ChinaXiv合作期刊

第55卷 第1期
2017年1月

古 脊 椎 动 物 学 报
VERTEBRATA PALASIATICA

pp. 1–23
figs. 1–9

First complete fossil *Scleropages* (Osteoglossomorpha)

ZHANG Jiang-Yong[1] Mark V H WILSON[2]

(1 *Key Laboratory of Vertebrate Evolution and Human Origins of Chinese Academy of Sciences*, *Institute of Vertebrate Paleontology and Paleoanthropology*, *Chinese Academy of Sciences* Beijing 100044, China
zhangjiangyong@ivpp.ac.cn)
(2 *Department of Biological Sciences*, *University of Alberta* Edmonton, Alberta T6G 2E9, Canada, and *Department of Biology*, *Loyola University* Chicago, USA)

Abstract A new species of osteoglossid fish, *Scleropages sinensis* sp. nov., is described from the Early Eocene Xiwanpu Formation in Hunan and the Yangxi Formation in Hubei, China. The new species was attributed to *Scleropages*, an extant genus of Osteoglossidae, because it very closely resembles the genus in skull bones, caudal skeleton, the shape and position of fins, and reticulate scales. The new fish is very similar to extant *Scleropages* except: the nasals do not appear to be ornamented; the sensory pore in the antorbital is large; the posterior infraorbitals are not quite covering the dorsal limb of the preopercle; the posteroventral angle of the preopercle is produced to point; the posteroventral margin of the opercle is concave and the ventral end of the bone is produced to a point; the pectoral fin is very long and extends well behind the beginning of the pelvic fin; the vertebral count is about 46–48; the parapophyses are shorter and the upper and lower caudal rays are nearly as long as the inner rays. The new fish is closer to its Asian neighbor, *S. formosus*, than to its southern relative, *S. leichardti*. *Scleropages formosus* inhabits natural lakes, swamps, flooded forests, and slowly moving, deep parts of rivers with overhanging vegetative cover. It is a carnivorous fish and its food consists mainly of insects, fishes, worms, small amphibians, small mammals, and even birds. *S. sinensis* may live in the same natural environment and have a similar diet except for the largest items. Sexual dimorphism may exist in *S. sinensis*. The presumed male has a slimmer and shallower body, a relatively larger head, and a deeper mouth cleft. The discovery of *Scleropages sinensis* sp. nov. dates the divergence of *Scleropages* and *Osteoglossum* to no later than the Early Eocene.

Key words Hunan, Hubei, China; Early Eocene; Xiawanpu Formation; Yangxi Formation; Osteoglossidae

Citation Zhang J Y, Wilson M V H, 2017. First complete fossil *Scleropages* (Osteoglossomorpha). Vertebrata PalAsiatica, 55(1): 1–23

1 Introduction

Scleropages, an extant genus of Osteoglossidae, is a freshwater fish with a transoceanic distribution in Southeast Asia and Australia. It has four species, *S. formosus* (Müeller and

国家自然科学基金(批准号：91514302, 41688103, 41172019, 40772019)资助。
收稿日期：2016-12-06

chinaXiv:201711.01925v1

ChinaXiv合作期刊

Schlegel, 1844) and *S. inscriptus* (Roberts, 2012) distributed in Sumatra, Kalimantan, Peninsular Malaysia, Thailand, and Cambodia, *S. jardinii* (Saville-Kent, 1892) and *S. leichardti* (Günther, 1864) in Australia and New Guinea. Pouyaud et al. (2003) described three closely related new species of *Scleropages* by coloration, molecular data and morphometric characters, but these new species were questioned and regarded as synonyms of *S. formosus* by Kottelat and Widjanarti (2005) and Roberts (2012). Pouyaud et al. (2003) also designated a neotype for *S. formosus* in their redescription of this species. Martien et al. (2013) thought the designation to be unnecessary because the types are still extant.

The Asian arowana (*Scleropages formosus*), known as the dragon fish, is one of the most prized and expensive aquarium fishes in the world. Some Asians believe that the arowana brings them good luck and fortune and even believe this fish can cast out evil spirits. This custom is still current in Thailand, China (Taiwan and Hong Kong), and Japan in spite of the fact that the fish was listed in the first appendix as in the highest class of protected fishes by the Convention on International Trade in Endangered Species of Wild Fauna and Flora (CITES). At present, captive-bred dragon fish (F2 Generation) may be traded.

Fossil *Scleropages* are known from the Maastrichtian of India (Hora, 1938; Rana, 1988; Kumar et al., 2005; Nolf et al., 2008), the Maastrichtian/Late Paleocene of Africa (Taverne, 2009), the Paleocene of Europe (Taverne et al., 2007), the Eocene of Sumatra (Sanders, 1934; Forey and Hilton, 2010), the Oligocene of Australia (Hills, 1934, 1943; Unmack, 2001). All of these earlier records are scales, otoliths and isolated fragments of bones. Here we report the first skeletons of fossil *Scleropages* from Lower Eocene strata in Xiangxiang, Hunan Province and Songzi, Hubei Province, China. Some specimens are complete and well preserved. A local farmer in Xiangxiang first collected the specimens and sent them to IVPP (Institute of Vertebrate Paleontology and Paleoanthropology, Chinese Academy of Sciences), and later, Li Chun from IVPP obtained a beautiful specimen (the holotype) from a farmer in Songzi. Zhang Miman of IVPP recognized these specimens first and then encouraged and advised the first author of this paper to study the specimens (including one piece from Xiangxiang sent by Song Changqi, a senior geologist), as she often helps young researchers to study the specimens in her care. Thereafter, the first author of this paper and his colleagues from IVPP collected tens of specimens of the fish along with other fishes during three field seasons, one in Xiangxiang and two in Songzi.

The specimens from Xiangxiang were found in gray-black shale of the lacustrine Xiawanpu Formation consisting predominantly of greenish, blue-gray claystone and grey-black shale, grey-black paper shale, with marlstone lenses. The geological age of the Xiawanpu Formation was considered to be Eocene or probably somewhat later (Liu et al., 1962; Cheng, 1962), or Early Eocene to early Middle Eocene (ECSLC, 1999). In addition to osteoglossids, some other fishes (Cheng, 1962) including "*Osteochilus*" *hunanensis* (originally described as a cyprinid fish by Cheng (1962) and later revised to *Amyzon hunanensis*, a catostomid, by Chang et al. in 2001), *Aoria* (a genus of bagrid catfishes), *Tungtingichthys* (Perciformes), and *Cyclurus* (Amiidae, Chang et al., 2010), as well as ostracods, and plants were also found in the formation.

chinaXiv:201711.01925v1

ChinaXiv合作期刊

The Songzi specimens including the holotype were collected in the Yangxi Formation which is 100–150 m in thickness and contacts conformably or disconformably with the underlying Paomagang Formation and the overlying Pailoukou Formation. The Yangxi Formation comprises shallow lacustrine deposits consisting of finely laminated mudstones and siltstones. Tons of slabs of fossil fishes (most are *Jianghanichthys*, a cypriniform fish) were unearthed by farmers and commercial collectors. Up to now, many vertebrate fossils have been found in this locality including the osteoglossid *Phareodus songziensis* (Zhang, 2003), *Jianghanichthys* (Liu et al., 2015), catfishes, perciforms, two rail-like birds *Songzia heidangkouensis* and *S. acutunguis* (Hou, 1990; Wang et al., 2012), and a pantodont mammal *Asiocoryphodon* cf. *A. conicus* (Chen and Gao, 1992). In addition, the oldest known primate was found in the same formation near this locality (Ni et al., 2013). Other fossils seen in the locality are ostracods, gasteropods, charaphytes, spores and pollen. The age of the strata is Early Eocene (ECSLC, 1999).

2 Material and methods

The specimens studied are deposited in the collection of Institute of Vertebrate Paleontology and Paleoanthropology (IVPP), Chinese Academy of Sciences. The comparative materials of extant *Scleropages* (*S. formosus*, IVPP V OP 80; *S. leichardti*, IVPP V OP 81) were bought at a fish market in Beijing and are also deposited in the IVPP. *Scleropages jardinii* and *S. inscriptus* were not found in Beijing fish market.

3 Systematic paleontology

Teleostei Müller, 1846

Osteoglossomorpha Greenwood et al., 1966

Osteoglossidae Bonaparte, 1832

***Scleropages* Günther, 1864**

***Scleropages sinensis* sp. nov.**

(Figs. 1–5, 7)

Etymology The specific name refers to China where the specimens were found.

Holotype IVPP V 13672.2, a complete skeleton.

Referred specimens IVPP V 12749.1–8, V 12750, V 13672.1, 3.

Locality and horizon Specimens V 13672.1–3 and V 12750 are from Songzi County, Hubei Province, China; Yangxi Formation, Lower Eocene. Specimens V 12749.1–8 are from Xiangxiang, Hunan Province, China; Xiawanpu Formation, Eocene.

Diagnosis A fossil species of *Scleropages* different from the extant species of the genus in: nasals not appearing to be ornamented, sensory canal exposed in prominent groove on nasals, supraorbital sensory canal enclosed in bone on frontal only for middle third of its length, unornamented posterior portion of parietal is only 1/4 of length rather than 2/3,

chinaXiv:201711.01925v1

ChinaXiv合作期刊

commissure in extrascapular tubes rather than passing through parietals, pterotic thicker in lateral portion, sensory pore in antorbital larger than in extant species, posterior infraorbitals not as large as in extant species and not quite covering dorsal limb of preopercle and their width to height ratio about 0.75 rather than 1–1.2, preopercle posteroventral angle produced to point, unlike condition in the extant species, posteroventral margin of opercle concave and ventral end of bone produced to point, supracleithrum recurved, dorsal process of cleithrum long and strong, pectoral fin very long and extending well behind beginning of pelvic fin, vertebrae about 46–48, parapophyses shorter, neural spine on U1 partly doubled, upper and lower caudal rays nearly as long as inner rays.

4 Description

The body of the fish is fusiform in adults, with median fins posteriorly positioned and pelvic fins in abdominal position. Skull bones are thick and squamation is heavy. The standard length of the largest specimen is 175 mm, that of the holotype is 140 mm, and that of the smallest is 78 mm. Unless otherwise indicated, the following description is based on the holotype (Fig. 1), which is the best-preserved example.

Cranium The bone interpreted as the probable dermethmoid has an elongate, spear-point shape, with a pointed anterior end and a long, tapered posterior end (Fig. 4). The nasals are large and suture in the midline along the anterior half of their length, but are separated by the tapered frontals posteriorly. The nasals are not noticeably ornamented, unlike the condition in extant *Scleropages formosus* (Taverne, 1977:fig. 73) and *S. leichardti* (IVPP dried skeleton). Also unlike the condition in the two extant species of *Scleropages* examined, the sensory canal appears to be exposed in a prominent groove in the fossil species.

The frontal is similar in shape and ornamentation to that of extant species of *Scleropages* (Taverne, 1977:fig. 73; IVPP dried skeleton of *S. leichardti*). It is long and subrectangular, with an anterior embayment for the reception of the nasal, and a posterior sinuous suture with its opposite member. In proportions it is slightly shorter and wider than that of *S. leichardti* and more like that of *S. formosus*. The lateral margin is embayed to conform to the medial margin of the dermosphenotic. Parallel to the lateral margin, the sensory canal is enclosed in bone for the middle third of its length, while being exposed in deep grooves for the anterior and posterior thirds of its length in the frontal. In *S. leichardti* and *S. formosus*, in contrast, the canal is enclosed in bone to or almost to its entry into the nasal.

As in other species of the genus, the parietal is subrectangular and sutures with its opposite at the midline and with the pterotic laterally. The surface of the anterior three-quarters of the bone is sculptured, while the posterior quarter lies at a lower level, beneath the canal-bearing extrascapulars, and is not sculptured. Length-to-width proportions of the parietal are about 2:3, similar to those of *S. formosus* but unlike the 1:1 ratio seen in *S. leichardti*.

The external portion of the pterotic is a little larger and thicker than it is in extant species of *Scleropages*. The anterior half of the bone, lateral to the parietal, is sculptured and bears the

chinaXiv:201711.01925v1

ChinaXiv合作期刊

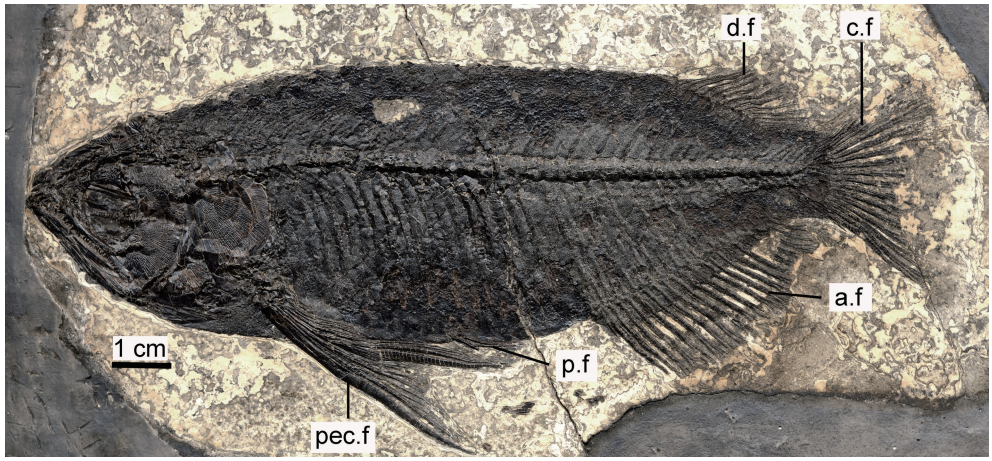

Fig. 1 *Scleropages sinensis* sp. nov., holotype (IVPP V 13672.2) in left lateral view
Abbreviations: a.f. anal fin; c.f. caudal fin; d.f. dorsal fin; p.f. pelvic fin; pec.f. pectoral fin

Fig. 2 *Scleropages sinensis* sp. nov., a complete fish (IVPP V 13672.3a) in right lateral view

temporal sensory canal in an open groove, whereas it is a simple tube in *S. formosus* (Taverne, 1977:fig. 73). The epiotic, supratemporal and supraoccipital are not visible in the available specimens.

Scleropages sinensis appears to have its extrascapular sensory commissure carried within tubular 'extrascapulars' situated dorsal to the unsculptured area of the parietals, rather than passing directly through the parietals as seen in extant species of *Scleropages* (Taverne, 1977:fig. 71). In both fossil and extant species, the canal is carried in paired extrascapular tubes between the previously mentioned bones and the posttemporals.

The orbital portion of the parasphenoid is toothless, moderately broad, and parallel-sided (V 12749.5). The remainder is covered by infraorbitals in available specimens.

The circumorbital series (Fig. 4) is composed of six bones: an antorbital, four infraorbitals and a dermosphenotic. A supraorbital is absent. The antorbital, infraorbitals 1, 3 and 4, and

chinaXiv:201711.01925v1

ChinaXiv合作期刊

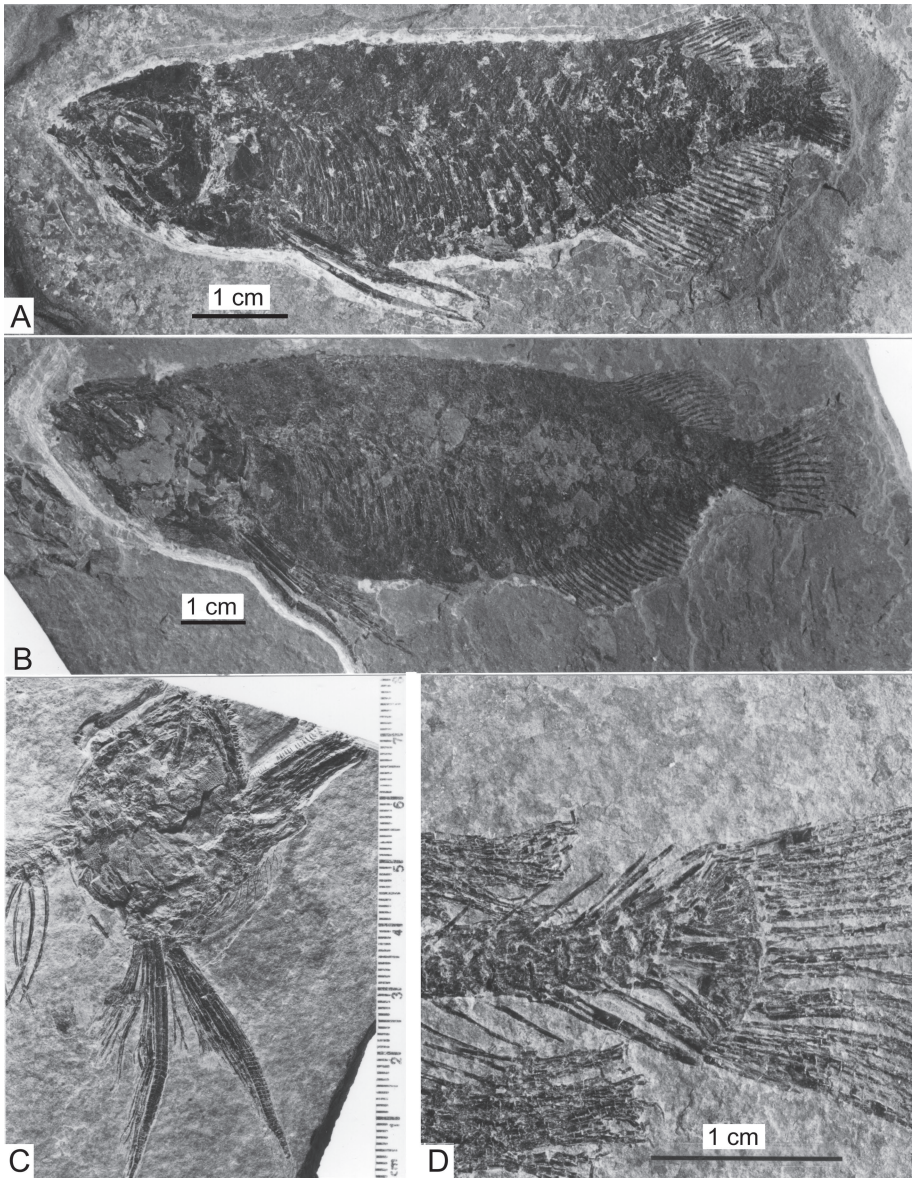

Fig. 3 *Scleropages sinensis* sp. nov.
A. a complete fish (IVPP V 12749.4) in left lateral view, B. a complete fish (V 12749.2) in left lateral view, C. a skull (V 12749.7a), D. a caudal skeleton (V 12749.8)

the dermosphenotic are all prominently sculptured, while infraorbital 2 is not preserved well enough for assessment of its sculpture.

The antorbital is polygonal, making contact with the dermopterotic posterodorsally, the frontal and parietal dorsomedially, and the first infraorbital ventrally. The concave anterior and orbital margins are free. The shape is similar to that of *S. formosus* (Taverne, 1977:fig. 71). Dorsally the circumorbital sensory canal enters the antorbital via a short, broad groove, then passes through the bone in a tube, entering the first infraorbital where a large pore communicates

chinaXiv:201711.01925v1

ChinaXiv合作期刊

with the exterior. In *S. formosus* as illustrated by Taverne (1977:fig. 71), the latter pore is small and the canal is completely enclosed in bone throughout its length. The antorbital in *Osteoglossum bicirrhosum* (Taverne, 1977:fig. 42) is more tubular and parallel-sided and unornamented; in *S. leichardti* (IVPP dried skeleton) it is also less polygonal but is ornamented.

The first and the second infraorbitals are narrow and tubular. The first is slightly expanded, longer, and more ornamented than the second, but the latter is not well preserved.

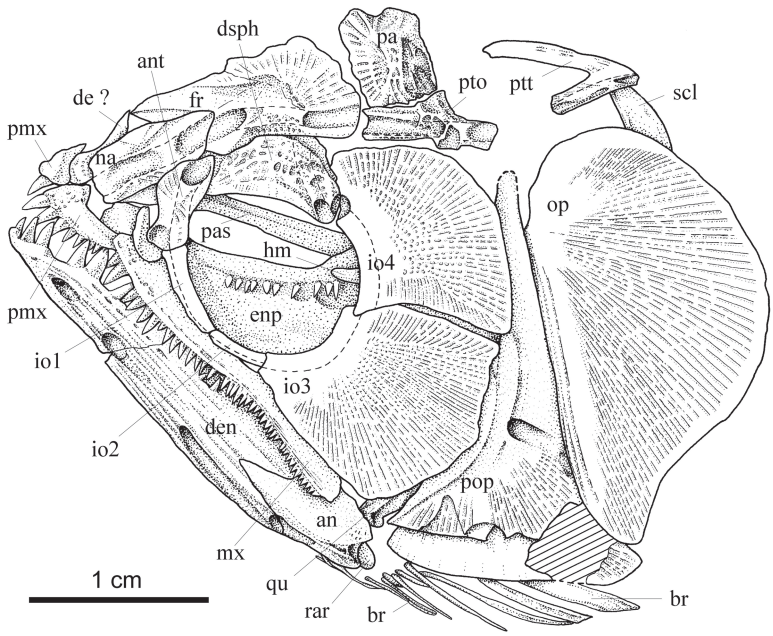

Fig. 4 *Scleropages sinensis* sp. nov., skull as preserved in holotype, left lateral view
Abbreviations: an. angular; ant. antorbital; br. branchiostegals; de. dermethmoid; den. dentary; dsph. dermosphenoid; enp. endopterygoid; fr. frontal; hm. hyomandibula; io1–4. first to fourth infraorbitals; mx. maxilla; na. nasal; op. opercle; pa. parietal; pas. parasphenoid; pmx. premaxilla; pop. preopercle; pto. pterotic; ptt. posttemporal; qu. quadrate; rar. retroarticular; scl. supracleithrum

The two posterior infraorbitals (third and fourth) are very large but do not quite reach the size of those in extant *Scleropages* and *Osteoglossum*, in which they extend posteriorly to the articulation of the opercle, completely concealing the dorsal end of the preopercle and covering the posterior suspensorium. In *S. sinensis* there is a narrow gap through which the dorsal limb of the preopercle may be seen. The two posterior infraorbitals have a ratio of width to height of about 0.75, compared to about 1.0–1.2 in the two extant species of *Scleropages*. The two bones are nearly equal in size, like those in extant *Scleropages* but differing from those in *Osteoglossum*, in which the lower one is much larger than the upper. The infraorbital sensory canal is carried in a tube near the orbital margin of both posterior infraorbitals, with only a single small pore opening externally near the anteroventral end of the third infraorbital, as in the specimen of *S. formosus* figured by Taverne (1977:fig. 71). In *O. bicirrhosum* the pore is much larger and directed posteroventrally into a large groove (Taverne, 1977:fig. 42).

chinaXiv:201711.01925v1

ChinaXiv合作期刊

The complete or near-complete enclosure by infraorbitals of the cheek posteroventral to the orbit is considered to be a synapomorphy of Osteoglossidae by Li and Wilson (1996) and Hilton (2003). Among early osteoglossomorphs, this character is found only in *Paralycoptera*. Accordingly, *Paralycoptera* was considered to be closely related to or included within Osteoglossidae by different authors (Chang and Chou, 1977; Ma and Sun, 1988; Jin et al., 1995; Zhang, 2002).

The dermosphenotic is large, thick, sculptured, and approximately triangular. It bears the infraorbital canal internally near its posterior margin. The canal emerges from the posterodorsal corner of the dermosphenotic, where it enters the frontal to join with the supraorbital sensory canal near the anterior end of the posterior sensory groove of the frontal. In *S. formosus* the canal also joins within the frontal, but within a bone-enclosed tube. In V 12749.5 there is a suggestion of a branch in the infraorbital canal within the dermosphenotic, but the course of this branch cannot be detailed. Taverne (1977:fig. 71) did not show any branching within the dermosphenotic.

Jaws The premaxilla is small, approximately triangular, and sculptured. It bears a blunt ascending process in its anterior half. There are seven teeth on the left premaxilla of the holotype, the anterior three teeth being much larger than the posterior ones. The number of teeth on the premaxilla of extant *Scleropages* has been counted differently, 4–5 by Ridewood (1905), 3–5 by Kershaw (1976), and 11 by Taverne (1977). In the four specimens of extant *Scleropages* that we examined, this number is 6–8, a condition agreeing with that of *S. sinensis*.

The maxilla is long and slender, and takes an angle of about 45º with the long axis of the fish when the mouth is closed. It extends posteriorly nearly to the level of the mandibular articulation and ends well behind the posterior margin of the orbit. The posterior end is slightly expanded and downturned, especially immediately posterior to the marginal teeth. Ornament is present all along the external surface but is most prominent at the anterior and posterior ends. As in all living osteoglossomorphs, there is no supramaxilla.

The maxilla bears 40 conical teeth in an external row in the holotype, a resemblance in number with *S. formosus* and a difference from *S. leichardti*, in which the teeth number about 35 (IVPP dried skeletons). The teeth decrease in size steadily from anterior to posterior. Here and there, a few smaller teeth seen behind and between these marginal teeth might represent replacement teeth.

The mandible is also very long, makes a 45º angle with the long axis of the fish, lacks a distinct coronoid process, and consists of three bones: dentary, angulo-articular, and retroarticular. The dentary forms the great majority (3/4) of the length of the mandible. Anteriorly, the dentary curves medially to meet its opposite at a shallow symphysis. As for the premaxilla, the anterior five or six teeth of the dentary are much larger than the posterior ones.

As in extant *Scleropages* (Taverne, 1977:fig. 71), the angulo-articular is relatively small, articulates with the quadrate as seen in lateral view, and the posterior tip of the retroarticular is visible laterally posterior to the quadrate articulation. Both dentary and angulo-articular bear longitudinal ridges on their lateral surfaces.

chinaXiv:201711.01925v1

ChinaXiv合作期刊

The mandibular sensory canal extends the length of the dentary and angulo-articular within a canal, with one pore located near the ventral end of the suture between the angulo-articular and dentary, as in *S. formosus* (Taverne, 1977:fig. 71) and three more pores evenly spaced and opening onto posteriorly directed grooves more anteriorly in the dentary, as in *S. formosus* and *S. leichardti* (IVPP dried skeletons).

Palato-quadrate arch The toothed palato-ectopterygoids are preserved in V 12749.5, in which both have a row of uniform-sized small teeth on their lateral margins. On the right one can be seen more medially an area of much smaller teeth. Both conditions are matched in extant *S. formosus* (Taverne, 1977:fig. 83) and *S. leichardti* (IVPP dried skeleton). According to Taverne (1977:134–135), the anterior end of this bone in *S. formosus* includes the fused dermopalatine, with the autopalatine ossified only in the largest, oldest individuals. We were unable to confirm these details in *S. sinensis*.

The entopterygoid in extant species of *Scleropages* is triangular, a single row of large conical teeth existing on the medial edge, and fine denticles covering the remainder of the surface. The detailed shape is not seen in the fossils of *S. sinensis*, but part of the medial row of large teeth on the right entopterygoid is visible in the holotype. These teeth are larger posteriorly than anteriorly, and each is curved slightly ventrolaterally, as in *S. leichardti* (IVPP dried skeleton). In V 12750 the medial row and more lateral denticles are visible in cross section. The metapterygoid, symplectic, and most of the quadrate are covered by the posterior infraorbitals in available specimens, although the quadrate and symplectic are exposed in inner view in V 12750.

Hyoid arch and branchiostegals Only a very small part of the hyomandibular can be seen in the holotype. The tip of a bone protruding from beneath the anterior margin of the fourth infraorbital in the holotype might be the entopterygoid process of the hyomandibular as characteristically seen in extant osteoglossids, but it seems rather too stout. On the other hand, it is not oriented appropriately to be identified with the basipterygoid process of the parasphenoid, which might be expected to occur in the same area of the fossil.

A small triangular hypohyal, most of the anterior ceratohyal and basihyal are seen in V 12749.5. There are 9 slender, acinaciform branchiostegal rays in the holotype, and at least two broad, spatulate ones. In *S. formosus*, Taverne (1977:fig. 84) illustrates 9 acinaciform and 7 spatulate branchiostegals; thus we might estimate that *S. sinensis* had a similar number, perhaps 16 in total, given that only two spatulate branchiostegals are preserved.

Opercular series The preopercle is similar but not identical to that in the extant species of *Scleropages*. The upper limb is not completely covered by posterior infraorbitals as it is in the extant species of the genus (Taverne, 1977:fig. 71). The dorsal limb tapers uniformly dorsally, as far as can be seen, and is about twice as long as the ventral limb. The latter is bluntly rounded anteroventrally. The posteroventral angle of the preopercle is produced posteriorly to a point, located immediately below the ventral extremity of the opercle. This last feature is not seen in the preopercles of extant species of *Scleropages* but is met with in a more extreme form in some African osteoglossiforms such as *Chauliopareion* Murray and Wilson,

chinaXiv:201711.01925v1

ChinaXiv合作期刊

2005, and *Singida* as redescribed by Murray and Wilson (2005).

The preopercular sensory canal in *S. sinensis* has features typical for osteoglossids. The canal is open ventrally beneath a long, horizontal shelf. On the shelf, and dorsal to it, the preopercle is sculptured, but ventral to it the surface of the preopercle is smooth. From the posterior end of this shelf to the dorsal end of the vertical limb, the preopercular canal is enclosed in bone beneath the anterior edge of the exposed portion of the bone, except for a single, large pore at about half the height of the preopercle. This pore opens posteriorly from the main canal into a prominent groove directed posteroventrally.

In other osteoglossids the relative height of this single pore varies, but essentially the same feature is seen, where preservation permits, in many genera of Osteoglossidae and Notopteridae including extant species of *Scleropages* and fossil taxa such as *Phareodus* and *Musperia* (e.g., Taverne, 1977, 1978). *Arapaima* and *Heterotis* do not exhibit the shelf and single large pore, showing instead a bone-enclosed canal opening via pores, while the condition in *Pantodon* is perhaps somewhat intermediate (Taverne, 1978).

The opercle in *S. sinensis* is large and nearly semicircular in shape, but differs from that in the extant species of *Scleropages* and *Osteoglossum* in having its ventral end produced to a point and its posteroventral margin concave. The opercle is also prominently sculptured except for its anterior margin and dorsal extremity. The opercle in the holotype has a height of 24 mm and a maximum width, at right angles to the anterior edge, of 13 mm. The hyomandibular facet is located at a height of 19 mm from the ventral end, judging by the arrangement of ornamental ridges on the external surface. The subopercle and the interopercle are not visible.

Appendicular skeleton The pectoral girdle is partially seen in the holotype and in V 12749.8. The posttemporal is a forked bone with the dorsal limb longer than the ventral one. The lateral line runs near the ventral margin of the bone and probably goes into the trunk scales directly, without passing through the supracleithrum, as in the living osteoglossids.

The supracleithrum is strap-like dorsally and broadens ventrally; it is recurved rather than following a uniform curve as seen in extant species of *Scleropages*. In *Osteoglossum* the bone broadens ventrally but is not recurved (Taverne, 1977). A small postcleithrum is present and lies medial to the junction between the supracleithrum and cleithrum.

The cleithrum is best exposed in specimen V 12749.8, in which it is seen to have a long dorsal limb of uniform width, terminating dorsally in a long, rod-like process. In contrast, the cleithrum of extant species of *Scleropages* (Taverne, 1977:fig. 86; IVPP dried skeletons) has only a smaller, acuminate dorsal extremity, much shorter and more slender than that of *S. sinensis*. The coracoid, scapula, and mesocoracoid have not been seen.

Four proximal pectoral radials that support the pectoral rays except for the first ray can be recognized in the holotype, with the first thick and stout and the others becoming small posteriorly.

The pectoral fin (Figs. 1, 3C) is very long and extends well behind the beginning of the pelvic fin, a difference from the extant species of *Scleropages* where it does not reach the beginning of the pelvic fin. In the holotype the longest rays are 47 mm long, whereas the pelvic

chinaXiv:201711.01925v1

ChinaXiv合作期刊

fin originates 35 mm posterior to the origin of the pectoral fin.

The pectoral fin contains seven rays, resembling that of *S. formosus* rather than *S. leichardti* where the fin has eight rays (IVPP dried skeletons); all rays are branched and segmented except the first one which is exceptionally thick and unbranched, though segmented. Adjacent to the base of the smallest ray there is a claw-shaped bone.

The pelvic girdle and fin are very small. The pelvic fin originates slightly closer to the anal fin than to pectoral fin. The pelvic bone (seen in V 12749.8) is short and flat. There appear to be six pelvic fin rays, all branched but the first, a condition agreeing with that of *S. leichardti* and differing from *S. formosus* which has five fin rays in specimens examined.

Dorsal and anal fins Both dorsal and anal fins are rounded in outline and located posteriorly. The dorsal fin is small and originates posterior to the origin of anal fin, opposite the middle of the anal fin. In the holotype there are two short procurrent dorsal rays, the second one segmented, followed by one full-length unbranched ray, and 11 branched rays, the last one apparently double, for a total of 12 principal rays. Fourteen short dorsal pterygiophores can be counted, matching the fin rays one-to-one. Other specimens (V 12749.1,2) may have slightly more principal rays, 12–15 in available specimens, with 14–17 pterygiophores.

The anal fin is much larger than the dorsal fin, with three very small, unsegmented procurrent rays and 22 principal rays, supported by 23 anal pterygiophores in the holotype, and 21–24 anal pterygiophores in other specimens (V 12749.1,4). This resembles the condition in *S. formosus* and differs from that in *S. leichardti*, in which 28 principle fin rays are present.

Vertebral column and caudal fin There are 46–48 vertebrae in available specimens, of which in the holotype about 22 are abdominals and 24 are caudals including the two ural centra. This number is much less than in extant osteoglossids and agrees more with that of early osteoglossomorphs such as *Kuntulunia* and *Xixiaichthys* (Zhang, 1998, 2004). The first three centra are covered by the opercle. The centra are slightly deeper than long.

The first four neural spines are paired and the remainder anterior to the dorsal fin are fused into a single element. In extant *Scleropages* and *Osteoglossum*, this condition varies, neural spines being fused beginning with the third in *S. formosus* and with the eighth in *O. bicirrhosum* (e.g., Taverne, 1977:108, 147). Parapophyses are difficult to see but appear (V 12749.8) to be much shorter than in extant *Scleropages*, *Osteoglossum*, and *Phareodus* (Li et al., 1997) and even shorter than in most early osteoglossomorphs (Zhang and Jin, 1999; Zhang, 1998, 2004).

There are 22 pairs of pleural ribs, which extend to the ventral margin of the trunk, except for the last pair, which is only about half the length of the more anterior ones.

Long, slender epineurals are present, their proximal ends not fused with the neural arches. The last epineural is related to the second vertebra following the last abdominal vertebra.

Some 22 long, slender supraneurals are seen in specimen V 12749.8, anterior to the dorsal fin and lying at a shallow angle to the long axis of the body so that each one overlaps the dorsal end of one or two neural spines.

The caudal skeleton (Figs. 3D, 5) is very similar to that of the extant species of

chinaXiv:201711.01925v1

ChinaXiv合作期刊

Scleropages with a couple of exceptions. Unfortunately, these details can only be seen in a single specimen of *S. sinensis* (V 12749.8). The caudal skeletons in the two examined extant species of *Scleropages* (Fig. 6) display important differences, each resembling that of *S. sinensis* in some ways but not in others.

Three neural and haemal spines in *S. sinensis* are lengthened to support the caudal fin rays; these haemal spines gradually thicken posteriorly. The first preural centrum bears a complete neural spine, while in some specimens of *S. leichardti* the centrum bears two.

The first ural centrum (U1) appears to have two incompletely fused neural spines, with the first complete and the second one shorter. The second ural centrum (U2) is fused with the proximal ends of hypurals 3–5. There are six hypurals. Hypural 1 is very deep and does not reach U1 proximally. Hypural 2 is less than half the width of the first and either articulates with or is fused to the centrum as in extant species of *Scleropages*. Hypurals 3 through 5 are fused proximally and fit tightly together distally. A rod-like bone dorsal to hypurals 3–5 is probably the sixth hypural. Just above this bone, a similarly shaped bone is interpreted here as fused uroneurals (see Hilton, 2003, for discussion of this unusual feature of osteoglossiforms).

In *S. leichardti*, centrum U1 supports three hypurals in every specimen available to us, a very unusual situation for a teleostean fish. The first two of these hypurals are fused to each other proximally but separated distally, and the combined first two hypurals do not reach U1. In contrast, both *S. formosus* and *O. bicirrhosum* have the more usual situation of two lower hypurals, the first not reaching U1 and the second joins it.

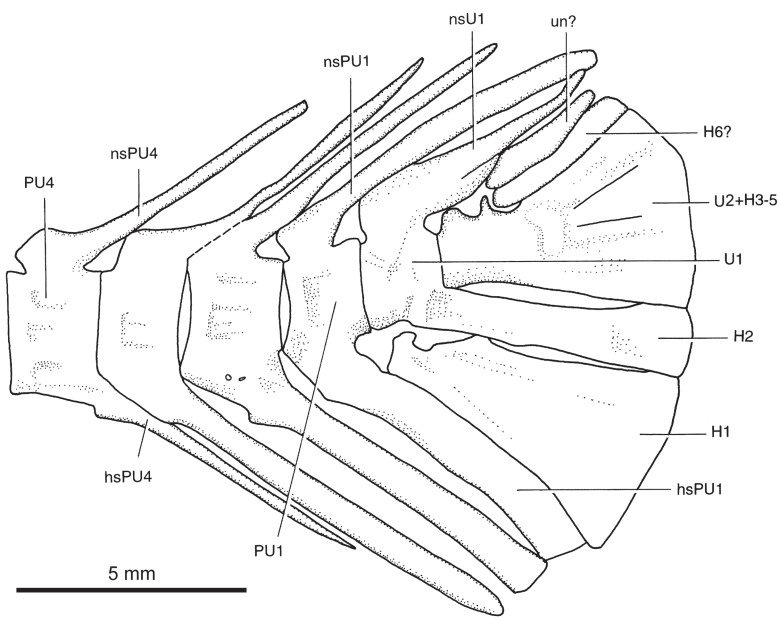

Fig. 5 *Scleropages sinensis* sp. nov., caudal skeleton, IVPP V 12749.8
Abbreviations: H1–6. hypurals 1–6; hsPU1, 4. haemal spines on PU1, 4; nsPU1, 4. neural spines on PU1, 4; nsU1. neural spine on U1; PU1, 4. preural vertebrae 1, 4; U1, 2. ural centra 1, 2; un. uroneural

chinaXiv:201711.01925v1

ChinaXiv合作期刊

The greatly enlarged first hypural in *S. sinensis* seems deep enough to correspond to the two partially fused hypurals of extant *S. leichardti* specimens. This hypural is as deep as the first two (of three lower) hypurals in *S. leichardti*. However, we do not see any evidence of a division into two hypurals in this specimen. The occurrence in *S. sinensis* of two incompletely separated neural spines on U1 might suggest an origin by fusion of centra. However, the neural spine of *S. leichardti* specimens examined by us is not doubled, whereas they have an extra lower hypural. Additional specimens showing the caudal skeleton of *S. sinensis* and a study of the development of the caudal skeleton in *S. leichardti* could be very informative in light of these findings.

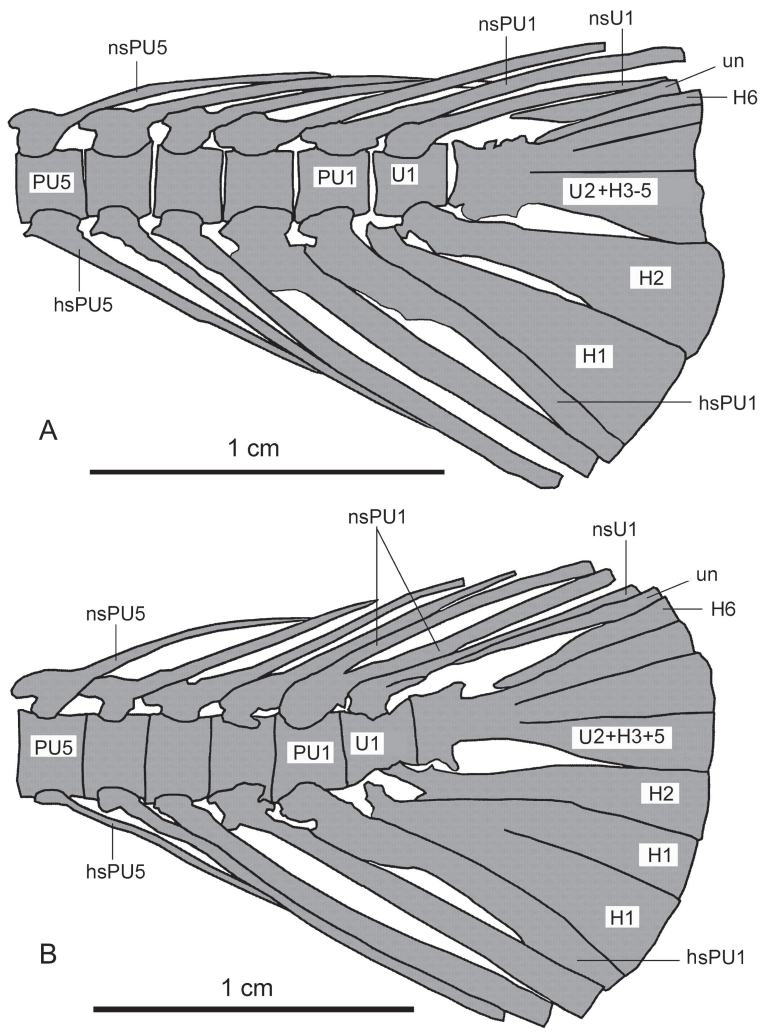

Fig. 6 Caudal skeletons of *Scleropages formosus* (A, IVPP V OP 80) and *S. leichardti* (B, IVPP V OP 81) Abbreviations: H1–6. hypurals 1–6; hsPU1, 5. haemal spines on PU1, 5; nsPU1, 5. neural spines on PU1, 5; nsU1. neural spine on U1; PU1, 5. preural vertebrae 1, 5; U1, 2. ural centra 1, 2; un. uroneural

chinaXiv:201711.01925v1

ChinaXiv合作期刊

Fig. 7 *Scleropages sinensis* sp. nov., scales, IVPP V 13672.3a

The caudal fin is rounded. There are 16 principal caudal rays, the first and the last being unbranched and almost as long as the remaining rays, whereas in living species of *Scleropages* and *Osteoglossum*, the upper and lower rays are only half the length of the innermost ones. One or two procurrent rays are present anterior to the principal rays.

Squamation The scales are large (Figs. 2, 7), cycloid, oval, and exhibit the reticulate pattern, involving small units called squamules, typical of osteoglossids (Fig. 8). The external surface of the scale shows circuli in the basal portion and granular ornamentation in the apical area. The squamules (Gayet and Meunier, 1983) are rhombic, polygonal, or irregular in shape. The mesial surface of each squamule may be smooth or bear 1–25 rounded, raised tubercles, each of which has a minute transversal-pore (Jolly and Bajpai, 1988) at its center.

The lateral line (Fig. 2) runs just below the vertebral column and the scales along the lateral line number about 24, a similar number to that in *S. formosus* and 10 scales fewer than is seen in *S. leichardti* (IVPP specimens).

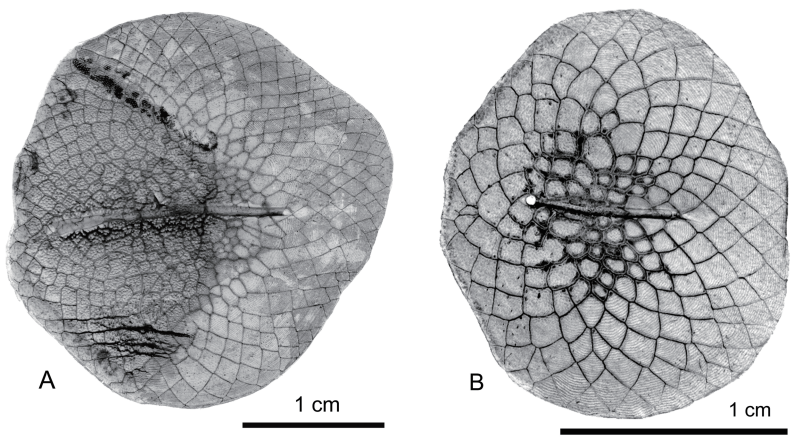

Fig. 8 Scales of *Osteoglossum bicirrhosum* (A) and *Scleropages formosus* (B)

5 Discussion

The new fish found in Hubei and Hunan provinces of China very much resembles *Scleropages* in skull bones, caudal skeleton, the shape and position of fins, and reticulate scales (Fig. 9). Therefore, it must belong to the genus. *Scleropages* has four species, two in Australia and New Guinea (*S. jardinii* and *S. leichardti*) and the other two in Asia (*S. formosus* and *S. inscriptus*). *S. jardinii* and *S. leichardti* are very similar to each other, while *S. formosus*

chinaXiv:201711.01925v1

ChinaXiv合作期刊

and *S. inscriptus* are nearly identical except the latter has complex maze-like markings on circumorbitals, opercular series and scales. For this reason and because specimens of the other two species were not available to us, only *S. leichardti* and *S. formosus* were used as representatives of extant *Scleropages* for comparison study.

The new fish is very similar to *S. leichardti* and *S. formosus*, except: the nasals do not appear to be ornamented; the sensory canal is exposed in prominent groove on the nasals (unless a preservational artifact); the supraorbital sensory canal is enclosed in bone on the frontal only for middle third of its length; unornamented posterior portion of the parietal is only 1/4 of its length rather than 2/3; the commissure is in extrascapular tubes rather than passing through the parietals; the pterotic is thicker in its lateral portion; the sensory pore in the antorbital is larger than in the extant species; the two posterior infraorbitals are not as large as in extant species of *Scleropages*, not quite covering the dorsal limb of the preopercle, and their width to height ratio is about 0.75 rather than 1–1.2; the posteroventral angle of the preopercle is produced to a point, unlike the condition in the extant species; the posteroventral margin of opercle is concave and the ventral end of the bone is produced to a point (in the extant species the ventral end of the opercle is not as produced and the posteroventral margin is not concave); the supracleithrum is recurved vs uniformly curved; the dorsal process of the cleithrum is long, strong, and rod-shaped vs shorter and acuminate in the extant species; the pectoral fin is very long and extends well behind the beginning of the pelvic fin; vertebrae number about 46–48 vs ~60 in extant species and other Recent osteoglossids; the parapophyses are shorter; the neural spine on U1 is partly doubled; the upper and lower caudal rays are nearly as long as the inner rays (vs much shorter). Based on these differences, a new species is established, *Scleropages sinensis* sp. nov.

Scleropages sinensis is similar to *S. formosus* but different from *S. leichardti* in that: proportions of length to width of parietal are 2:3 vs 1:1; the antorbital proportions are similar to those in *S. formosus* but in *S. leichardti* the antorbital is not as polygonal; maxillary teeth number about 40 vs about 35 in *S. leichardti*; principal anal rays are 21–24 vs 28 in *S. leichardti*; there are two lower hypurals vs three in *S. leichardti*; there are 24 scales along the lateral line, vs ~34 in *S. leichardti*.

Scleropages sinensis also shares some similarities with *S. leichardti* but differs from *S. formosus*. These characters include six pelvic rays vs five in *S. formosus*, the first hypural very deep (as deep as the first two in *S. leichardti*, and unlike the slender first hypural in *S. formosus*). Pelvic fin rays are seven in Hiodontidae, six principle plus one short in *Kuntulunia* and *Xixiaichthys*, six in *Lycoptera* and *Asiatolepis* (Zhang, 2010: five in original description, but clearly six in V 11982.28a). Therefore, having more pelvic rays is likely to be a primitive condition in osteoglossomorphs. Centrum U1 supporting three hypurals in *S. leichardti* is a very unusual situation in teleosts. The same condition was noticed by Hilton (2003) in *S. jardinii* (152 mm SL) and by Xu and Chang (2009) in *S. jardinii* and *S. leichardti*. Hilton thought that study of more specimens was needed to confirm if this is due to ontogeny (i.e., if hypural 1 typically is composed of two elements) or is an individual variation. Although

chinaXiv:201711.01925v1

ChinaXiv合作期刊

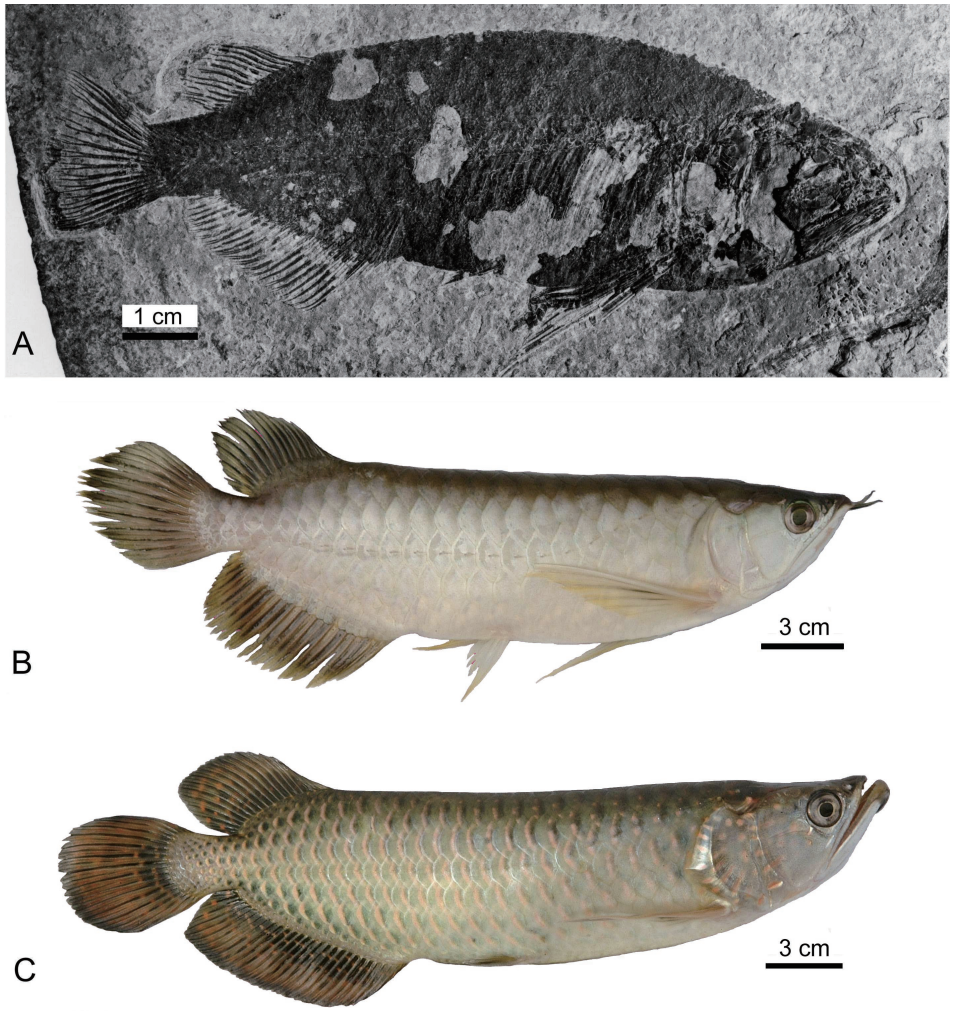

Fig. 9 Comparison between *Scleropages sinensis* sp. nov. (A, IVPP V 12749. 1) and *S. formosus* (B, IVPP V OP 80), *S. leichardti* (C, V OP 81)

the first hypural in *S. sinensis* seems deep enough to correspond to the first two hypurals in *S. leichardti*, no evidence of a possible division into two hypurals can be seen. The caudal skeleton is usually covered by scales in *S. sinensis* that make it difficult to know if there is any variation in the hypural pattern.

According to the above comparison between *S. sinensis* sp. nov. and the extant *Scleropages*, it is clear that the new fish is closer to its Asian neighbor, *S. formosus* than to its southern relative, *S. leichardti*.

The Asian arowana *S. formosus* is distributed in the Mekong Basin in Viet Nam and Cambodia, southeastern Thailand, Tenassarim (Myanmar), the Malay Peninsula from Sungai Golok southwards, Borneo, and Sumatra. It inhabits natural lakes, swamps, flooded forests, and slowly moving, deep parts of rivers with overhanging vegetative cover. The Asian arowana is a carnivorous fish and its food consists mainly of insects, fishes, worms, small amphibians,

chinaXiv:201711.01925v1

ChinaXiv合作期刊

small mammals, and even birds. It can jump very high in the wild to get food hanging on trees. *S. sinensis* may have lived in the same natural environment and could have had a similar diet except for the largest items considering the smaller body size of the new fish.

Arowana are paternal mouthbrooders. The Asian arowana is not easy to sex. Scott and Fuller (1976) found no obvious external sexual differences in 170 specimens (32 were fry) they obtained in Malaya. But Suleiman (2003) argued that the differences become apparent after maturity is reached at about 3–4 years of age. The determination of sex is based on the body shape and the size of the mouth cavity. Males have a slimmer and shallower body depth (while females have a more rounded body), a bigger mouth and more intense color than the females. A larger mouth and a deeper lower jaw in males are beneficial for holding more eggs and fry. These sexual differences can also be seen in *S. sinensis*. The holotype (Fig. 1) and another fish (Fig. 3A) have a slimmer and shallower body, a relatively larger head and a deeper mouth cleft. In contrast, some other individuals (Fig. 2) have a more rounded body and a smaller head. This suggests a possible sexual dimorphism in *S. sinensis*. The deeper mouth cleft in the holotype and V 12749.4 (Fig. 3A) also suggests the possibility of paternal mouthbrooding in *S. sinensis*. Unfortunately, no direct evidences such as eggs and fry can be found on the fossils.

Except for *Hiodon*, which lives only in North America, all the other extant osteoglossomorphs are distributed in the tropical or subtropical fresh waters of southern continents. Fossil osteoglossomorphs were found from fresh water deposits (some forms, such as *Brychaetus*, may live in brackish water and even marine) in all the continents except Antarctica. The explanation for such a transoceanic distribution of freshwater fishes is a challenge for paleogeography and historical biogeography. Nelson (1969) argued that Africa was probably the center of the ancestral distribution of osteoglossomorphs. Greenwood (1970) and Chang and Chou (1976) supposed that East Asia might be the ancestral of osteoglossomorphs. Gayet (1987) explained the present distribution of osteoglossomorphs by a hypothetical “lost Pacifica”. All these hypotheses failed to resolve the transoceanic distribution of the superorder Osteoglossomorpha satisfactorily. Li (1997) and Xu and Chang (2009), in contrast, suggested that the early evolution of Osteoglossomorpha occurred in Pangea.

The earliest fossil record of Osteoglossomorpha is *Lycoptera* (Barremian) (Swisher et al., 2002). Early osteoglossomorphs have mostly been recovered from China, but have also been found in other parts of the world, such as *Chandlerichthys* from North America (Cenomanian), *Laeliichthys* from South America (Aptian), *Kipalaichthys* from Africa (Cenomanian). Since Osteoglossomorpha were already widely distributed on both northern and southern continents in the Early and mid-Cretaceous, it is reasonable to suggest that the superorder originated in Pangea.

Li (1997) believed that the earliest member of the main lineages of Osteoglossomorpha had already extended their distribution to most parts of Pangea before its final break up and the recent relict distribution of the superorder resulted from extinction. Li conceived that the transoceanic dispersal and vicariance of Osteoglossomorpha did not happen after the final split of Pangea. *Phareodus*, a very common genus of fossil osteoglossid also seen in the same

chinaXiv:201711.01925v1

ChinaXiv合作期刊

formation with *S. sinensis*, has been found in Pakistan, India, Sumatra (*Musperia*), North America and Australia. If transmarine migration never happened, a Pangea origin would be the most likely model to interpret the transoceanic distribution of *Phareodus*. Based on their study on molecular phylogeny of osteoglossoids, Kumazawa and Nishida (2000) concluded that the divergence time between Asian arowana (*Scleropages formosus*) and Australia arowana (*S. leichardti* and *S. jardinii*) is about 138 million years, which is close to or slightly older than the probable time of the India-Madagascan separation from Gondwanaland (120–130 Ma, Smith et al., 1994). They consequently argued that the Asian arowana originated on a part of Gondwanaland and was carried to Eurasia by the Indian subcontinent. Therefore, the transoceanic migration of Osteoglossomorpha might have occurred after the split of Pangea.

The Eocene collision of the Indian subcontinent with Asia has been accepted for a long time (Besse et al., 1984; Metcalfe, 1999), but recent data support the view that terrestrial continuity between India and mainland Asia was already established by the time of the K/T boundary, 65 Ma ago, or probably slightly earlier (Beck et al., 1995; Jaeger et al., 1989; Prasad et al., 1994; Rage et al., 1995). The discovery of *Scleropages* and *Phareodus* from mainland Asia suggests the possibility that the genus originated in Gondwana and dispersed to Asia through the Indian subcontinent, and then *Phareodus* to North America via the Bering Strait. The Eocene fish fauna along the coast of the Bohai Gulf, eastern China, shows striking similarity in composition to those of the same age along the west coast of North America, demonstrating a “transpacific” distributional pattern (Chang and Chen, 2000). The Arctic connection of the northern continents and the broad connection between Asia and North America in the Bering Strait area may have served as a passage for the fishes from both sides of the Pacific (Chang and Chen, 2000). With those connections between the two places, *Phareodus* could have dispersed from Asia to North America. *Scleropages* has been found in the Maastrichtian, Paleocene, Eocene and Oligocene and *Phareodus* was cosmopolitan in the Eocene, but their Late Cretaceous representatives were only found in southern continents. The fossil records thus seem to support the view of a Gondwanian origin of osteoglossids.

However, a recent work (Lavoué, 2015) rejected the Gondwanian origin of *Scleropages*. Lavoué reported an age CI of *Scleropages* ranging from 79.9 to 101.4 Ma, which is significantly younger than the (138 ± 18) Ma age inferred by Kumazawa and Nishida (2000). Recent paleogeographical reconstructions (Gibbons et al., 2013; Scotese, 2014) give a latest possible age (115.0 Ma) for a direct connection of the Indian subcontinent to Australia–Antarctica. Lavoué’s result suggests that the divergence between the Sundaland–Indochina *Scleropages* and the Australia–New Guinea *Scleropages* is younger than 115.0 Ma. The early divergence of *Scleropages* therefore occurred after the final separation between India and Antarctica–Australia. Consequently, his study rejects the Gondwanian origin hypothesis to explain the distribution of *Scleropages*.

More recently, Lavoué (2016) used newly reconstructed time-calibrated phylogenetic trees based on a large dataset combining extant and fossil taxa and molecular and

chinaXiv:201711.01925v1

ChinaXiv合作期刊

morphological characters to test whether the divergence of Osteoglossiformes was compatible with the breakup of Gondwana. He thought that the most convincing evidence that some osteoglossomorphs may have achieved their current transmarine distribution through marine dispersal is from the genus *Scleropages*. Marine dispersal in *Scleropages* was also mentioned by Cracraft (1974), Briggs (1979) and Wilson and Murray (2008). Taverne et al. (2007) argued that Recent freshwater Osteoglossiformes generally tolerate brackish waters and sometimes enter in marine waters near the estuaries. In contrast, Lavoué (2015) suggested that *Scleropages* species are highly intolerant of salt water according to the investigations of Gehrke et al. (2011) and Roberts (1978).

The distribution of osteoglossids remains a zoogeographical enigma. Marine fossils of *Scleropages* or an unknown vicariance event are wanted to explain the intercontinental distribution of the genus. In such a situation, the discovery of *Scleropages sinensis* dates the divergence of *Scleropages* and *Osteoglossum* as at least old as the Early Eocene, which is a significant step toward solving this zoogeographical puzzle.

Acknowledgements We are most grateful to Prof. Zhang Miman (IVPP) for permission to study the specimens under her care. Our best thanks are due to Mr. Xu Yong (IVPP) for drawings and to Mr. Gao Wei (IVPP) for photographs. Thanks also go to Profs. Song Changqi and Li Chun (IVPP) for collecting the specimens, to Liu Juan, Wang Min, Dong Liping, Wang Qiuyuan, Wang Zhao, Huo Yulong and Guo Yanfang (all from IVPP) for their helps in the field works, to Wang Zhao and Huo Yulong for preparing the specimens. This work was supported by the National Natural Science Foundation of China (NSFC) (Grant Nos. 91514302, 41688103, 41172019, 40772019).

chinaXiv:201711.01925v1

金龙鱼(*Scleropages*: Osteoglossomorpha)化石的首次发现

张江永[1] Mark V H WILSON[2]

(1 中国科学院古脊椎动物与古人类研究所，中国科学院脊椎动物演化与人类起源重点实验室 北京 100044)

(2 加拿大阿尔伯塔大学生物系 埃德蒙顿 T6G 2E9, 美国洛约拉大学生物系 芝加哥)

摘要：金龙鱼化石的鳞片和骨骼碎片在过去时有报道，但鉴定并非十分可靠，因为在骨舌鱼科鱼类中这些鳞片和骨骼十分相似。首次记述了保存完美的金龙鱼化石，标本产于湖南湘乡下湾铺组和湖北松滋洋溪组，确立为骨舌鱼科金龙鱼属一新种：中华金龙鱼 *Scleropages sinensis* sp. nov.。新种与现生金龙鱼(*Scleropages*)在头部骨骼、尾骨骼、各鳍的形状和位置以及具有网状鳞片等方面极为相似，因而归入该属。然而，新种在以下特征上不同于金龙鱼的现生种：鼻骨无纹饰，鼻骨上的感觉管显露于沟内，感觉管联合不经过顶骨，翼耳骨侧向加厚，眶前骨上的感觉孔大，眼眶后的眶下骨不完全覆盖前鳃盖骨上支，其宽高比例为0.75而非现生种的1–1.2, 前鳃盖骨后下角变尖，鳃盖骨后下缘凹形、下端变

ChinaXiv合作期刊

尖，匙骨背突长大，脊椎46–48, 椎体横突短小，胸鳍十分长大，上下两端的尾鳍条和内部鳍条等长。亚洲的现生种发现于各种河流和小溪中，比较喜欢水草茂盛的静水环境，一般游弋于表层水中，以鱼虾、昆虫等为食，新种中华金龙鱼也应该有相似的生长环境和食性。新种似具有性二形性，雄鱼体形略纤细，头部略大，口裂更深。中华金龙鱼化石的发现，说明金龙鱼属(*Scleropages*)和骨舌鱼属(*Osteoglossum*)在早始新世以前就已经分化，这对解释骨舌鱼类的跨洋分布具有十分重要的意义。

关键词：湖南、湖北，早始新世，下湾铺组，洋溪组，骨舌鱼类

中图法分类号：Q915.862　　**文献标识码**：A　　**文章标号**：1000–3118(2017)01–0001–23

References

Beck R A, Burbank D W, Sercombe W J et al., 1995. New stratigraphic constraints on the collision of NW India and Asia. Nature, 373: 55–58

Besse J, Courtillot V, Pozzi J P et al., 1984. Palaeomagnetic estimates of crustal shortening in the Himalayan thrusts and Zangbo suture. Nature, 311: 621–626

Briggs J C, 1979. Ostariophysan zoogeography: an alternative hypothesis. Copeia, 1979: 111–118

Chang M M, Chen Y Y, 2000. Late Mesozoic and Tertiary ichthyofaunas from China and some puzzling patterns of distribution. Vert PalAsiat, 38(3): 161–175

Chang M M, Chou C C, 1976. Discovery of *Plesiolycoptera* on Songhuajiang-Liaoning Basin and origin of Osteoglossomorpha. Vert PalAsiat, 14(3): 146–153

Chang M M, Chou C C, 1977. On late Mesozoic fossil fishes from Zhejiang Province, China. Mem Inst Vert Palaeont Palaeoanthrop Acad Sin, 12: 1–59

Chang M M, Miao D S, Chen Y Y et al., 2001. Suckers (Fish, Catostomidae) from the Eocene of China account for the family's current disjunct distributions. Sci China Ser D: Earth Sci, 44: 577–586

Chang M M, Wang N, Wu F X, 2010. Discovery of *Cyclurus* (Amiinae, Amiidae, Amiiformes, Pisces) from China. Vert PalAsiat, 48(2): 85–100

Chen Q, Gao Q, 1992. The discovery of *Asiocoryphodon conicus* in Yangxi Formation on the northwest margin of Jianghan Basin and its stratigraphic significance. Acta Petrolei Sin, 13(2): 127–129

Cheng C G, 1962. Fossil fishes from the Early Tertiary of Hsianghsiang, Hunan, with discussion of age of the Hsiawanpu Formation. Vert PalAsiat, 6(2): 333–348

Cracraft J, 1974. Continental drift and vertebrate distribution. Ann Rev Ecol Syst, 5: 215–262

Editorial Committee of Stratigraphical Lexicon of China (ECSLC), 1999. Stratigraphical Lexicon of China–The Tertiary. Beijing: Geological Publishing House. 1–166

Forey P L, Hilton E J, 2010. Two new Tertiary osteoglossid fishes (Teleostei: Osteoglossomorpha) with notes on the history of the family. In: Elliott D K, Maisey J G, Yu X et al. eds. Morphology, Phylogeny and Paleobiogeography of Fossil Fishes. Munich: Friedrich Pfeil. 215–246

Gayet M, 1987. Consideraciones preliminare sobre la paleobiogeografía de les Osteoglossomorpha. IV Congreso Latinoamericano de Paleontología, Bolivia, 1: 379–398

Gayet M, Meunier F, 1983. Ecailles actuelles et fossiles d'Osteoglossiformes (Pisces, Téléostéens). C R Acad Sci, Pairs, 297: 867–870

Gehrke P C, Sheaves M J, Boseto D et al., 2011. Vulnerability of freshwater and estuarine fisheries in the tropical Pacific to

chinaXiv:201711.01925v1

ChinaXiv合作期刊

climate change. In: Bell J D, Johnson J E, Hobday A J eds. Vulnerability of Tropical Pacific Fisheries and Aquaculture to Climate Change. Nouméa, New Caledonia: Secretariat of the Pacific Community. 577–646

Gibbons A D, Whittaker J M, Müller R D, 2013. The breakup of East Gondwana: assimilating constraints from Cretaceous ocean basins around India into a best-fit tectonic model. J Geophys Res, 118: 808–822

Greenwood P H, 1970. On the genus *Lycoptera* and its relationships with the family Hiodontidae (Pisces, Osteoglossomorpha). Bull Br Mus (Nat Hist), Zool, 19: 259–285

Günther A, 1864. On a new generic type of fishes discovered by the late Dr. Leichardt in Queensland. Ann Mag Nat Hist Ser 3, 14(81): 195–197

Hills E S, 1934. Tertiary fresh water fishes from southern Queensland. Mem Queen Mus, 10: 157–174

Hills E S, 1943. Tertiary freshwater fishes and crocodilian remains from Gladstone and Duaringa, Queensland. Mem Queen Mus, 12: 96–100

Hilton E J, 2003. Comparative osteology and phylogenetic systematics of fossil and living bony-tongue fishes (Actinopterygii, Teleostei, Osteoglossomorpha). Zool J Linn Soc, 137: 1–100

Hora S L, 1938. On some fossil fish-scales from the intertrappean beds at Deothan and Kheri, Central Provinces. Rec Geol Surv India, 73: 267–294

Hou L H, 1990. An Eocene bird from Songzi, Hubei Province. Vert PalAsiat, 28(1): 34–42

Jaeger J J, Courtillot V, Tapponnier P, 1989. Paleontological view of the ages of the Deccan Traps, the Cretaceous/Tertiary boundary, and the India/Asia collision. Geology, 17: 316–319

Jin F, Zhang J Y, Zhou Z H, 1995. Late Mesozoic fish fauna from western Liaoning, China. Vert PalAsiat, 33(3): 169–193

Jolly A, Bajpai S, 1988. Fossil Osteoglossidae from the Kalakot Zone (Middle Eocene): implications for palaeoecology, palaeobiogeography and correlation. Bull Indian Geol Assoc, 21: 71–79

Kershaw D R, 1976. A structural and functional interpretation of the cranial anatomy in relations to the feeding of osteoglossoid fishes and a consideration of their phylogeny. Trans Zool Soc London, 33: 173–252

Kottelat M, Widjanarti E, 2005. The fishes of Danau Sentarum National Park and the Kapuas Lake Area, Kalimantan Barat, Indonesia. Raffles Bull Zool Supp, 13: 139–173

Kumar K, Rana R S, Paliwal B S, 2005. Osteoglossid and lepisosteid fish remains from the Paleocene Palana Formation, Rajasthan, India. Palaeontology, 48: 1187–1209

Kumazawa Y, Nishida M, 2000. Molecular phylogeny of osteoglossoids: a new model for Gondwanian origin and plate tectonic transportation of the Asian Arowana. Mol Biol Evol, 17(12): 1869–1878

Lavoué S, 2015. Testing a time hypothesis in the biogeography of the arowana genus *Scleropages* (Osteoglossidae). J Biogeogr, 42: 2427–2439

Lavoué S, 2016. Was Gondwanan breakup the cause of the intercontinental distribution of Osteoglossiformes? A time-calibrated phylogenetic test combining molecular, morphological, and paleontological evidence. Mol Phylogenet Evol, 99: 34–43

Li G Q, 1997. Notes on the historical biogeography of Osteoglossomorpha (Teleostei). In: Jin, Dineley eds. Proceedings of the 30th International Geological Congress, 12. Zeist, Netherlands: VSP International Science Publishers. 54–66

Li G Q, Wilson M V H, 1996. Phylogeny of Osteoglossomorpha. In: Stiassny M L J, Parenti L R, Johnson G D eds. Interrelationships of Fishes. New York: Academic Press. 163–174

Li G Q, Grande L, Wilson M V H, 1997. The species of †*Phareodus* (Teleostei: Osteoglossidae) from the Eocene of North

chinaXiv:201711.01925v1

ChinaXiv合作期刊

America and their phylogenetic relationships. J Vert Paleont, 17: 487–505

Liu J, Chang M M, Wilson M V H et al., 2015. A new family of Cypriniformes (Teleostei, Ostariophysi) based on a redescription of †*Jianghanichthys hubeiensis* (Lei, 1977) from the Eocene Yangxi Formation of China. J Vert Paleont, 35: 6, e1004073, doi: 10.1080/02724634.2015.1004073

Liu T S, Liu H T, Tang X, 1962. A new percoid fish from South China. Vert PalAsiat, 6(2): 121–127

Ma F Z, Sun J R, 1988. Jura-Cretaceous ichthyofaunas from Sankeyushu section of Tonghua, Jilin. Acta Palaeont Sin, 27(6): 694–711

Martien J P, Oijen V, Sancia E T et al., 2013. The types of *Osteoglossum formosum* Müller & Schlegel, 1840 (Teleostei, Osteoglossidae). Zootaxa, 3722: 361–371

Metcalfe I, 1999. Gondwana dispersion and Asian accretion: an overview. In: Metclfe I ed. Gondwana Dispersion and Asian Accretion. Rotterdam: A. A. Balkema. 9–28

Müller J, 1846. On the structure and characters of the Ganoidei, and on the natural classification of fish. Sci Mem, 4: 499–558

Müller S, Schlegal H, 1844. Beschrijving van een' nieuwen Zoetwater-visch van Borneo, *Osteoglossum formosum*. Verhandlingen over de Natuurlijke Geschiedenis der Nederlandsche Overzeesche Bezittengen, 2: 1–7

Murray A M, Wilson M V H, 2005. Description of a new Eocene osteoglossid fish and additional information on †*Sindiga jacksonoides* Greenwood and Patterson, 1967 (Osteoglossomorpha), with an assessment of their phylogenetic relationships. Zool J Linn Soc, 144: 213–228

Nelson G J, 1969. Infraorbital bones and their bearing on the phylogeny and geography of osteoglossomorphs. Am Mus Novit, 2394: 1–37

Ni X J, Daniel L G, Marian D et al., 2013. The oldest known primate skeleton and early haplorhine evolution. Nature, 498: 6, doi: 10.1038/nature12200

Nolf D, Rana R S, Prasad G V R, 2008. Late Cretaceous (Maastrichtian) fish otoliths from the Deccan Intertrappean Beds, India: a revision. Bull Inst R Sci Nat Belg, Sci Terre, 78: 239–259

Pouyaud L, Sudarto, Teugels G G, 2003. The different colour varieties of the Asian arowana *Scleropages formosus* (Osteoglossidae) are distinct species: morphologic and genetic evidences. Cybium, 27(4): 287–305

Prasad G V R, Jaeger J J, Sahni A et al., 1994. Eutherian mammals from the Upper Cretaceous (Maastrichtian) intertrappean beds of Naskal, Andhra Pradesh, India. J Vert Paleont, 14: 260–277

Rage J C, Cappetta H, Hartenberger J L, 1995. Collision age. Nature, 375: 286

Rana R S, 1988. Freshwater fish otoliths from the Deccan Trap associated sedimentary (Cretaceous–Tertiary transition) beds of Rangapur, Hyderabad District, Andhra Pradesh, India. Geobios, 21: 465–493

Ridewood W G, 1905. On the cranial osteology of the fishes of the families Osteoglossidae, Pantodontidae, and Phractolaemidae. J Linn Soc Lond, Zool, 29: 252–282

Roberts T R, 1978. An Ichthyological Survey of the Fly River in Papua New Guinea with the Descriptions of New Species. Washington, DC: Smithsonian Institution Press. 1–72

Roberts T R, 2012. *Scleropages inscriptus*, a new fish species from the Tananthayi or Tenasserim River Basin, Malay Peninsula of Myanmar (Osteoglossidae: Osteoglossiformes). Aqua Int J Ichthyol, 18: 113–118

Sanders M, 1934. Die fossilen Fische der Alttertiären Süsswasserablagerungen aus mittel-Sumatra. Verhandelingen van het Geologisch-Mijnbouwkundig Genootschap voor Nederland en Kolonien. Geol Ser, 11: 1–144

Saville-Kent W, 1892. Description of a new species of true Barrimundi, *Osteoglossum jardinii*, from northern Queensland. Proc R Soc Queens, 8(3): 105–108

chinaXiv:201711.01925v1

ChinaXiv合作期刊

Scotese C R, 2014. Atlas of Late Cretaceous Maps, Paleomap Atlas for ArcGIS, Vol. 2, The Cretaceous. Mollweide Projection. Evanston, IL: Paleomap Project. 16–22

Scott D B C, Fuller J D, 1976. The reproductive biology of *Scleropages formosus* (Müller & Schlegel) (Osteoglossomorpha, Osteoglossidae) in Malaya, and the morphology of its pituitary gland. J Fish Biol, 8: 45–53

Smith A G, Smith D G, Funnell B M, 1994. Atlas of Mesozoic and Cenozoic Coastlines. New York: Cambridge University Press. 1–99

Suleiman M Z, 2003. Breeding technique of Malaysian golden arowana, *Scleropages formosus* in concrete tanks. Aquac Asia, 8(3): 5–6

Swisher C C I, Wang X L, Zhou Z H et al., 2002. Further support for a Cretaceous age for the feathered-dinosaur beds of Liaoning, China: new $^{40}Ar/^{39}Ar$ dating of the Yixian and Tuchengzi formations. Chinese Sci Bull, 47(2): 2009–2013

Taverne L, 1977. Ostéologie, phylogénèse et systématique des Téléostéens fossiles et actuels du super-ordre des Ostéoglossomorphes, Première partie. Ostéologie des genres *Hiodon*, *Eohiodon*, *Lycoptera*, *Osteoglossum*, *Scleropages*, *Heterotis* et *Arapaima*. Acad R Belg, Mém Clas Sci, Collect in-8º-2e sér, 42(3): 1–235

Taverne L, 1978. Ostéologie, phylogenèse et systématique des Téléostéen fossiles et actuels du super-ordre des Ostéoglossomorphes. Deuxième partie. Ostéologie des genres *Phareodus*, *Phareoides*, *Brychaetus*, *Musperia*, *Pantodon*, *Singida*, *Notopterus*, *Xenomystus* et *Papyrocranus*. Acad R Belg, Mém Clas Sci, Collect in-8º-2e sér, 42(6): 1–213

Taverne L, 2009. On the presence of the osteoglossid genus *Scleropages* in the Paleocene of Niger, Africa (Teleostei, Osteoglossomorpha). Bull Inst R Sci Nat Belg, Sci Terre, 79: 161–167

Taverne L, Nolf D, Folie A, 2007. On the presence of the osteoglossid fish genus *Scleropages* (Teleostei, Osteoglossiformes) in the continental Paleocene of Hainin (Mons Basin, Belgium). Belg J Zool, 137: 89–97

Unmack P J, 2001. Biogeography of Australian freshwater fishes. J Biogeogr, 28: 1053–1089

Wang M, Mayr G, Zhang J Y et al., 2012. Two new skeletons of the enigmatic, rail-like avian taxon *Songzia* Hou, 1990 (Songziidae) from the Early Eocene of China. Alcheringa, 36: 487–499

Wilson M V H, Murray A M, 2008. Osteoglossomorpha: phylogeny, biogeography, and fossil record and the significance of key African and Chinese fossil taxa. In: Cavin L, Longbottom A, Richter M eds. Fishes and the Break-up of Pangaea. Geol Soc London, Spec Publ, 295: 185–219

Xu G H, Chang M M, 2009. Redescription of †*Paralycoptera wui* Chang & Chou, 1977 (Teleostei: Osteoglossoidei) from the Early Cretaceous of eastern China. Zool J Linn Soc, 157: 83–106

Zhang J Y, 1998. Morphology and phylogenetic relationships of *Kuntulunia* (Teleostei: Osteoglossomorpha). J Vert Paleont, 18: 280–300

Zhang J Y, 2002. New fossil osteoglossomorphs from China and the phylogeny of osteoglossomorpha. Ph.D. Thesis. Beijing: Graduate School of the Chinese Academy of Sciences. 1–172

Zhang J Y, 2003. First *Phareodus* (Osteoglossomorpha: Osteoglossidae) from China. Vert PalAsiat, 41(4): 327–331

Zhang J Y, 2004. New fossil osteoglossomorph from Ningxia, China. J Vert Paleont, 24: 515–524

Zhang J Y, 2010. Validity of the osteoglossomorph genus †*Asiatolepis* and a revision of †*Asiatolepis muroii* (†*Lycoptera muroii*). In: Nelson J S, Schultze H P, Wilson M V H eds. Origin and Phylogenetic Interrelationships of Teleosts. München: Verlag Dr Friedrich Pfeil. 239–249

Zhang J Y, Jin F, 1999. A revision of †*Tongxinichthys* MA 1980 (Teleostei: Osteoglossomorpha) from the Lower Cretaceous of northern China. In: Arratia G, Schultze H P eds. Mesozoic Fishes 2 – Systematics and Fossil Record. München: Verlag Dr. Friedrich Pfeil. 385–396

chinaXiv:201711.01925v1

ChinaXiv合作期刊

第55卷 第1期
2017年1月

古 脊 椎 动 物 学 报
VERTEBRATA PALASIATICA

pp. 24–40
figs. 1–7

Therocephalian (Therapsida) and chroniosuchian (Reptiliomorpha) from the Permo-Triassic transitional Guodikeng Formation of the Dalongkou Section, Jimsar, Xinjiang, China

LIU Jun[1,2] Fernando ABDALA[3]

(1 *Key Laboratory of Vertebrate Evolution and Human Origins of Chinese Academy of Sciences*, *Institute of Vertebrate Paleontology and Paleoanthropology*, *Chinese Academy of Sciences* Beijing 100044, China liujun@ivpp.ac.cn)
(2 *University of Chinese Academy of Sciences* Beijing 100039)
(3 *Evolutionary Studies Institute*, *University of the Witwatersrand* Private Bag 3, WITS 2050, Johannesburg, South Africa)

Abstract The Guodikeng Formation encompasses the terrestrial Permo-Triassic transition sequence in China. This formation crops out in the Dalongkou section, Jimsar, Xinjiang where remains of the dicynodonts *Jimusaria* and *Lystrosaurus* were found. We are describing here a therocephalian and a chroniosuchian from the Dalongkou section, which are the first records of these groups for the Guodikeng Formation. Diagnostic characters of the new therocephalian, *Dalongkoua fuae* gen. and sp. nov., include maxillary ventral margin strongly concave in lateral view; incisors spatulated and rounded; incisors and canines with faint serrations; coronoid process of the dentary with a marked external adductor fossa; triangular reflected lamina of the angular with two smooth concavities. Chroniosuchians are represented by several postcranial elements and the vertebral morphology is similar to *Bystrowiana* and *Bystrowiella*. These remains are interpreted as representing a Bystrowianidae indeterminate. The new findings increase the diversity of the Guodikeng Formation that is now represented by three or four dicynodonts, one therocephalian and one chroniosuchian. All these groups survived the massive P-T extinction but disappear from the fossil record in the Middle to Upper Triassic.

Key words Dalongkou, Xinjiang; Permian; Triassic; Guodikeng Formation; chroniosuchian; therocephalian

Citation Liu J, Abdala F, 2017. Therocephalian (Therapsida) and chroniosuchian (Reptiliomorpha) from the Permo-Triassic transitional Guodikeng Formation of the Dalongkou Section, Jimsar, Xinjiang, China. Vertebrata PalAsiatica, 55(1): 24–40

chinaXiv:201711.01925v1

1 Introduction

Dalongkou section, Jimsar, in Xinjiang is a famous terrestrial section with Permo-Triassic transitional sequences. The southern limb Dalongkou anticline section (SLS) has been suggested as a candidate for the global non-marine Permian-Triassic boundary (PTB) reference section (Cheng and Lucas, 1993, Liu, 1994). This section was originally known by its fossil

国家重点基础研究发展计划项目(编号：2012CB821902)、国家自然科学基金(批准号：41572019)、现代古生物学和地层学国家重点实验室基金(编号：20161101)、中国科学院国际人才计划(编号：2016VBB054)和科技部中南联合研究计划项目(编号：CS08-L02)资助。

收稿日期：2016-06-30

ChinaXiv合作期刊

vertebrate bearings. This formation produced the dicynodonts *Jimusaria sinkianensis* and the first specimen of *Lystrosaurus* from China (Sun, 1963; Yuan and Young, 1934a, b), later the co-occurrence of these taxa on the same horizon of the Dalongkou section were noticed (Cheng, 1993). The lowest occurrence of *Lystrosaurus* at the SLS is at the base of bed 63 or 54 of the measured lithostratigraphic section (Fig. 1), ~65 m below the base of the Jiucaiyuan Formation (Cheng, 1993; Liu et al., 2002). The exact position of the holotype of *Jimusaria sinkianensis* is unknown, but Cheng (in Yang et al., 1986) suggested it could lies within the top 20 m of the Guodikeng Formation. This is perhaps the reason why Kozur and Weems (2011) located the stratigraphic position of this dicynodont 15 m below the base of the Jiucaiyuan Formation. Besides dicynodonts, the procolophonid *Santaisaurus yuani* and the archosauriform *Chasmatosaurus yuani* were discovered from horizons of the Jiucaiyuan Formation at the Dalongkou section (Koh, 1940; Li et al., 2008; Young, 1958, 1963).

The PTB in the Junggar Basin was traditionally positioned at the base of the Jiucaiyuan Formation, but a joint team of the Chinese Academy of Geological Sciences and the Xinjiang Bureau of Geology and Mineral Resources first proposed the PTB within the Guodikeng Formation (Yang et al., 1986). They tentatively located the PTB at the uppermost Guodikeng Formation; one major reason for this decision was the position of the lowest occurrence of *Lystrosaurus*. For a long time, *Lystrosaurus* was a Triassic index fossil, and its lowest occurrence marked (or at least approximate) the base of the Triassic (cf. Lucas, 1998).

Based on palynomorph evidence, Ouyang and Norris (1999) placed the PTB at the base of Unit 3 in the uppermost Guodikeng Formation, ~50 m below the base of the Jiucaiyuan Formation. Hou (2004) discovered overlapping interval of sporomorphs from the middle part of the Guodikeng Formation at SLS, and placed the PTB at the base of Bed 51 of the measured lithostratigraphic section 1 (Fig. 1). Furthermore, Pang and Jin (2004) observed a distinct turnover in the ostracod assemblages between Bed 54 and 55 in the Guodikeng Formation (Fig. 1), approximately 10 m above the PTB suggested by the palynological analysis of Hou (2004). Foster and Afonin (2005) studied the abnormal pollen grains from Russia and China, and suggested that the latest Permian mass extinction level lies at the upper lower Guodikeng Formation, between Bed 63 to 65 on s1. Using conchostracan biostratigraphy, Kozur and Weems (2011) proposed the continental extinction event horizon at the middle part of the Guodikeng Formation at SLS; and they proposed that the first appearance datum (FAD) of *Falsisca verchojanica*, ~25 m below the base of the Jiucaiyuan Formation at SLS, correlates to the PTB. Based on the paleomagnetic data, Li et al. (2003) put the PTB between their Bed 41 and 42 at the SLS. Cao et al. (2008) suggested an isotopically defined PTB at the base of Bed 65 (Fig. 1).

In summary, there are distinct faunal and floral turnovers in the middle part of the Guodikeng Formation. As suggested by Kozur and Weems (2011), their relationships with the end-Permian mass extinction need to be studied carefully, but they must not equate to the PTB.

A recent revision of *Dicynodon* restricted the name to two species from the African

chinaXiv:201711.01925v1

ChinaXiv合作期刊

Permian and *Jimusauria*, that was synonymized to *Dicynodon*, is considered as a valid taxon different of *Dicynodon* (Kammerer et al., 2011). The phylogeny presented by Kammerer et al. (2011:fig. 156) found *Jimusauria* as a basal form in a clade of Permian and Triassic dicynodonts. Metcalfe et al. (2009) points out the poor record of *Lystrosaurus* in the Guodikeng Formation in opposition to the rich representation of this taxon in the overlying Jiucaiyuan Formation. Considering the faunal composition of the Permo-Triassic transition in South Africa, they argue that the combined presence of *Lystrosaurus* and the *Jimusauria* is more likely representing levels of the Late Permian, in which the former taxon is poorly represented (Smith and Botha-Brink, 2014). As a result the PTB is interpreted on the top of the Guodikeng Formation, near the base of the Jiucaiyuan Formation. Recently, Gastaldo et al. (2015) reported a dicynodontoid skull of characteristically Permian aspect more than 10 m above the previous last occurrence of *Dicynodon* and a zircon age of (253.48 ± 0.15) Ma from a layer ~60 m below the current vertebrate-defined boundary from Karoo Basin. They suggested the PTB should be higher than that recognized by Ward et al. (2005). The work in Karoo Basin suggested an older occurrence of *Lystrosaurus*, and the PTB could be around the base of the Jiucaiyuan Formation in Junggar Basin.

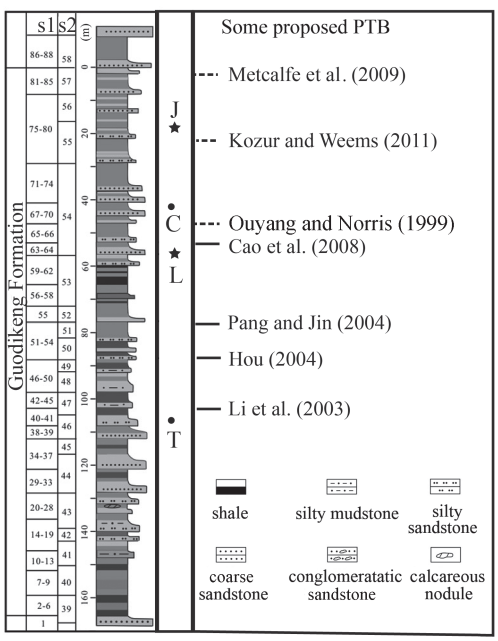

Fig. 1 Position of some vertebrate fossils and proposed PTB from the Guodikeng Formation in the SLS

The stratigraphic column adapted from Cao et al. (2008). Subunits of lithological stratigraphy listed as s1 are from team work of 2000 (published in Li et al., 2003; Hou, 2004 and Pang and Jin, 2004), s2 from Yang et al. (1986)

C. IVPP V 23295, a chroniosuchian; J. the possible position of *Jimusaria sinkiangensis*; L. the lowest occurrence of *Lystrosaurus*; T. IVPP V 23296, the therocephalian *Dalongkoua fuae*. The continuous lines mean the exact position of PTB, while the dashed lines indicate unsure on the position

In 2000, some bones were collected from the SLS while digging a trench for paleomagnetic study. One specimen (IVPP V 23296) was produced from a green mudstone close to the yellow sandstone in Bed 40. All bones of this specimen are badly weathered, before being buried. Another specimen came from the red mudstone of Bed 70, including several vertebrae and a nearly complete humerus (IVPP V 23295). These materials were prepared and identified as a therocephalian and a chroniosuchian. Therocephalian therapsids were important component of Middle Permian to Middle Triassic terrestrial faunas (Abdala et al., 2008, 2014; Huttenlocker et al., 2015; Ivakhnenko, 2011). In China, therocephalians are only known from the Triassic, including *Urumchia lii* recovered from the Jiucaiyuan Formation of Xinjiang, which was originally assigned as Late Permian (Li et al., 2008;

chinaXiv:201711.01925v1

ChinaXiv合作期刊

Young, 1952). The new discoveries represent, thus, the first report of a Permian therocephalian for China. Chroniosuchians is an enigmatic and a recent addition to the group of tetrapods. It was first reported in the Permian and Triassic of Russia (Golubev, 1998; Novikov and Shishkin, 2000; Shishkin et al., 2014), and later from the Permian of China (Li and Cheng, 1999; Young, 1979), and the Triassic of Kyrgyzstan and Germany (Schoch et al., 2010; Witzmann et al., 2008). The new material here presented is a new Permian record for China, and the first one from Xinjiang.

Abbreviation IVPP, Institute of Vertebrate Paleontology and Paleoanthropology, Chinese Academy of Sciences.

2 Systematic paleontology

Therapsida Broom, 1905

Therocephalia Broom, 1903

Eutherocephalia Hopson & Barghusen, 1986

***Dalongkoua fuae* gen. et sp. nov.**

Holotype IVPP V 23296, incomplete left premaxilla with three teeth, incomplete right premaxillae with four teeth, snout and part of the orbital region with the maxilla on both sides featuring functional and replacement canines, isolated vertebrae, left humerus, two phalanges and some bone fragments (Figs. 2–4).

Etymology 'Dalongkou', the name of locality; 'fu', dedicated to the preparator Ms. Fu Hua-Lin.

Diagnosis Maxillary ventral margin strongly concave in lateral view; incisors spatulated and rounded; incisors and canines with faint serrations; coronoid process of the dentary with a marked external adductor fossa; triangular reflected lamina of the angular with two smooth concavities.

Description Skull The skull is strongly deformed as a flat plate and broken into small blocks. The anterior portions of the premaxillae are separated from the rest of the skull (Fig. 2).

Both premaxillae are represented as independent elements, with the right being better preserved. It forms a curved plate housing the alveoli for four incisors (Fig. 2C). Posteromedially, it has the process for contacting the vomer. The posterolateral side of the palatal surface curves dorsally, forming the anterior margin of the palatal fenestra for the lower canine (Fig. 2C). There are four preserved teeth, three of them with the main axis of their bases oriented longitudinally, whereas the second is circular in section. The latter tooth, is completely preserved, presenting spatulated crown, concave lingually, and mesiolingual and distal smooth ridges (Fig. 2E). Remaining teeth are incomplete lacking any ridge at their bases, where the external surface is relatively smooth. Based on the preservation, we interpret the probable presence of at least five incisors. Two replacing teeth lie on the lingual side of the first and third functional incisors (Fig. 2C). The crown of the first replacement incisor show fainted

chinaXiv:201711.01925v1

ChinaXiv合作期刊

serrations on the medial margin. A tiny foramen lies posterior to the first replacing incisor. A long diastema separated the last incisor and the canine. The left premaxilla has three poorly preserved incisors and an extra alveolus for the fourth incisor, without tooth. There are pits with replacement teeth behind the second and third incisors.

The maxilla is a long bone with large facial plate. It extends anteriorly and covers the lateral surface of the premaxilla anterior to the canine. Ventrally, there is a concave ventral step. The maxilla is laterally expanded to encapsulate the canine, and the snout seems

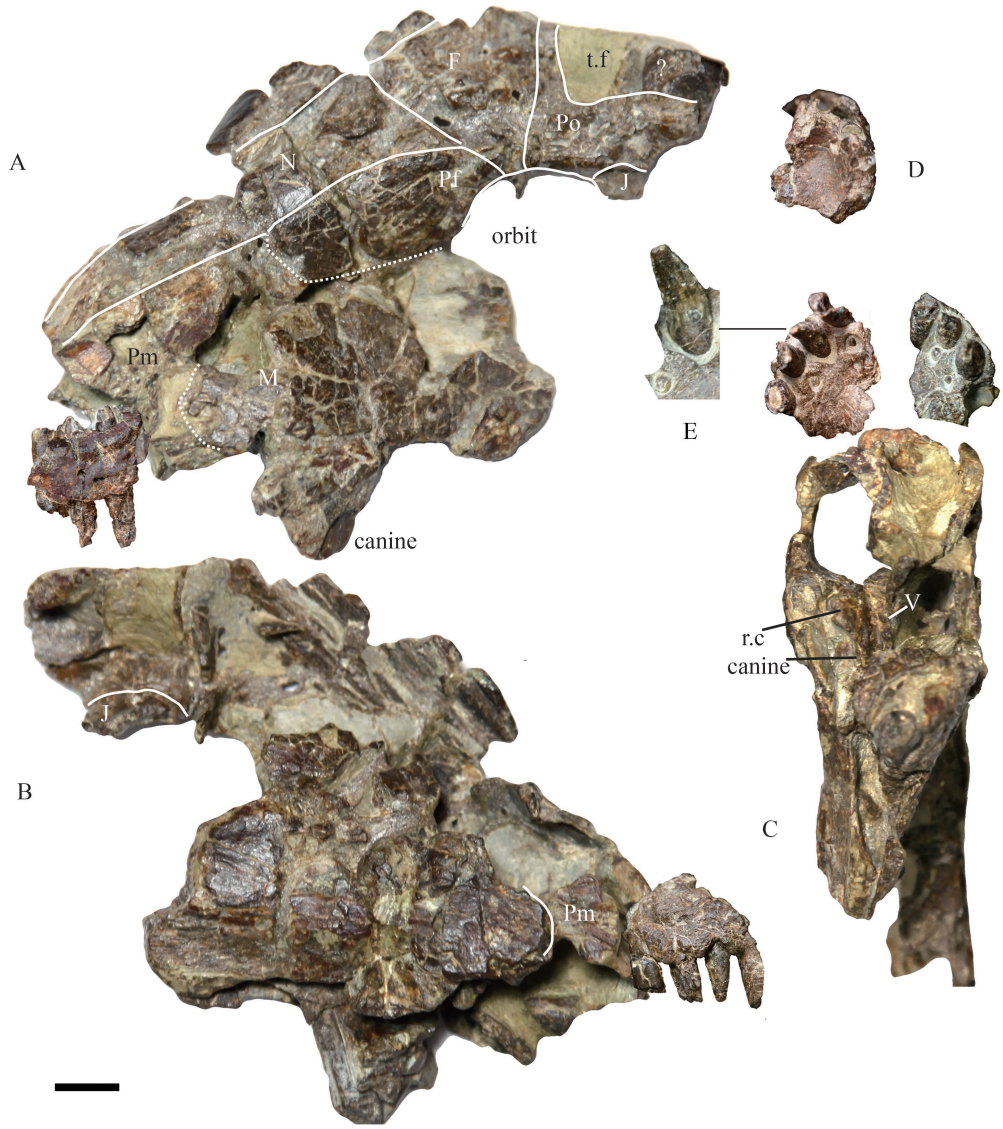

Fig. 2 Holotype of *Dalongkoua fuae* gen. et sp. nov. (IVPP V 23296)
Skull, including premaxilla in left lateral (A), right lateral (B) and ventral (C) views; right premaxilla in dorsal view (D); the second preserved right incisor in lingual view (E)
Abbreviations: F. frontal; J. jugal; M. maxilla; N. nasal; Pf. prefrontal; Pm. premaxilla; Po. postorbital; r.c. replacing canine; t.f. temporal fenestra; V. vomer. Scale bar equals 1 cm

chinaXiv:201711.01925v1

ChinaXiv合作期刊

constricted behind the canine. On the right side, the facial plate is folded medially, and a remarkable longitudinal ridge is present, suggesting a well exposed maxillary platform. The platform is posteriorly concave in lateral view as in *Theriognathus microps* (Huttenlocker and Abdala, 2016). The root of the left canine is exposed posteriorly. An erupting replacing canine lies anteromedially to the canine on both sides. The maxillary ventral margin is strongly concave in lateral view. The postcanines are not observed on the skull, but some isolated teeth could be postcanines. Two of them preserved the base of the crown, and it is possible to see strong ridges on two margins without serration. One margin is remarkable concave, the other is straight to slightly concave. One preserved tip of postcanine have faint serrations on both margins of the cusp. The putative preserved postcanines are much smaller than the incisors.

The nasal is long and forms the dorsal surface of the snout. A middle ridge is present on the posterior portion of the nasal. It is sutured with the frontal on the level of the anterior margin of the orbit (Fig. 2A). Laterally, it contacts the maxilla and the prefrontal. The prefrontal, frontal and postorbital form the dorsal margin of the orbit, whereas the postorbital bar is formed by the postorbital and jugal.

Lower jaw Dentary The symphyseal region and the posterior part of the left dentary is preserved, as well as the right reflected lamina of the angular (Fig. 3). The articular symphysis with the right dentary is broken, and the lower margin is incomplete (Fig. 3B). The symphyseal region bears a marked constriction lateral to the lower canine where the upper canine rests. The anterior part of this region bears pits and grooves, whereas the surface that will be contacting the medial side of the upper canine is smooth. The posteroventral portion of the dentary forms a thickened lower border that supports the angular in a trough on its medial surface (Fig. 3B). The posteroventral corner of the dentary forms an angle of 137°. The coronoid process is well developed, with a dorsal adductor fossa on the lateral surface (Fig. 3A). The posteroventral margin of the dentary, below the bulged ridge that limits ventrally the adductor fossa, forms a descending flange ending in a sharp ridge. Although the posterodorsal corner is incomplete, the preserved portion shows a nearly straight posterodorsal margin. Six teeth are preserved on the symphyseal region. The biggest one is the canine, and anteromedially there is a replacing canine that is partially wrapped by it (Fig. 3C). Faint serrations developed on the anterior margin of the replacing canine. There are four lower incisors, including three preserved teeth and one alveolus (Fig. 3C). A tiny tip of an erupting tooth lies immediately anterior to the canines. The last incisor is small and partially preserved; whereas two other incisors, medial to the later, are also preserved. One of them is faceted showing a well-developed ridge laterally (the medial side is not exposed). Very fine serrations, only visible under microscope magnification, are present on the margins of the larger two preserved incisors.

Angular The right angular is nearly complete. This bone is flat and elongated posteriorly with a triangular-like reflected lamina (Fig. 3D, E). The large reflected lamina bears a deep ‘U’-shaped dorsal notch which is posterodorsally directed (Fig. 3D). The lateral surface of the reflected lamina is ornamented by fine, radiating ridges and grooves, and is divided into three

chinaXiv:201711.01925v1

ChinaXiv合作期刊

parts by large grooves directed ventrally and posteriorly (Fig. 3D).

Prearticular The prearticular lies on the medial side of the angular (Fig. 3E). It is an elongate element forming an anterior rod to contact the splenial. Posteriorly, it is a triangular plate, whose posterior process contacts the articular.

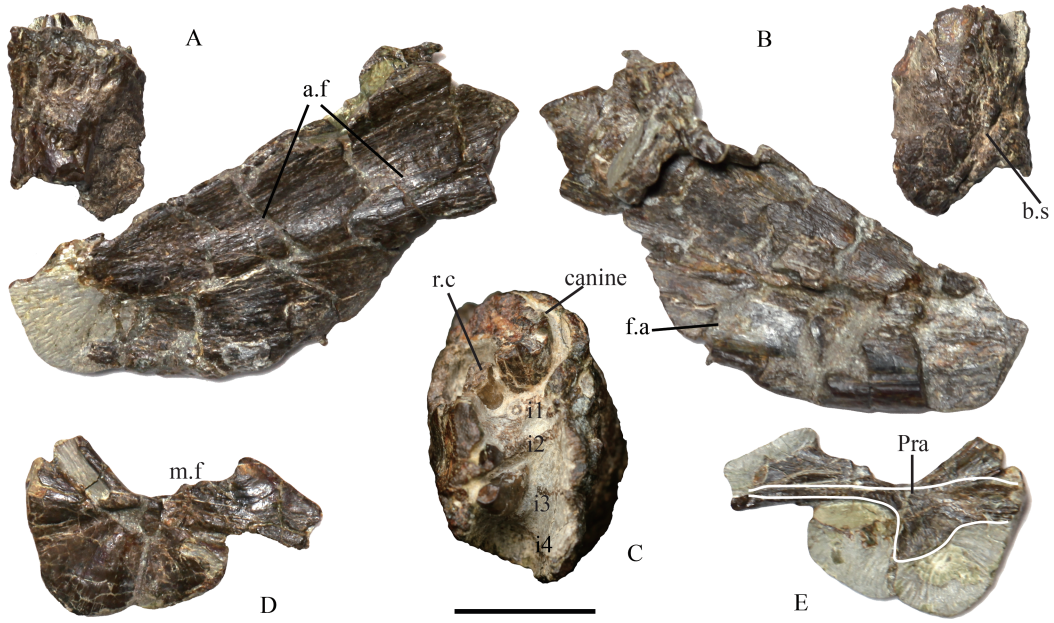

Fig. 3 Holotype of *Dalongkoua fuae* gen. et sp. nov. (IVPP V 23296)
Symphysis and posterior portion of the left dentary in lateral (A) and medial (B) views; left dentary symphysis in dorsal view (C); right angular in lateral (D) and medial (E) views
Abbreviations: a.f. adductor fossa; b.s. broken surface; f.a. facent on the dentary for the angular; i. incisor; m.f. mandibular fenestra; Pra. prearticular; r.c. replacing canine. Scale bars equal 1 cm

Vertebrae Two partial vertebrae including centra and a left partial neural arch are represented. The complete centrum in one of them, interpreted as dorsal vertebra, is amphicoelous, and deeply hollowed. The second element has an incomplete centrum and a clear suture between the centrum and the right partial neural arch shows lack of synostosis between them (Fig. 4A, B). The transverse process extends dorsolaterally and is angled posterolaterally, with a vertical flange on the ventral side. This is similar to the dorsal vertebra of *Promoschorhynchus platyrhinus* (Huttenlocker et al., 2011).

The isolated arch is possible of a cervical vertebra, with its zygapophyses bearing more or less horizontal articulating surfaces (Fig. 4C, D). The transverse process is not preserved and should lie well down on the neural arches. The neural spine is robust and inclines anteriorly. This is similar to the cervical of *Olivierosuchus parringtoni* (Botha-Brink and Modesto, 2011).

Sternum A partial posterior margin of the sternum is preserved (Fig. 4G, H). It is a large plate with convex ventral surface and concave dorsal surface. There is no posterior notch, and a weak midline ridge is developed on the ventral surface, as in *Promoschorhynchus platyrhinus* (Huttenlocker et al., 2011).

chinaXiv:201711.01925v1

ChinaXiv合作期刊

Fig. 4 Holotype of *Dalongkoua fuae* gen. et sp. nov. (IVPP V 23296)
An incomplete dorsal vertebra in lateral (A) and posterior (B) views; an incomplete cervical neural arch in left lateral (C) and medial (D) views; two phalanges in dorsal (E) and ventral (F) views, distal to the top; sternum in ventral (G) and dorsal (H) views; left humerus in dorsal (I), anterior (J), ventral (K) and posterior (L) views. Scale bars equal 1 cm

Humerus The humerus is robust with expanded proximal end, missing the distal end and the deltopectoral crest (Fig. 4I–L). The proximal half is curved dorsally relative to the shaft (Fig. 4J, L). A low ridge lies on the rough posterodorsal side, possible representing part of the wide posteroventral ridge described by Kemp (1986). The long shaft is broken on the place of the entepicondylar foramen.

Phalanges Two phalanges are well preserved (Fig. 4E, F). A longitudinal middle groove develops on the ventral surface. They are nearly as wide as length. Nearly quadrangular phalanges are represented in several therocephalians including the Scylacosauridae *Glanosuchus*, the Akidnognathidae *Olivierosuchus*, the Hofmeyriid *Mirotenthes* and the Whaitsiidae *Theriognathus* (Attridge, 1956; Boonstra, 1964; Botha-Brink and Modesto, 2011; Fourie and Rubidge, 2007; Abdala, pers. obs).

Chroniosuchia Tatarinov, 1972

Bystrowianidae Vjuschkov, 1957

Genus and species undetermined

Referred specimen IVPP V 23295, five vertebrae, rib, gastral scales, partial ilium, left femur, and partial fibula (Figs. 5, 6).

Description Vertebrae Three articulated vertebrae show two intercentra, two isolated pleurocentra are fused to the neural arches, and there are three isolated intercentra. Four larger vertebrae are tentatively identified as dorsals and the smallest as caudal.

The morphology of the vertebrae is very similar to that of *Bystrowiana sinica* or *Bystrowiella schumanni* (Liu et al., 2014; Witzmann et al., 2008) (Fig. 5).

The length of the large pleurocentrum is approximately 14 mm, whereas the length in the other two is 12 and 10 mm. The pleurocentrum are roughly twice as long anteroposteriorly as the intercentra. The height of the pleurocentra is about 10 mm. All pleurocentra are deeply amphicoelous with a round cross-section, and they are not perforated by the notochord. In

chinaXiv:201711.01925v1

ChinaXiv合作期刊

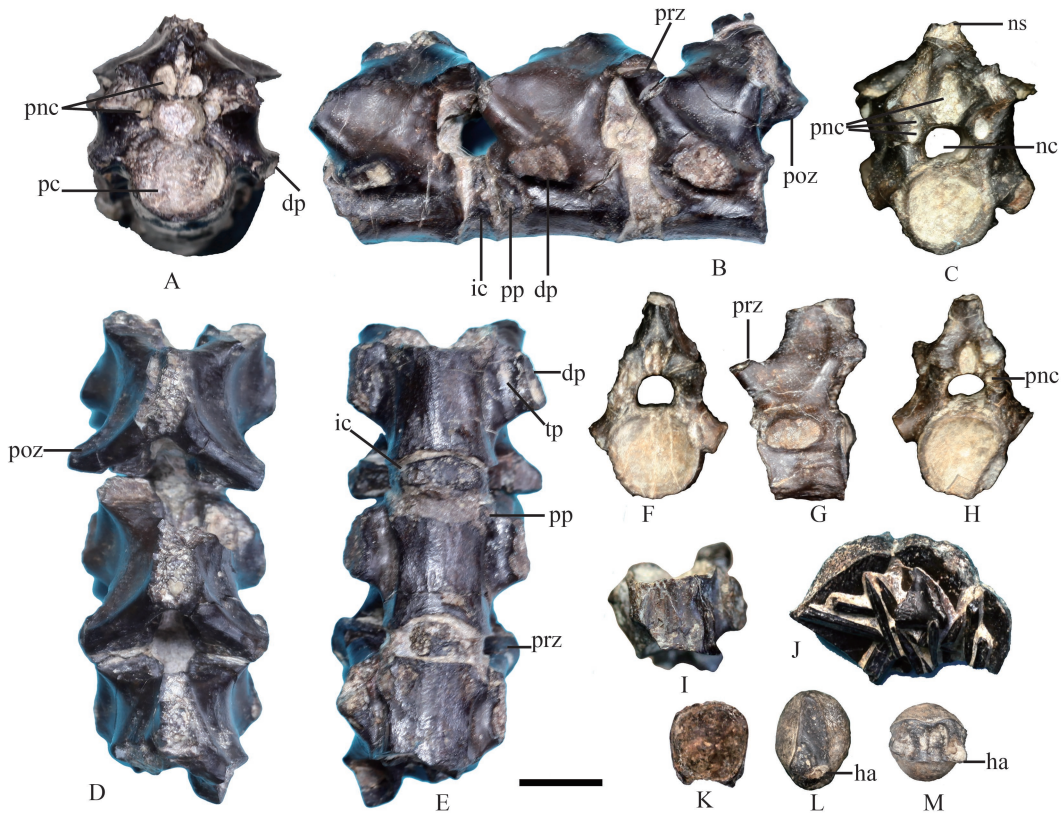

Fig. 5 Chroniosuchian specimen (IVPP V 23295) from Dalongkou section
Three dorsal vertebrae in anterior (A), left lateral (B), posterior (C), dorsal (D) and ventral (E) views; one caudal vertebra in anterior (F), left lateral (G), posterior (H), and ventral (I) views; J. gastral scales; caudal intercentrum in anterior (K), left lateral (L), and ventral (M) views
Abbreviations: dp. diapophysis; ha. haemal atch; ic. intercentrum; nc. neural canal; ns. neural spine; pc. pleurocentrum; pnc. paraneural canal; poz. postzygapophysis; pp. parapophysis; prz. prezygapophysis; tp. transverse process. Scale bar equals 1 cm

lateral view, the anterior and posterior margins of the pleurocentrum are curved but the ventral margin is nearly straight. A small knob (parapophysis) for the capitulum lies on the middle of the pleurocentrum anterior margin (Fig. 5B, E), and a longitudinal faint ridge runs posterior to it. The parapophysis is separated from the diapophysis by an anterodorsally directed incisure. On the larger pleurocentrum, the ventral surface is slightly convex to smooth (Fig. 5E). On the smallest pleurocentrum, two anteroposteriorly directed, low ridges delimit the faintly concave ventral margin (Fig. 5I) as in *Bystrowiella schumanni* (Witzmann et al., 2008).

The intercentra are about as tall as the pleurocentra in lateral view. The articular intercentra show smooth periosteal bone, without haemal arch on the ventral surface. They appear wedge-like in articulation (Fig. 5B, E), but actually are ball-like (Fig. 5K–M). On three free caudal intercentra, the ventral surface consists of slightly concave, smooth periosteal bone, and bears the ventrolateral bases of the hemapophyses as in *Bystrowiella schumanni* (Witzmann et al., 2008). The roughened dorsal surface of the intercentrum is convex and did not articulate

chinaXiv:201711.01925v1

ChinaXiv合作期刊

with the neural arch, forming part of the base of the neural canal. The largest intercentrum measures 9.7 mm long, while the others range from 8 to 9 mm. The exposed length of them in ventral view is nearly 5 mm.

All neural arches are fused to the pleurocentrum and the spines only preserved at their base. The zygapophyses are widely spaced (Fig. 5D, E) and the facets slope medially at a small angle to the horizontal plane in anterior view. There are two pairs of well-developed paraneural canals at the base of the zygapophyses, with the anterior openings of the dorsal pair being larger than those of the lateral pair (Fig. 5A). As in *Bystrowiana permira*, the number and shape of the openings on the two sides could be different (Liu et al., 2014). The neural canal is compressed dorsoventrally. The short transverse process lies on the upper half of the pleurocentrum, bearing small, unfinished diapophyses (Fig. 5A–C).

Rib and gastral scales A proximal rib fragment, and some gastral scales are preserved on a bone plate (Fig. 5J). The gastral scales are thin, some ending in a sharp point.

Ilium The preserved acetabular area of the right ilium is similar to that of *Dendrysecos helogenes* or *Chroniosaurus* (Clack and Klembara, 2009; Holmes et al., 1998; Schoch and Milner, 2014). The anterior margin is slightly concave (Fig. 6A). There is a distinct crescent supra-acetabular buttress, and, anteroventrally, a notch on the anterior margin of acetabulum. The iliac blade is only preserved as a narrow base above the acetabular rim. On the medial side, a strong iliac ridge runs dorsoventrally and divides the medial surface in two portions (Fig. 6B).

Femur The slender left femur is well-ossified and nearly complete (Fig. 6C–H). The general shape of the bone is same as that of *Chroniosaurus* (Clack and Klembara, 2009). The length of the bone is 73 mm, and the width is 21 mm for proximal and distal ends. The distal side deflects ventrally relative to the proximal part, so the bone is curved dorsally. The anterior margin is curved while the posterior margin is relatively straight. Differing from *Chroniosaurus dongusensis*, the articular surface on the proximal side is smoothly convex and dorsoventrally flattened (Fig. 6C). The dorsoventral height of the articular surface is near half its anteroposterior length (Fig. 6G). The proximal extensor surface of the femur bears some striations on the posterior side (Fig. 6C), indicating the insertion for the ischiotrochantericus.

On the anteroflexor side, the ventrally directed adductor blade demarcates the anterior side of the deep intertrochanteric fossa (Fig. 6D, E). The broken internal trochanter is separated from the femoral head by a narrow ridge, and it continues distally as a low crest, the fourth trochanter (Fig. 6D). The anterior surface of the adductor blade is rugose with deep muscle scars.

From the distal end of the fourth trochanter, the adductor crest follows a strongly diagonal course posteroventrally to a point distal to the middle of the shaft (Fig. 6E, F). A low ridge continues distally on the posterior side of the shaft ending on the distal posterior corner. This ridge does not seem to be for muscle attachment. In other groups such as captorhinomorphs, seymouriamorphs and temnospondyls, the adductor crest generally runs towards the popliteal area (Fox and Bowman, 1966; Klembara and Bartik, 2000; Pawley, 2007).

The popliteal area is pitted and concave on the flexor side (Fig. 6E). The fibular (posterior)

chinaXiv:201711.01925v1

ChinaXiv合作期刊

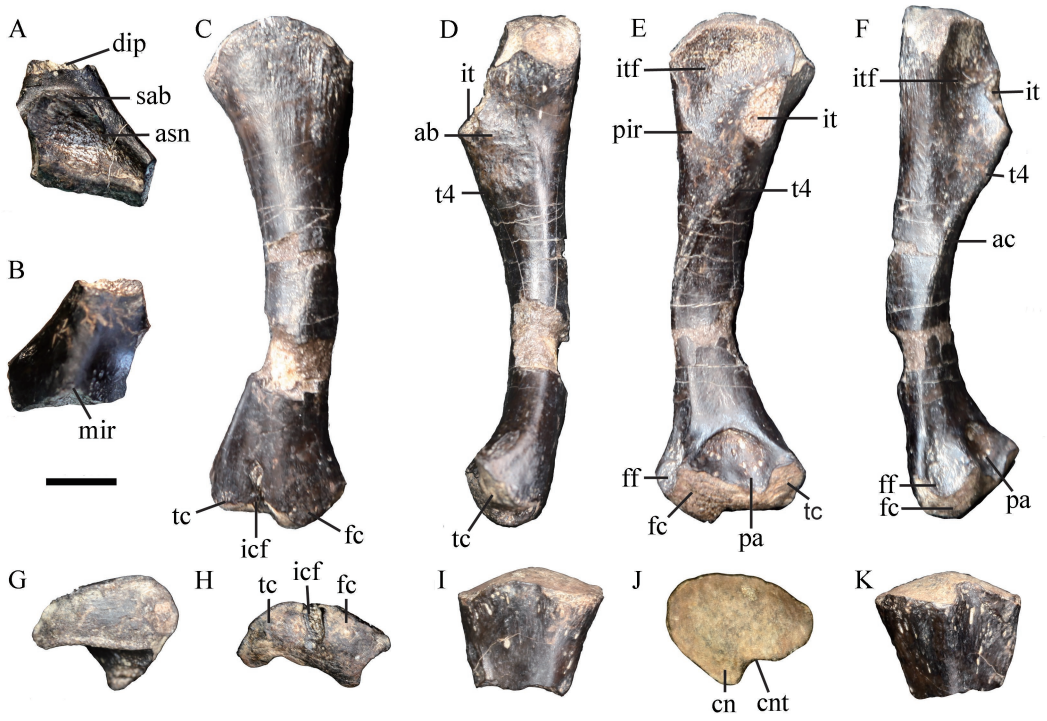

Fig. 6 Chroniosuchian specimen (IVPP V 23295) from Dalongkou section
Right ilium in lateral (A) and medial (B) views; left femur in extensor (C), anterior (D), flexor (E), posterior (F), proximal (G), and distal (H) views; left fibula in flexor (I); proximal (J) and extensor (K) views
Abbreviations: ab. adductor blade; ac. adductor crest; asn. anterior supracetabular notch; cn. cnemial crest; cnt. cnemial trough; dip. dorsal iliac process; fc. fibular condyle; ff. fibula fossa; icf. intercondylar fossa; it. internal trochanter; itf. intertrochanteric fossa; mir. mesial iliac ridge; pa. popliteal area; pir. posterior intertrochanteric ridge; sab. supracetabular buttress; tc. tibial condyle; t4. fourth trochanter. Scale bar equals 1 cm

condyle projects more distally than the tibial (anterior) condyle. Proximal to the fibular condyle is a narrow but deep fibular fossa. In extensor view, a deeply incised intercondylar fossa is oriented posteroventrally towards the midline of the fibular condyle (Fig. 6H).

Fibula The proximal end of the left fibula is preserved (Fig. 6I–K). The head is convex to fit on the concave articular surface of the femur. Small striae distribute around the proximal articular surface (Fig. 6I, K), indicating the presence of cartilage or perhaps ligamentous connective tissue. The extensor surface is incised by a cnemial trough, which is bordered anteriorly by the prominent cnemial crest (Fig. 6J). Another crest is on the posterior surface of the bone. A striate area on the medial side of this ridge, distal to the proximal articular surface, provided attachment for muscles.

3 Discussion

The new therapsid specimen (IVPP V 23296) can be diagnosed as a therocephalian for the presence of palatal fenestra for the lower caniniform confluent with choana, and the

chinaXiv:201711.01925v1

ChinaXiv合作期刊

posterventral portion of the dentary forming a thickened lower border that extends below the angular bone and supports the latter in a trough on its medial surface. It has four lower incisors, and can be then diagnosed as an eutherocephalian (Huttenlocker, 2009). In addition, the shape of the reflected lamina, lacking an anterodorsal rounded portion in front of the notch that makes this structure circular in basal therocephalians is also an indication that the new species is member of Eutherocephalia.

Dalongkoua fuae show evidence of faint serrations in the margin of a replacement incisor and canine and on the tip of a postcanine. These findings are contrary to the assumed absence of serrations in the dentition of eutherocephalia (e.g. van den Heever, 1994; Abdala et al., 2008; Huttenlocker, 2009; and Huttenlocker et al., 2015, for incisors and Huttenlocker and Sidor, 2012 for anterior dentition). The serrations in the teeth of *Dalongkoua fuae* are exceedingly faint and it is clear that they will disappear with a minimum wear as demonstrated by the smoothly ridged crown of the preserved elements.

This specimen represents a new species on the basis of the following characters: maxillary ventral margin is strongly concave in lateral view; incisors spatulated and rounded; incisors and canines with faint serrations; coronoid process of the dentary with a marked adductor fossa; triangular reflected lamina with two concavities.

The maxillary ventral margin is convex or nearly straight in most therocephalians, but it is slightly concave in *Moschowhaitsia* (Ivakhnenko, 2011), and strongly concave in *Euchambersia* and *Theriognathus* (Broom, 1931; Huttenlocker and Abdala, 2016). Recent studies (e.g., Huttenlocker et al., 2015) indicate that spatulated incisors are restricted to a group of akidnognathids. In *Dalongkoua fuae* the completely preserved second left incisor is spatulated, whereas remaining left incisors, although incomplete, show the crown enough preserved to suggest the presence of rounded (non-spatulated) incisors. The adductor fossa is developed in the dorsolateral portion of the coronoid process, above of the through for the postdentary bones. This fossa is different to the one described on the lateral surface of the dentary in the bauriids *Microgomphodon oligocynus* (Abdala et al., 2014) and in the Russian *Notogomphodon danilovi* (Abdala, pers. obs.), as in these taxa there is no connection between the fossa and the through for the postdentary bones. The incomplete left dentary of *Urumchia lii* also seems to have an adductor fossa, although less developed than in *D. fuae* (Fig. 7). A triangular reflected lamina is also present in the holotype of *Tetracynodon darti*, but the lamina show a more complex lateral surface with several ridges and valley. In the lamina of *D. fuae* there is a posterior deep canal and a dorso-ventrally oriented shallow and wide depression.

Urumchia lii is the only known therocephalian from the Xinjiang, documented in the Jiucaiyuan Formation (Sun, 1991; Young, 1952). Diagnostic characters in this species are concentrated in the palate and in the postcanine morphology (Li et al., 2008; Sun, 1991). Unfortunately both palate and postcanines are incompletely preserved in *Dalongkoua fuae*, the postcanines only represented by isolated fragments including two crown bases and one tip. There are however a set of characters shared between these two species indicating perhaps

chinaXiv:201711.01925v1

ChinaXiv合作期刊

relationships (Fig. 7): medial margin of the frontal bones directed dorsally in *Dalongkoua fuae* indicating the presence of a central ridge in the posterior internasal and interfrontal sutures, the presence of a depressed facial area of the maxilla immediately above of the dental series, also described recently in *Ichibengops* of East Africa by Huttenlocker et al (2015), an apparent development of an adductor fossa, although clearly smaller, in the left dentary of *Urumchia lii*; and the presence of spatulated incisors. The putative relationship between these two taxa should be considered as a working hypothesis, whose validation will require finding of additional material.

Fig. 7 *Urumchia lii* (IVPP V 702)
Skull in dorsal (A) and right lateral (B) views; lower jaws in left lateral view (C). Showing the sharing characters with *Dalongkoua fuae*: 1. the mid-ridge between the posterior portions of the nasals and the anterior portions of the frontals; 2. depressed facial area of the maxilla; 3. adductor fossa on the dentary
Scale bars equal 1 cm

The new specimen of Reptiliomorpha (IVPP V 23295) is referred to chroniosuchian for the characteristic ball-and-socket joint between pleurocentra and intercentra (Ivakhnenko and Tverdokhlebova, 1980). It can be further assigned to Bystrowianidae for paired paraneural canals on the vertebrae (Novikov et al., 2000). The vertebrae show the similar morphology as other bystrowianids, and intercentra is similar to the figured for *Bystrowiella schumanni* (Novikov and Shishkin, 2000; Witzmann et al., 2008). The morphology of ilium, femur, and fibula is consistent with this taxonomic identity (Clack and Klembara, 2009; Ivachnenko and Tverdochlebova, 1980). Unfortunately, no dermal scute was discovered, and no further identification could be made.

Chroniosuchian specimens in China were first reported from the Upper Permian Jiyuan fauna (Young, 1979), and then from the Middle Permian Dashankou fauna (Li and Cheng, 1999). The new findings here reported represent the latest occurrence of chroniosuchians in

chinaXiv:201711.01925v1

ChinaXiv合作期刊

China. This group however is known from the Middle/Upper Triassic Madygen Formation of Kyrgyzstan (Schoch et al., 2010), indicating their continued presence in Laurasia after the Permian exctinction.

These new findings allow recognizing that the diversity of tetrapod near the Permo-Triassic boundary in China, and particularly in Xinjiang, was higher than previously recognized. Only dicynodonts were previously reported from the Guodikeng Formation, including *Lystrosaurus*, *Jimsaria*, *Turfanodon*, and possibly *Diictodon* (Li et al., 2008). Both chroniosuchians and therocephalians crossed the P-T boundary; therocephalians become extinct in the Middle Triassic (Abdala et al., 2014), whereas the youngest record of chroniosuchians is in the Middle or Late Triassic (Schoch et al., 2010).

Acknowledgements The authors thank the field crew to Dalongkou in 2000 (Cheng Zheng-Wu, Pang Qi-Qing, Li Yong-An, Sun Dong-Jiang and Jin Xiao-Chi), FU Hua-Lin prepared the specimens, Jozef Klembara kindly provided some photos of *Chroniosaurus*. Adam Huttenlocker and Florian Witzmann provided valuable comments. JL is supported by National Basic Research Foundation (973 grant no. 2012CB821902), NSFC grants (41572019), and State Key Laboratory of Palaeobiology & Stratigraphy (Nanjing Institute of Geology & Palaeontology, CAS) grants (No. 20161101). FA research is supported by the National Research Foundation of South Africa and a research trip to China funded by the Chinese Academy of Sciences President's International Fellowship Initiative Grant (2016VBB054).

chinaXiv:201711.01925v1

新疆吉木萨尔大龙口剖面锅底坑组新发现的兽头类和迟滞鳄类

刘 俊[1,2] Fernando ABDALA[3]

(1 中国科学院古脊椎动物与古人类研究所，中国科学院脊椎动物演化与人类起源重点实验室 北京 100044)

(2 中国科学院大学 北京 100039)

(3 南非金山大学进化研究所 约翰内斯堡 WITS2050)

摘要：锅底坑组是重要的二叠—三叠系过渡序列，本组在新疆吉木萨尔大龙口出露广泛，产出吉木萨尔兽以及水龙兽两类二齿兽类。本文报道了在大龙口剖面首次发现的兽头类和迟滞鳄类，这也是此二类群在锅底坑组的首次报道。新发现的兽头类被命名为付氏大龙口兽(*Dalongkoua fuae*)。其鉴定特征包括上颌骨犬后齿齿槽外边缘向背向凹入；切齿有圆形和匙形；切齿和犬齿有微弱的锯齿；齿骨冠状突有显著的收肌窝；反折翼近三角形，有两个平滑的凹陷。锅底坑组目前有3～4属二齿兽类、1属兽头类和1属迟滞鳄类，这一发现增加了其多样性。这些类群都在二叠纪末的大灭绝中幸存下来，直到中晚三叠世才消失。

关键词：新疆大龙口，二叠纪，三叠纪，锅底坑组，兽头类，迟滞鳄类

中图法分类号：Q915.864 **文献标识码**：A **文章编号**：1000−3118(2017)01−0024−17

ChinaXiv合作期刊

References

Abdala F, Rubidge B S, Van Den Heever J A, 2008. The oldest therocephalians (Therapsida, Eutheriodontia) and the early diversification of Therapsida. Palaeontology, 51(4): 1011–1024

Abdala F, Kammerer C F, Day M O et al., 2014. Adult morphology of the therocephalian *Simorhinella baini* from the Middle Permian of South Africa and the taxonomy, paleobiogeography, and temporal distribution of the Lycosuchidae. J Paleont, 88(6): 1139–1153

Attridge J, 1956. IV.—The morphology and relationships of a complete therocephalian skeleton from the *Cistecephalus* Zone of South Africa. Proc R Soc Edinburgh B, 66(1): 59–93

Boonstra L D, 1964. The girdles and limbs of the pristerognathid Therocephalia. Ann S Afr Mus, 48: 121–165

Botha-Brink J, Modesto S P, 2011. A new skeleton of the therocephalian synapsid *Olivierosuchus parringtoni* from the Lower Triassic South African Karoo Basin. Palaeontology, 54(3): 591–606

Broom R, 1931. Notices of some new genera and species of Karroo fossil reptiles. Rec Albany Mus, 4: 161–166

Cao C Q, Wang W, Liu L J et al., 2008. Two episodes of ^{13}C-depletion in organic carbon in the latest Permian: evidence from the terrestrial sequences in northern Xinjiang, China. Earth Planet Sci Lett, 270: 251–257

Cheng Z W, 1993. On the discovery and significance of the nonmarien Permo-Triassic transition zone at Dalongkou in Jimsar, Xinjiang, China. New Mexico Mus Nat Hist Sci Bull, 3: 65–67

Cheng Z W, Lucas S G, 1993. A possible nonmarine GSSP for the Permian-Triassic boundary. Albertiana, 12: 39–44

Clack J A, Klembara J, 2009. An articulated specimen of *Chroniosaurus dongusensis* and the morphology and relationships of the chroniosuchids. Spec Pap Palaeontol, 81: 15–42

Foster C B, Afonin S A, 2005. Abnormal pollen grains: an outcome of deteriorating atmospheric conditions around the Permian-Triassic boundary. J Geol Soc, 162(4): 653–659

Fourie H, Rubidge B S, 2007. The postcranial skeletal anatomy of the therocephalian *Regisaurus* (Therapsida: Regisauridae) and its utilization for biostratigraphic correlation. Palaeontol Afr, 42: 1–16

Fox R C, Bowman M, 1966. Osteology and relationships of *Captorhinus aguti* (Cope) (Reptilia: Captorhinomorpha). Univ Kansas Paleontol Contrib Vertebr, 11: 1–79

Gastaldo R A, Kamo S L, Neveling J et al., 2015. Is the vertebrate-defined Permian-Triassic boundary in the Karoo Basin, South Africa, the terrestrial expression of the end-Permian marine event? Geology, 43(10): 939–942

Golubev V K, 1998. Narrow-armored chroniosuchians (Amphibia, Anthracosauromorpha) from the Late Permian of Eastern Europe. Paleontol J, 32(3): 278–287

Holmes R B, Carroll R L, Reisz R R, 1998. The first articulated skeleton of *Dendrerpeton acadianum* (Temnospondyli, Dendrerpetontidae) from the Lower Pennsylvanian locality of Joggins, Nova Scotia, and a review of its relationships. J Vert Paleont, 18(1): 64–79

Hou J P, 2004. Two sporo-pollen assemblages of Guodikeng formation and discussion on the Permo-Triassic boundary in Junggar Basin, Xinjiang. Prof Pap Stratigr Palaeont, 28: 177–204

Huttenlocker A, 2009. An investigation into the cladistic relationships and monophyly of therocephalian therapsids (Amniota: Synapsida). Zool J Linn Soc, 157(4): 865–891

Huttenlocker A K, Abdala F, 2016. Revision of the first therocephalian, *Theriognathus* Owen (Therapsida: Whaitsiidae), and implications for cranial ontogeny and allometry in nonmammaliaform eutheriodonts. J Paleont, 89(04): 645–664

chinaXiv:201711.01925v1

ChinaXiv合作期刊

Huttenlocker A K, Sidor C A, 2012. Taxonomic revision of Therocephalians (Therapsida: Theriodontia) from the Lower Triassic of Antarctica. Am Mus Novit, 3738: 1–19

Huttenlocker A K, Sidor C A, Smith R M H, 2011. A new specimen of *Promoschorhynchus* (Therapsida: Therocephalia: Akidnognathidae) from the Lower Triassic of South Africa and its implications for theriodont survivorship across the Permo-Triassic boundary. J Vert Paleont, 31(2): 405–421

Huttenlocker A K, Sidor C A, Angielczyk K D, 2015. A new eutherocephalian (Therapsida, Therocephalia) from the Upper Permian Madumabisa Mudstone Formation (Luangwa Basin) of Zambia. J Vert Paleont, 35(5): e969400

Ivakhnenko M F, 2011. Permian and Triassic therocephals (Eutherapsida) of Eastern Europe. Paleontol J, 45(9): 981–1144

Ivakhnenko M F, Tverdochlebova G I, 1980. Systematics, Morphology, and Stratigraphic Significance of the Upper Permian Chroniosuchians from the East of the European Part of the USSR. Saratov: Izdatel'stvo Saratovskogo Universiteta. 1–69

Kammerer C F, Angielczyk K D, Fröbisch J, 2011. A comprehensive taxonomic revision of *Dicynodon* (Therapsida, Anomodontia) and its implications for dicynodont phylogeny, biogeography, and biostratigraphy. J Vert Paleont, 31(sup1): 1–158

Kemp T S, 1986. The skeleton of a baurioid therocephalian therapsid from the Lower Triassic (*Lystrosaurus* Zone) of South Africa. J Vert Paleont, 6(3): 215–232

Klembara J, Bartik I, 2000. The postcranial skeleton of *Discosauriscus* Kuhn, a seymouriamorph tetrapod from the Lower Permian of the Boskovice Furrow (Czech Republic). Trans R Soc Edinb- Earth Sci, 90(4): 287–316

Koh T P, 1940. *Santaisaurus yuani* gen. et sp. nov., ein neues Reptil aus der unteren Trias von China. Bull Geol Surv China, 20: 73–92

Kozur H W, Weems R E, 2011. Detailed correlation and age of continental late Changhsingian and earliest Triassic beds: implications for the role of the Siberian Trap in the Permian-Triassic biotic crisis. Palaeogeogr, Palaeoclimatol, Palaeoecol, 308(1-2): 22–40

Li J L, Cheng Z W, 1999. New anthracosaur and temnospondyl amphibians from Gansu, China - the fifth report on Late Permian Dashankou lower tetrapod fauna. Vert PalAsiat, 37(3): 234–247

Li J L, Wu X, Zhang F C, 2008. The Chinese Fossil Reptiles and Their Kin. 2nd ed. Beijing: Science Press. 1–473

Li Y A, Jin X C, Sun D J et al., 2003. Paleomagnetic properties of non-marine Permo-Triassic transitional succession of the Dalongkou Section, Jimsar, Xinjiang. Geol Rev, 49(5): 525–536

Liu J, Li J L, Chen Z W, 2002. The *Lystrosaurus* fossils from Xinjiang and their bearing on the terrestrial Permian-Triassic boundary. Vert PalAsiat, 40(4): 267–275

Liu J, Xu L, Jia S H et al., 2014. The Jiyuan tetrapod fauna of the Upper Permian of China–2. stratigraphy, taxonomical review, and correlation with other assemblages. Vert PalAsiat, 52(3): 328–339

Liu S, 1994. The non-marine Permian-Triassic boundary and Triassic conchostracan fossils in China. Albertiana, 13: 12–24

Lucas S G, 1998. Global Triassic tetrapod biostratigraphy and biochronology. Palaeogeogr, Palaeoclimatol, Palaeoecol, 143(4): 347–384

Metcalfe I, Foster C B, Afonin S A et al., 2009. Stratigraphy, biostratigraphy and C-isotopes of the Permian-Triassic nonmarine sequence at Dalongkou and Lucaogou, Xinjiang Province, China. J Asian Earth Sci, 36: 503–520

chinaXiv:201711.01925v1

ChinaXiv合作期刊

Novikov I V, Shishkin M A, 2000. Triassic chroniosuchians (Amphibia, Anthracosauromorpha) and the evolution of trunk dermal scutes in bystrowianids. Paleontol J, 34(S2): 165–178

Novikov I V, Shishkin M A, Golubev V K, 2000. Permian and Triassic anthracosaur from Eastern Europe. In: Benton M J, Shishkin M A, Unwin D M et al. eds. The Age of Dinosaus in Russia and Mongolia. Cambridge: Cambridge University Press. 60–70

Ouyang S, Norris G, 1999. Earliest Triassic (Induan) spores and pollen from the Junggar Basin, Xinjiang, northwestern China. Rev Palaeobot Palyno, 106(1–2): 1–56

Pang Q, Jin X C, 2004. Ostracoda of the Guodikeng Formation and the continental Permo-Triassic boundary of Dalongkou section, Jimsar, Xinjiang. Prof Pap Stratigr Palaeont, 28: 205–246

Pawley K A T, 2007. The postcranial skeleton of *Trimerorhachis insignis* (Temnospondyli: Trimerorhachidae): a plesiomorphic temnospondyl from the Lower Permian of North America. J Paleont, 81(5): 873–894

Schoch R R, Milner A R, 2014. Temnospondyli I. München: Verlag Dr. Friedrich Pfeil. 1–150

Schoch R R, Voigt S, Buchwitz M, 2010. A chroniosuchid from the Triassic of Kyrgyzstan and analysis of chroniosuchian relationships. Zool J Linn Soc, 160(3): 515–530

Shishkin M A, Novikov I V, Fortuny J, 2014. New bystrowianid chroniosuchians (Amphibia, Anthracosauromorpha) from the Triassic of Russia and diversification of Bystrowianidae. Paleontol J, 48(5): 512–522

Smith R M H, Botha-Brink J, 2014. Anatomy of a mass extinction: Sedimentological and taphonomic evidence for drought-induced die-offs at the Permo-Triassic boundary in the main Karoo Basin, South Africa. Palaeogeogr, Palaeoclimatol, Palaeoecol, 396: 99–118

Sun A L, 1963. The Chinese kannemeyerids. Palaeont Sin, New Ser C, 17: 1–109

Sun A L, 1991. A review of Chinese therocephalian reptiles. Vert PalAsiat, 29(2): 85–94

van den Heever J A, 1994. The cranial anatomy of the early Therocephalia (Amniota: Therapsida). Ann Univ Stellenbosch, 1994(1): 1–59

Vjuschkov B P, 1957. New kotlassiomorphs from the Tatarian of the European part of the USSR. Tr Paleontol Inst, 68: 89–107

Ward P D, Botha J, Buick R et al., 2005. Abrupt and gradual extinction among Late Permian land vertebrates in the Karoo Basin, South Africa. Science, 307: 709–714

Witzmann F, Schoch R R, Maisch M W, 2008. A relict basal tetrapod from Germany: first evidence of a Triassic chroniosuchian outside Russia. Naturwissenschaften, 95: 67–72

Yang J D, Qu L F, Zhou H Q et al., 1986. Permian and Triassic strata and fossil assemblages in the Dalongkou area of Jimsar, Xinjiang. Beijing: Geological Publishing House. 1–262

Young C C, 1952. On a new therocephalian from Sinkiang, China. Acta Sci Sin, 2: 152–165

Young C C, 1958. On the occurrence of *Chasmatosaurus* from Wuhsiang, Shansi. Vert PalAsiat, 2(4): 259–262

Young C C, 1963. Additional remains of *Chasmatosaurus yuani* Young from Sinkiang, China. Vert PalAsiat, 7(3): 215–222

Young C C, 1979. A Late Permian fauna from Jiyuan, Henan. Vert PalAsiat, 17(2): 99–113

Yuan P L, Young C C, 1934a. On the discovery of a new dicynodon in Sinkiang. Bull Geol Surv China, 1934: 563–573

Yuan P L, Young C C, 1934b. On the Occurrence of *Lystrosaurus* in Sinkiang. Bull Geol Surv China, 1934: 575–580

chinaXiv:201711.01925v1

ChinaXiv合作期刊

第55卷 第1期
2017年1月

古 脊 椎 动 物 学 报
VERTEBRATA PALASIATICA

pp. 41–58
figs. 1–8

The morphology of *Chiappeavis magnapremaxillo* (Pengornithidae: Enantiornithes) and a comparison of aerodynamic function in Early Cretaceous avian tail fans

Jingmai K. O'CONNOR[1] ZHENG Xiao-Ting[2,3] HU Han[1]
WANG Xiao-Li[2] ZHOU Zhong-He[1]

(1 *Key Laboratory of Vertebrate Evolution and Human Origins of Chinese Academy of Sciences*, *Institute of Vertebrate Paleontology and Paleoanthropology*, *Chinese Academy of Sciences* Beijing 100044 jingmai@ivpp.ac.cn)
(2 *Institute of Geology and Paleontology*, *Linyi University* Linyi, Shandong 276000)
(3 *Shandong Tianyu Museum of Nature* Pingyi, Shandong 273300)

Abstract We provide a complete description of the skeletal anatomy of the holotype of *Chiappeavis magnapremaxillo*, the first enantiornithine to preserve a rectricial fan, suggesting that possibly rectricial bulbs were present in basal members of this clade. Notably, *Chiappeavis* preserves a primitive palatal morphology in which the vomers reach the premaxillae similar to *Archaeopteryx* but unlike the condition in the Late Cretaceous enantiornithine *Gobipteryx*. If rectricial bulbs were present, pengornithid pygostyle morphology suggests they were minimally developed. We estimate the lift generated by the tail fan preserved in this specimen and compare it to the tail fans preserved in other Early Cretaceous birds. Aerodynamic models indicate the tail of *Chiappeavis* produced less lift than that of sympatric ornithuromorphs. This information provides a possible explanation for the absence of widespread aerodynamic tail morphologies in the Enantiornithes.

Key words Mesozoic, Jehol Biota, Aves, rectrix

Citation O'Connor J K, Zheng X T, Hu H et al., 2016. The morphology of *Chiappeavis magnapremaxillo* (Pengornithidae: Enantiornithes) and a comparison of aerodynamic function in Early Cretaceous avian tail fans. Vertebrata PalAsiatica, 55(1): 41–58

chinaXiv:201711.01925v1

1 Introduction

Enantiornithes is the most diverse recognized group of Mesozoic birds, considered the first major avian radiation. Although specimens have been collected from continental and marine sediments on all continents with the exception of Antarctica, like other bird fossils, these remains are typically isolated and fragmentary (O'Connor et al., 2011). The major exception is the Early Cretaceous deposits in northeastern China that have produced

国家重点基础研究发展计划项目(编号：2012CB821906)和国家自然科学基金(批准号：41172020, 41372014, 41172016)资助。
收稿日期：2016-04-15

ChinaXiv合作期刊

the 130.7–120 Ma Jehol Biota (Pan et al., 2013), preserving the second oldest recognized fossil avifauna surpassed only by the Late Jurassic Solnhofen Limestones in Germany that produce *Archaeopteryx* (Wellnhofer, 2008). Despite its age, the Jehol avifauna accounts for approximately half of the entire diversity of Mesozoic birds including a huge diversity of enantiornithines (Wang M et al., 2014; Wang X et al., 2014; Zhou and Zhang, 2006). As new species steadily continue to be discovered, several distinct clades have been recognized (e.g., the Bohaiornithidae, Longipterygidae). The most temporally successful of these enantiornithines lineages is the Pengornithidae. The first specimen, the holotype of *Pengornis houi*, was described by Zhou et al. in 2008 and already this group is one of the most diverse enantiornithine clades in the Jehol avifauna. Currently there are five specimens representing four genera (*Pengornis*, *Parapengornis*, *Eopengornis*, and *Chiappeavis*) (Hu et al., 2015; O'Connor et al., 2016; Wang X et al., 2014; Zhou et al., 2008). The holotype of *Pengornis houi* is the largest known Early Cretaceous enantiornithine. *Eopengornis* is from the 130.7 Ma *Protopteryx*-horizon of the Huajiying Formation and all other taxa are from the 120 Ma Jiufotang Formation. Pengornithids are the most recognizable enantiornithines, with their characteristic numerous small, low-crowned teeth, hooked scapular acromion, bilaterally formed sternum without intermediate trabeculae, elongate femur, unreduced fibula, metatarsal V, and elongate metatarsal I and hallux. These characters are mostly primitive features strongly suggesting that pengornithids are basal within the Enantiornithes, consistent with recent phylogenetic analyses and the fact *Eopengornis* is among the oldest known enantiornithines (Wang X et al., 2014).

The most recently described pengornithid, *Chiappeavis magnapremaxillo*, preserves the first clear evidence that some members of the Enantiornithes possessed rectricial fans (Fig. 1), similar to those present in the basal pygostylian *Sapeornis* and members of the Ornithuromorpha (Clarke et al., 2006; Zheng et al., 2013), the clade that includes all living birds nested within. The unique shape of the pengornithid pygostyle, being relatively more similar to that of ornithuromorphs and *Sapeornis* than other enantiornithines, suggests that the rectricial fan evolves together with the rectricial bulbs necessary to control them, which in turn shapes the pygostyle (O'Connor et al., 2016). The holotype and only known specimen of *Chiappeavis magnapremaxillo* STM 29-11 was only briefly described with regards to its skeletal morphology. Here we provide a complete description and further explore the unique morphology of the pengornithid pygostyle. We reconstruct the tail fans of several well preserved Jehol ornithuromorphs and compare the aerodynamic lift generated by different tail shapes and discuss the significance of this information.

chinaXiv:201711.01925v1

ChinaXiv合作期刊

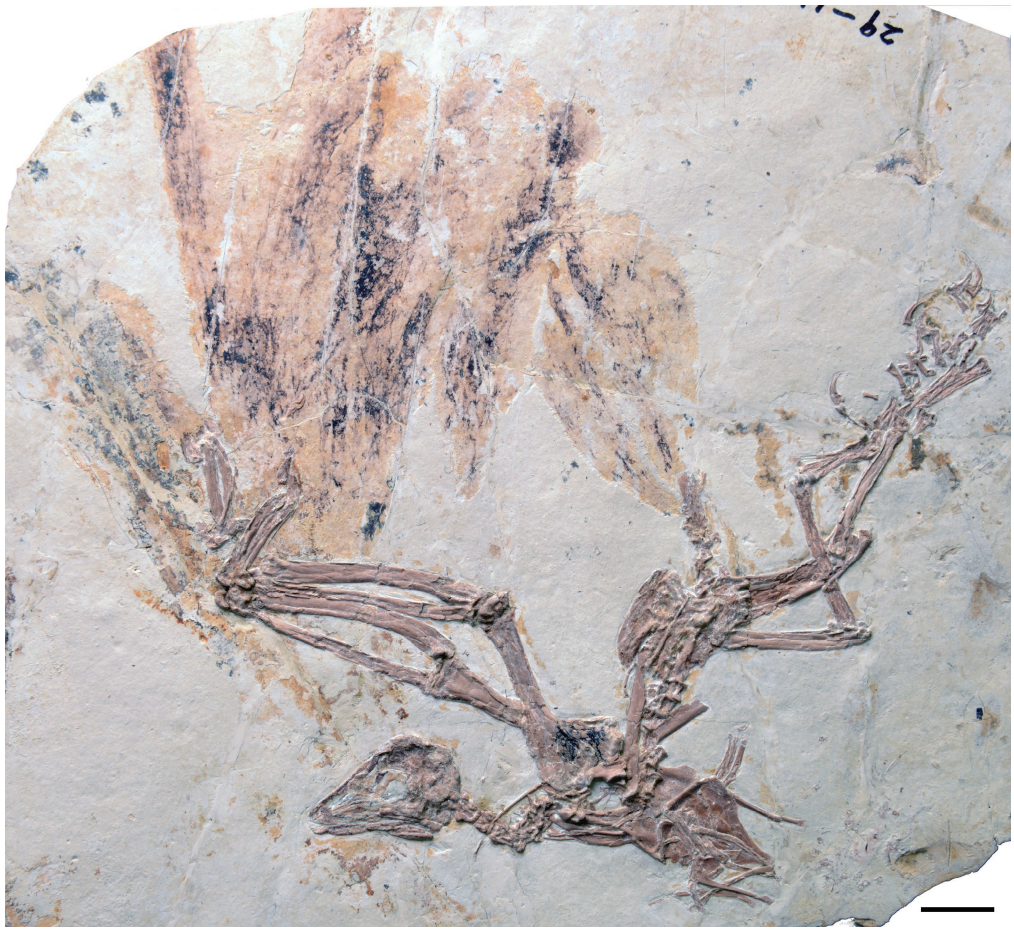

Fig. 1 Photograph of the holotype and only known specimen of *Chiappeavis magnapremaxillo* STM 29-11 Scale bar equals 2 cm

2 Description

This description provides only new anatomical information regarding STM 29-11 (Fig. 2). The enlarged premaxillary corpus and elongate nasal processes that distinguish *Chiappeavis* from other pengornithids have already been described in detail (O'Connor et al., 2016). The maxillary process of the premaxilla is robust, sharply tapered, and roughly equal to the length of the corpus (Fig. 3). The premaxillae form a medial wedged articulation with the nasals although the extent of this articulation is unclear due to poor preservation of the nasals. A fragment of the left nasal is preserved articulating with the frontal; it appears narrower than the nasal in *Pengornis* IVPP V 15336 (Zhou et al., 2008). Although the maxilla forms most of the facial margin in *Pengornis* V 15336 (Zhou et al., 2008) and all other known pengornithids (Hu et al., 2014, 2015; Wang X et al., 2014), only possible fragments are preserved in *Chiappeavis* STM 29-11. Part of the scleral ring is preserved in the orbit. Other fragments may represent pieces of the pterygoids. Ventrally, a thin, distally upturned rod-like element is identified as

chinaXiv:201711.01925v1

ChinaXiv合作期刊

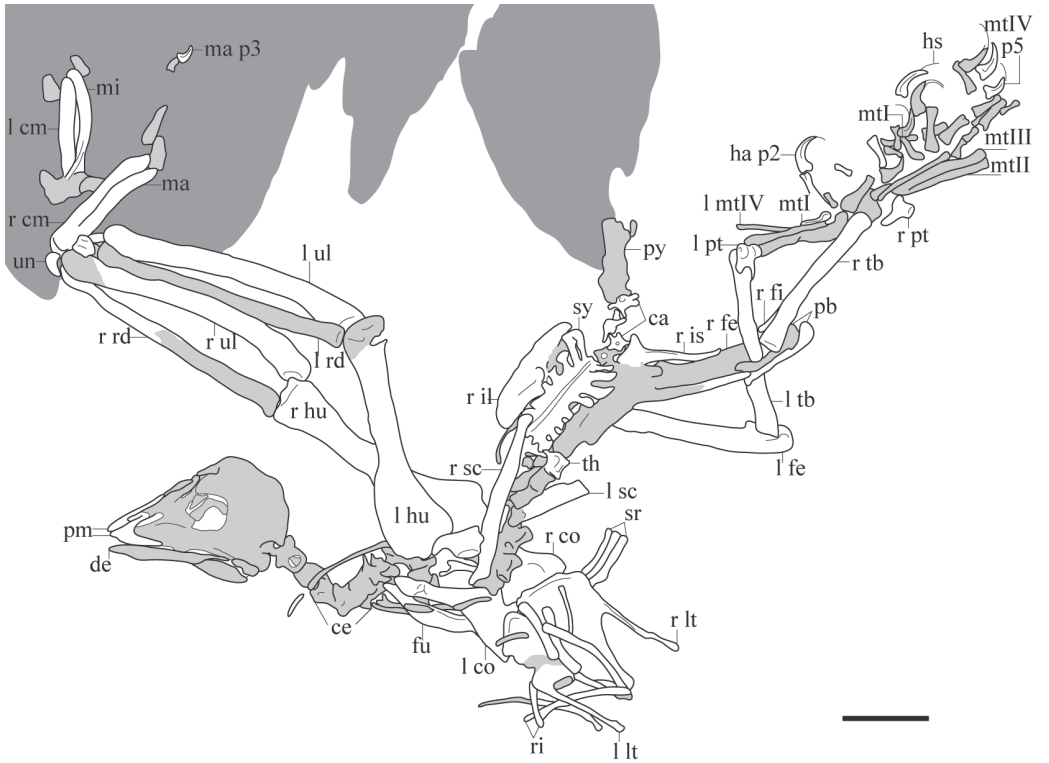

Fig. 2 Interpretative line drawing of the preserved elements in STM 29-11
Anatomical abbreviations: ca. caudal vertebrae; ce. cervical vertebrae; cm. carpometacarpus; co. coracoid; de. dentary; fe. femur; fi. fibula; fu. furcula; ha. hallux; hs. horny sheath; hu. humerus; il. ilium; is. ischium; l. left; lt. lateral trabecula; ma. major metacarpal; mi. minor metacarpal; mt I-IV. metatarsals I-IV; p. phalanx; pb. pubes; pm. premaxilla; pt. proximal tarsals; py. pygostyle; r. right; ri. thoracic ribs; sc. scapula; sr. sternal ribs; sy. synsacrum; tb. tibia; th. thoracic vertebrae; ul. ulna; un. ulnare
Scale bar equals 2 cm. Light grey indicates areas of bone that are broken or poorly preserved; dark grey indicates soft tissue impression of feathers

the jugal. A robust fragment of bone is preserved dorsal and in parallel to the jugal; this bone may be a piece of the jugal process of the maxilla but it appears unusually robust. Part of the palate is visible through the left external nares (Fig. 3). Both vomers are preserved presumably in dorsal view. As in *Gobipteryx* they appear to be fused along their rostral halves, caudally diverging at a 15° angle (nearly parallel in *Gobipteryx*). This suggests that like *Gobipteryx* the choana was rostrally located compared to neornithines (Chiappe et al., 2001). However, unlike in *Gobipteryx* and neognathous birds, as preserved the vomers appear to retain the plesiomorphic tetrapod condition, reaching and presumably articulating with the premaxillae, as in paleognathous birds and potentially *Archaeopteryx* (Witmer and Martin, 1987). A fragment of bone preserved between the left vomer and the maxillary process of the premaxilla may be a piece of the maxillary contribution to the palate. The caudal half of the skull is poorly preserved, crushed and heavily abraded, revealing no anatomical details. The tip of the left dentary is blunt; barely visible, numerous small teeth are preserved in separate aveoli. The

chinaXiv:201711.01925v1

ChinaXiv合作期刊

postdentary bones are poorly preserved.

Approximately seven cervical vertebrae are poorly preserved in articulation with the skull (Fig. 2). The cranial articular surfaces appear to be slightly concave. Proximally the cervicals are preserved in ventral view; distally the series appears in caudal view. The third preserved vertebra reveals small carotid processes. The costal processes are short and sharply tapered. The proximal portion of the thoracic series is obscured by overlap with the thoracic girdle. There are five visible dorsal vertebrae; the first two are disarticulated but the distal three are in articulation with the synsacrum. The dorsal vertebrae show the typical enantiornithine condition with the parapophyses located one-third from the proximal end and the lateral surface deeply excavated by a groove (Chiappe and Walker, 2002). The neural spines of the synsacrum are fused into a continuous spinous crest, which narrows and decreases in height distally, as in V 15336. The first four transverse processes are quadrangular, short and wide; the last three are elongate and caudolaterally oriented and the fifth is intermediate in morphology (Figs. 1, 2). Five free caudal vertebrae are preserved, which is fewer than reported in other pengornithids (Hu et al., 2014, 2015); the cranial articular surface is exposed in the first caudal vertebra revealing a weakly concave surface. The transverse processes are long, approximately equal to the centrum width. The neural canal is smaller than the size of the exposed caudal articular surfaces. The unfused haemel arches are rectangular with blunt distal margins.

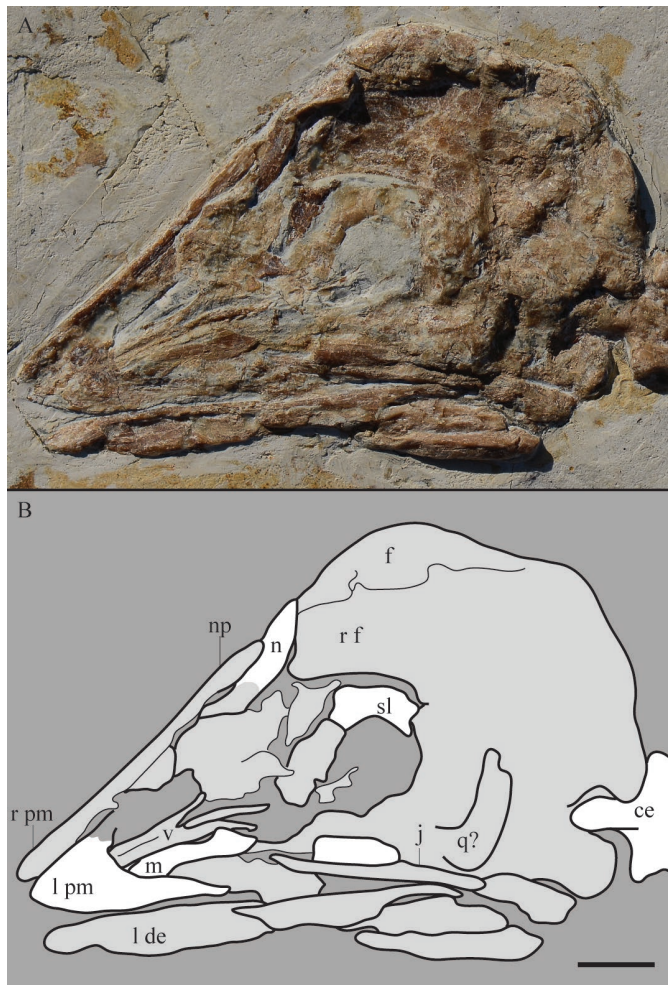

Fig. 3 Detail photograph (A) and line drawing (B) of the skull in STM 29-11
Anatomical abbreviations not listed in Fig. 2 caption: f. frontal; j. jugal; m. possible fragment of the palatal ramus of the maxilla; n. nasal; np. nasal process of premaxilla; q?. possible quadrate; sl. scleral ring; v. vomers. Scale bar equals 5 mm

As noted in a more detailed study of the pygostyle (Wang and O'Connor, in press) the pengornithid pygostyle bears all the same

chinaXiv:201711.01925v1

ChinaXiv合作期刊

characteristic features of other enantiornithines, although this clade differs in how these morphologies are expressed. The pygostyle of *Chiappeavis* has a pair of ventrolateral processes restricted to the proximal ventral half of the pygostyle whereas in other enantiornithines these processes extend for most of the pygostyle length (Chiappe and Walker, 2002). The ventrolateral processes project further ventrally and are limited to the proximal third of the pygostyle in *Pengornis* V 15336 (Fig. 4B). Visible on the right, a small cranial fork is present and continuous with a dorsolateral process that appears to extend the entire length of the pygostyle (Fig. 4A). The dorsal surface between these dorsolateral processes is broadly concave as in other pengornithids, whereas this concavity is narrow and deeper in other enantiornithines, even when preserved dorsoventrally crushed (Wang and O'Connor, in press).

The left ramus of the furcula is preserved in dorsal view; the rami are slightly bowed medially similar to *Pengornis* V 15336 (Fig. 5). The dorsolateral excavation is limited to the proximal 2/3 of the ramus; the dorsal surface of the omal third is flat. The omal tip tapers bluntly, as in *Pengornis* V 15336, and is pitted and striated suggesting incomplete ossification of the articular surfaces. A hypocleidium was present, as in other pengornithids. As in *Pengornis*, the process measures approximately half the length of the furcular rami, whereas the hypocleidium appears proportionately longer in *Parapengornis* IVPP V 18687 (Fig. 5). Both coracoids are in articulation with the coracoidal sulci of the sternum in dorsal view; the dorsal lips of the sulci cover the sternal margin of the coracoids indicating that the sulci are deep. The acrocoracoid, glenoid and scapular articular surface are weakly aligned, as in other enantiornithines (Chiappe and Walker, 2002). The poorly developed glenoid and scapular cotyla are separated by a deep pit, which may be an artefact of crushing and obscuring the presence of an acrocoracoidal tubercle. Just distal to the scapular articular surface the supracoracoid nerve foramen pierces the neck of the coracoid, separated from the medial margin by a complete boney bar; it does not appear to open into a medially located groove as it does in many other enantiornithines (Chiappe and Walker, 2002). The corpus makes up the distal half of the coracoid. The distal quarter of the lateral margin is convex, expanding the width of the sternal margin. The convex distal portion of the lateral margin appears distinctly thinner and flatter than the rest of the coracoidal corpus. This morphology of the lateral margin of the coracoid is also observed in other pengornithids (*Eopengornis*, *Parapengornis* V 18687) as well as bohaiornithid enantiornithines (Wang M et al., 2014). The corpus is weakly excavated by a

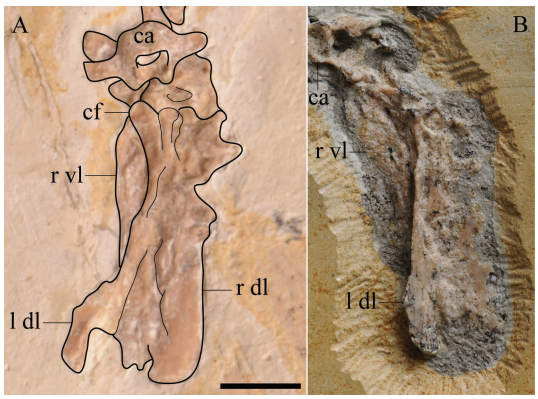

Fig. 4 Comparative photographs of the pygostyle preserved in *Chiappeavis* STM 29-11 (A) and *Pengornis* IVPP V 15336 (B)
Anatomical abbreviations not listed in Fig. 2 caption: cf. cranial fork; dl. dorsolateral process; vl. ventrolateral process. Scale bar equals 5 mm

chinaXiv:201711.01925v1

ChinaXiv合作期刊

shallow dorsal fossa, also observed in some ornithuromorph birds (e.g., *Yixianornis*), inferred to be the attachment of the m. supracoracoideus (Clarke et al., 2006).

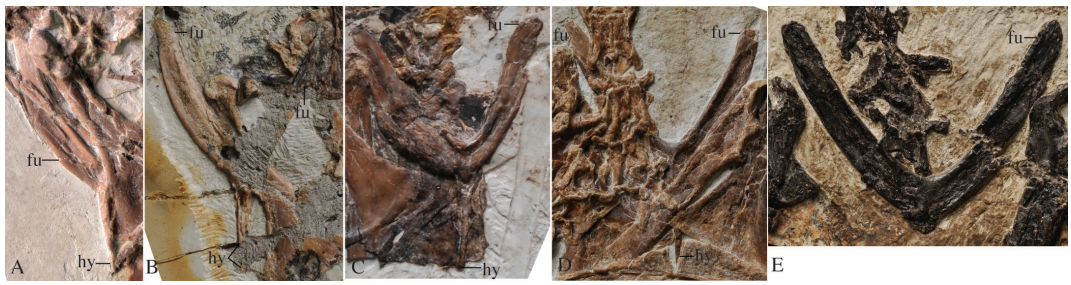

Fig. 5 Pengornithid furculae
A. *Chiappeavis* STM 29-11; B. *Pengornis* IVPP V 15336; C. *Eopengornis* STM 24-11; D. *Parapengornis* IVPP V 18687; E. *Parapengornis* IVPP V 18632
Note differences in *Parapengornis*: the straight furcular rami define a greater angle in IVPP V 18632 and the hypocleidium is proportionately longer in IVPP V 18687. Anatomical abbreviations listed in captions of Figs. 2, 4

The left scapula in lateral view overlaps the right in costal view, and where the two shafts overlap the left is missing a piece of the shaft; both distal ends are unclear. The scapular acromion process is slightly longer than the glenoid facet and hooked, as in other pengornithid enantiornithines (Wang X et al., 2014). The cranial margin of the process is wide and flat. The scapular glenoid facet is large, concave, slightly tapered distally and forming a labum where it contacts the scapular blade (Fig. 6). The body of the scapula is relatively wide and short as in other pengornithids. The costal surface is smooth, lacking the groove present in more derived enantiornithines (e.g. *Elsornis*, *Neuquenornis*) (Chiappe and Walker, 2002).

The straight coracoidal sulci meet at an 120° angle so that the rostral margin of the sternum is weakly vaulted (Fig. 6). The craniolateral corners are weakly developed into slight dorsolateral projections but no distinct craniolateral process is present. The entire lateral margin of the sternum including the lateral trabecula is weakly concave. The dorsal surface of each trabecula is keeled giving this process a triangular cross-section; distally the apex moves from dorsolaterally located to centered on the dorsal surface and the distal third is flat. The distal ends of the trabeculae are weakly expanded – this area of bone is also heavily pitted and striated indicating ossification was incomplete. The lateral trabeculae extend distally beyond the caudal margin of the xiphial region, as in V 18632 (level with caudal margin in *Eopengornis* STM 24-11). The lateral margins of the median trabeculae are concave as the sternal plates narrow caudally, whereas they are straight in *Eopengornis* and *Parapengornis*. Compared to other known pengornithids, the xiphial region is more elongate and narrow in STM 29-11 forming an incipient xiphoid process and defining approximately a 40° angle (75° in *Eopengornis* and 70° *Parapengornis*). The xiphial region bears a short, straight caudal margin, absent in *Eopengornis* and V 18632, in which the xiphial region defines a blunt V-shaped margin (Hu et al., 2014; Wang X et al., 2014). Given the lack of maturity in all specimens preserving sternal material, these apparent differences in the morphology of the

chinaXiv:201711.01925v1

ChinaXiv合作期刊

distal ends of the lateral trabeculae and proportions of the xiphial region may change with the discovery of adult material. However, features like the concavity of the lateral margins in *Chiappeavis* STM 29-11 are unlikely to change at this stage in maturity.

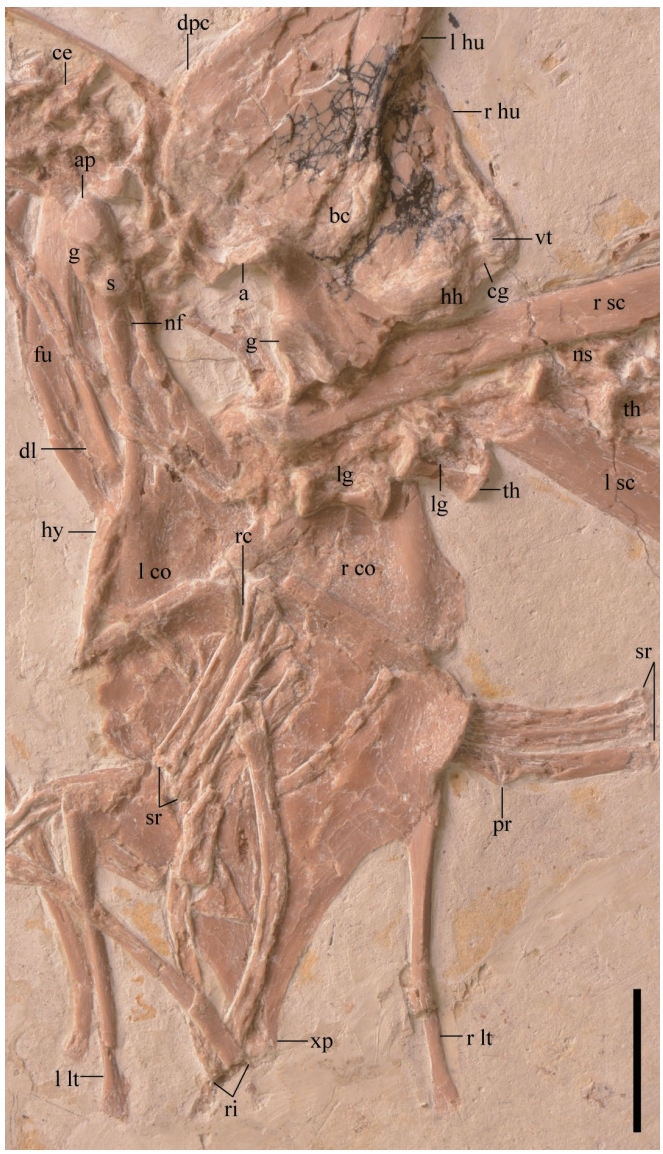

Fig. 6 Close up of the thoracic girdle in *Chiappeavis* STM 29-11
Anatomical abbreviations not listed in Fig. 2 caption: a. acromion process of scapula; ap. acrocoracoid process; bc. bicipital crest; cg. capital groove; dl. dorsolateral excavation of furcular rami; dpc. deltopectoral crest; g. glenoid facet; hh. humeral head; hy. hypocleidium; lg. lateral groove on thoracic vertebrae; nf. supracoracoidal nerve foramen; ns. neural spine of thoracic vertebrae; pr. pathologic rib; rc. rostral cleft of sternum; s. scapular cotyla of coracoid; vt. ventral tubercle; xp. xiphial process
Scale bar equals 5 mm

Well-defined costal facets are not visible but three robust sternal ribs are visible articulating on the right costal margin of the sternum. The third rib is more robust than the others and has an uneven caudal margin that may be pathological in origin (Fig. 6). The left sternal ribs are displaced over the dorsal surface of the sternum – they are short, robust, and weakly curved. Several disarticulated thoracic ribs are preserved; a few are located cranial to the sternum and a few are associated with this element. Compared to the cranially located ribs, the ribs preserved near and overlying the sternum are shorter, more robust, and more weakly curved, and probably articulated with the sternal ribs.

The left humerus is preserved in cranial view, while the right is in caudal view. Proximally in caudal view, the ventral tubercle is small, separated by a wide, shallow capital incision, and a pneumatic fossa is absent. In cranial view, a small bicipital crest is present, weakly projecting cranially. The width of the deltopectoral crest is less than the width of the shaft and extends along the proximal third of the humerus. The shaft weakly increases in width distally

chinaXiv:201711.01925v1

ChinaXiv合作期刊

from its narrowest point located midshaft, also observed in other pengornithids. The distal caudal surface is poorly preserved revealing no anatomical details. The distal condyles are small and located primarily on the cranial surface as in other birds. The circular dorsal condyle is larger than the oval ventral condyle, although the two are approximately equal in diameter. The long axis of the ventral condyle is transversely oriented. The round ventral epicondyle is smaller than the ventral condyle, and located on the craniodistal surface of the ventrodistal margin. The brachial fossa is not developed.

Both antebrachia are complete; the left is in caudal view and the right is cranially exposed. As in other basal birds the ulnae are bowed along their proximal halves. The dorsal cotyla is flat and the ventral cotyla appears slightly concave. The radii are straight and more than half the thickness of the ulna; crushing prevents identification of a longitudinal groove like that present on the interosseous surface of some enantiornithines (Chiappe and Walker, 2002).

The ulnare is U-shaped; one ramus is bluntly tapered, while the other is short and more robust, similar to that of *Pengornis* V 15336. The radiale is quadrangular but it is unclear which surface is exposed. The semilunate carpal appears only partially fused to the metacarpals. The right alular metacarpal is preserved unfused to the major metacarpal. It is narrow and approximately 1/5 the length of the carpometacarpus. The proximal end is rounded and the distal end appears ginglymous. As in V 15336 the proximal end of the minor metacarpal wraps onto the ventral surface of the major metacarpal and the ventral surface of the proximal third of the minor metacarpal forms a ridge rather than a distinct pisiform process, a morphology common in Early Cretaceous enantiornithines (O'Connor, 2009). The first phalanx of the major digit is incomplete but like other enantiornithines it maintains the plesiomorphic theropod condition and lacks any caudal expansion like that present in ornithuromorph birds. The penultimate phalanx is not preserved; the ungual phalanx is small and weakly curved. The first phalanx of the minor digit is wedge-shaped with a flat cranial margin and convex caudal margin, tapering to a blunt distal margin.

Both ilia are preserved in articulation with the synsacrum (Figs. 1, 2). The right ilium is preserved in medial view while the left appears in dorsal view. In lateral view, the dorsal margin is weakly convex. The ventral margins of the preacetabular and postacetabular alae are straight. The pubic pedicel of the ischium is wider than the iliac pedicel. The preacetabular wing is longer and dorsoventrally taller than the postacetabular wing and the postacetabular wing is bluntly tapered as in V 18632 and most enantiornithines. The right ischium, preserved in medial view, is long, delicate and gently tapered; the dorsal margin is concave and the ventral margin is convex (Figs. 1, 2). The pubes have a thick oval cross section with a craniodorsal-caudoventrally oriented long axis. The distal third is heavily pitted and striated.

Both femora are preserved although the right is overlain by the pubes and ischia and the proximal end is not exposed on either side (Figs. 1, 2). As described, a small tibiofibular crest is present distally (O'Connor et al., 2016). The right tibia is in caudal view exposing the

chinaXiv:201711.01925v1

ChinaXiv合作期刊

popliteal tuberosity and lateral articular facet on the proximocaudal surface, also developed in *Pengornis* and *Eopengornis* (Wang X et al., 2014). The flexor fossa is weak or absent. The left tibia is exposed in craniolateral view; the proximal tarsals are fused to each other forming the condyles. The medial condyle is wider than the lateral condyle. They are separated by a wide, shallow intercondylar incisure. The lateral margin of the lateral condyle and the medial margin of the medial condyle are both straight and the opposing surfaces are strongly convex, as in *Pengornis* V 15336. The lateral condyle is excavated by a deep concavity on the lateral surface as in some enantiornithines (e.g., *Qiliania*) (Ji et al., 2011). The ascending process is triangular, tapering proximally, and taller than the height of the condyles. Only the right fibula is preserved and it is incomplete so it cannot be determined if it reached the distal condyles as in other pengornithids (Wang X et al., 2014).

No distal tarsals are preserved, as in other pengornithids. The metatarsals are unfused and slightly disarticulated; the exposed surfaces are abraded, preserving very little information. Metatarsal IV is thinner than metatarsal III, which is in turn thinner than metatarsal II. The digit of metatarsal II is robust with a large ungual phalanx; the ungual phalanx in digit III is long but not as robust as those of digits I and II. The digit IV ungual is the smallest. No metatarsal V is preserved although it was likely present, as in other pengornithids (Wang X et al., 2014).

Ontogenetic status STM 29-11 is clearly immature based on the incomplete ossification of the periosteal surface of the bone evident from the striated pits that sparsely cover the surface of most elements. As would be expected, fusion is incomplete in the sternum and proximal carpometacarpus, and the compound bones of the hindlimb have yet to fully co-ossify. The compound bones of the axial skeleton, the pygostyle and synsacrum, are fully fused in all subadult enantiornithine specimens supporting the inference that the difference in the number of sacral vertebrae is a true distinction between *Chiappeavis* and *Pengornis*. The age of the specimen has not been explored through histology because there are no breaks in the long bones of STM 29-11 to allow non-destructive sampling of this particularly nice specimen. However, the sternum is fully fused in the subadult holotype of *Eopengornis martini* STM 24-1 and V 18632. This indicates that STM 29-11 is at a relatively earlier ontogenetic stage and strongly suggests it would have increased in size with maturity. The sternum in *Parapengornis* V 18687 is also medially unfused, despite its much smaller size (Table 1) and histology confirms that this specimen is immature, with no remodelling present to indicate the individual was mature or nearly so. *Parapengornis* sp. V 18632 has a fully fused sternum but is roughly 15% smaller than *Parapengornis* V 18687 indicating these specimens may represent different species (see phylogenetic analysis). As preserved STM 29-11 is 20% smaller than the holotype of *Pengornis houi* V 15336, although given the relative immaturity of the former specimen we suggest the terminal body size in *Pengornis* and *Chiappeavis* would have been similar.

chinaXiv:201711.01925v1

ChinaXiv合作期刊

Table 1 Select measurements of published pengornithids (mm)

	Pengornis		*Parapengornis*	*Eopengornis*	*Chiappeavis*	
	IVPP V 15336	IVPP V 18632	IVPP V 18687	STM 24-1	STM 29-11	
					right	left
Scapula	(36.3)	34.9	46.3	27.2	(40.9)	45.2
Coracoid L	39	(17.4)	26.3	17.8		30.1
Coracoid W	(18)	–	14	(9.7)	17.6	–
Sternum L	–	(22.7)	33	22	38	
Sternum W			32	22	31	
Humerus	72	45.7	52.1	38	55.7	57.8
Ulna	78	49	54.9	42.4	63.4	63.5
Radius	(66)	49	53.7	41.5	58.1	60.3
Carpometacarpus	34.2	23.8	30.7	23.3	30.9	30
Major metacarpal	29.1*	20.1	24.8	18.2	26.5	27.7
Minor metacarpal	31.4	19.7	27.4	20.1		29.8
Alular metacarpal	–	4.2	5.3	3.4	–	–
Alular digit ph1	–	10.7	11.4	9.5	–	–
Alular digit ph2	–	5.5	6.7	3.9	–	–
Major digit ph1	16	12.5	12.7	9.3	–	–
Major digit ph2	11.6	8.8	9.2	7.2	–	–
Major digit ph3	–	4.5	4.8	3.6	–	5.2
Minor digit ph1	6.9	6.3	8.1	6.3	–	8.4
Hand	56.8	45.9	1.2	38.3	–	–
Femur	53	34.8	39.8	27	–	42.9
Tibiotarsus	55	37.7	40.4	31	44.6	46.7
Femur/tibiotarsus	0.96	0.92	0.99	0.87		0.92
Fibula	(28)	(12)	34	29	(36)	(40)
Metatarsal I	8.2	6.9	8.6	6.9	–	8.2
Metatarsal I ph1	–	6.7	9.2	7.8	–	10.4
Metatarsal II	24	18.9	19.5	15.9	–	(22.4)
Metatarsal III	26.6	–	20.5	17	–	(22.5)
Metatarsal IV	25	–	18	15.9	–	20.5
Pygostyle	18.2	7.5	10	5.1	15	
Synsacrum	24	–	–	–	24	
Pubis	(31)	35	37.2	26	–	47.1
Ilium	–	(14)	30	–	29	–
Ischium	–	21	21	(5.2)	25.4	–

Notes: W. width; L. length; ph. phalanx. * estimated measurement, ( ) indicate incomplete elements.

3 Phylogenetic Analysis

We investigated the phylogenetic placement of *Chiappeavis* using a modified version of the O'Connor and Zhou (2013) dataset that includes the revised character 220 used by Wang X et al. (2014). The dataset includes five pengornithids: *Eopengornis*, *Parapengornis* IVPP V 18687 and IVPP V 18632, *Pengornis*, and *Chiappeavis*. (Hu et al., 2014, 2015; O'Connor et al., 2016; Wang X et al., 2014; Zhou et al., 2008). The matrix includes a total of 63 taxa, 24 of which are referable to the Enantiornithes. Using TNT software (Goloboff et al., 2008) we conducted a heuristic search using tree-bisection reconnection (TBR) retaining the single shortest tree out of every 1,000 replications. This produced 824 most parsimonious trees

chinaXiv:201711.01925v1

ChinaXiv合作期刊

with a length of 897 steps. A second round of TBR produced more than 10,000 trees of the same length. In the strict consensus, all nodes collapsed except Aves itself. Investigation of the MPTs revealed that in 78% of the trees Pengornithidae was resolved. The clade formed by *Jeholornis* + all more derived birds collapses due to the basal position of the fragmentary taxon *Chaoyangia* resolved by a small percentage of MPTs. In order to reduce the effects of homoplasy (Goloboff et al., 2008), which strongly characterizes early avian evolution (Brusatte et al., 2015), we reran the analysis with the same parameters using implied weighting (k = 1.0, 2.0, and 3.0) (Goloboff, 1993). With a k value of 1.0, the analysis produced 24 trees (TBR = 129.47). The strict consensus is well resolved with pengornithids forming successive outgroups to all other enantiornithines. With higher k values (2.0, 3.0) Pengornithidae is resolved as a clade that is sister taxon to all other enantiornithines (Fig. 7).

4 Discussion

Pengornithid diversity Five pengornithid specimens are now recognized, representing at least four distinct genera (*Chiappeavis*, *Eopengornis*, *Parapengornis*, and *Pengornis*). Pengornithids are unusual birds, differing from other enantiornithines in the morphology of the sternum (e.g., ossifying from a pair of medially fused bilateral plates and having only a single pair of caudal trabeculae), pygostyle (shorter, wider, with proximally restricted ventrolateral processes, often having a midline invagination on the caudal margin), and ischium (slender without a dorsal process). In addition, they possess features more typical of long boney-tailed birds or basal pygostylians, such as the presence of a metatarsal V and an elongate fibula. This marked increase in homoplasy caused by the inclusion of five pengornithids has thus resulted in a collapse in weakly resolved relationships from previous analyses, making a strong case for the use of implied weighting. Without the use of implied weighting Pengornithidae is only resolved in 78% of the MPTs, but in 98% of all MPTs V 18632 and *Eopengornis* form a clade, thus not supporting previous inferences that V 18632 should be referred to *Parapengornis* (Hu et al., 2015). This is further supported by differences in body size between V 18632 and *Parapengornis* V 18687 (see Ontogenetic status). Difference in size, morphology (Fig. 5), and stratigraphic level also suggest V 18632 is not referable to *Eopengornis martini*. Because the specimen is a subadult, Hu et al., (2014) originally refrained from naming V 18632 (*Pengornis* sp.), later referring it to *Parapengornis* (Hu et al., 2015). Here we regard this specimen as Pengornithidae indeterminate. Notably, *Eopengornis* and *Parapengornis* share a common tail morphology consisting of a pair of elongate, fully pennaceous rachis dominated feathers but are not found to be closely related; instead, *Eopengornis* is found to be more closely related to *Chiappeavis*, despite their disparate tail morphologies. This may suggest that this analysis does not accurately portray pengornithid relationships or that pengornithid plumage was as evolutionarily labile as in extant avian families (Gluckman, 2014). In favor of the former, the pygostyle of *Chiappeavis* is most similar to that of *Pengornis* with regards to

chinaXiv:201711.01925v1

ChinaXiv合作期刊

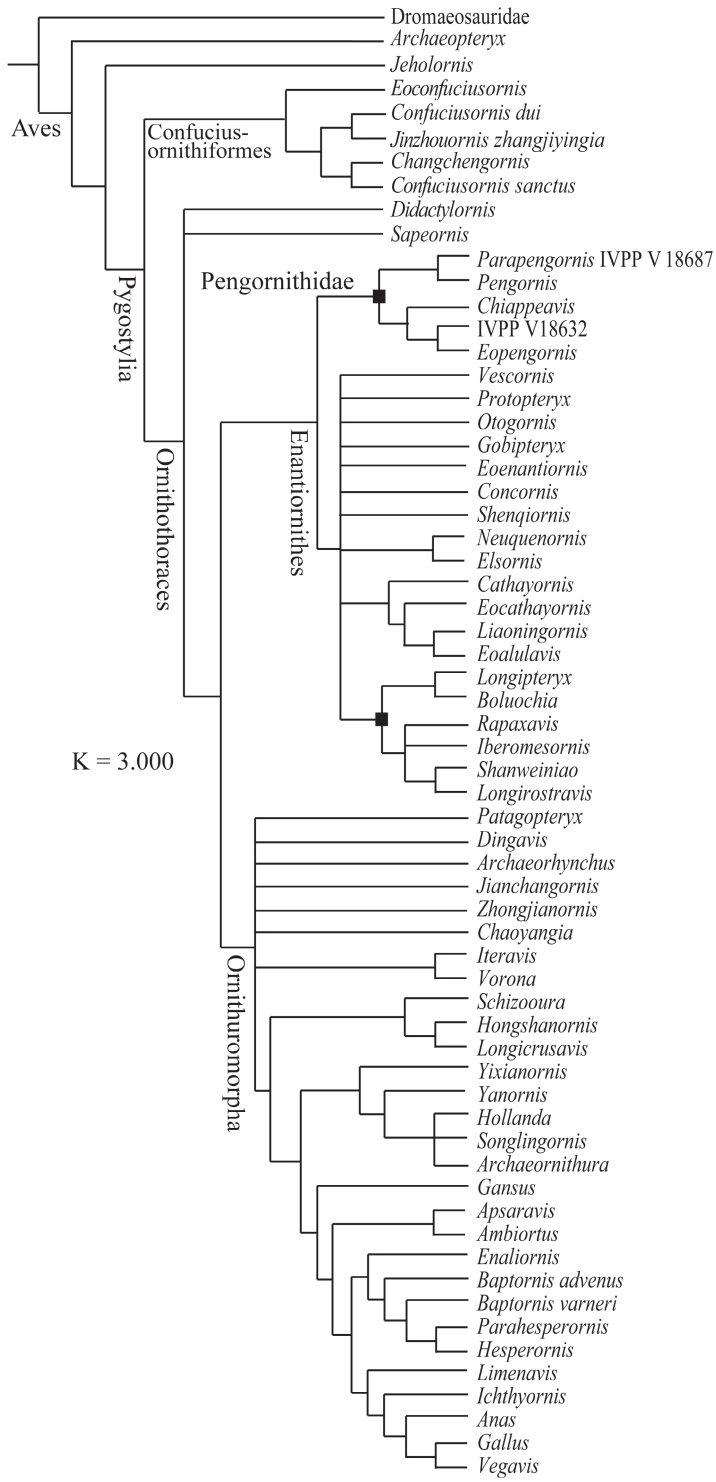

Fig. 7 Phylogenetic hypothesis of Mesozoic bird relationships using implied weighting (k=3.0)

chinaXiv:201711.01925v1

ChinaXiv合作期刊

proportions, whereas that of *Parapengornis* and *Eopengornis* are slightly shorter, suggesting that *Pengornis* may have had a rectricial fan. This subtle interclade diversity is not captured by the abstract morphologies encapsulated by this and other current character matrices used for the phylogenetic analysis of Mesozoic birds.

Large body size (Table 1) and stratigraphic level (Jiufotang) suggest that *Chiappeavis* is more closely related to *Pengornis* than to *Parapengornis* (smaller) or *Eopengornis* (smaller, Huajiying), which is further supported by the morphology of the furcula (furcular rami curved in *Chiappeavis* and *Pengornis* whereas they are straight in *Parapengornis*) (Fig. 5). The sternum in *Chiappeavis* is proportionately more elongate (length greater than width) than in *Parapengornis* and *Eopengornis* (length and width subequal). It further differs from smaller pengornithids in the morphology of the xiphial region of the sternum: the lateral margins of median trabeculae are concave in the new taxon, whereas they are straight in *Eopengornis* and *Parapengornis*. Ontogenetic and preservational differences obfuscate comparison with *Pengornis* V 15336. Postcranially, *Pengornis* V 15336 and *Chiappeavis* STM 29-11 are similar but STM 29-11 has a greater number of sacral vertebrae despite its immaturity (although the cranial margin of the synsacrum is obscured, clearly only seven sacrals are present in *Pengornis* V 15336) and the proximal articular surface of the tibia is inclined. The increased number of sacral vertebrae and expanded premaxillae suggest *Chiappeavis* is more advanced than other pengornithids.

Tail-fan performance in Early Cretaceous birds Even in the Jehol Biota, at the earliest known stage of pygostylian evolution with data limited by fossilization, there exist observable differences in the shape and relative size of the rectricial fan between clades and individual taxa. Compared to all Jehol ornithuromorphs preserving tail fans (*Yixianornis*, *Yanornis*, *Hongshanornis*, *Schizooura*, *Piscivoravis*) (Chiappe et al., 2014; Clarke et al., 2006) (Fig. 8), the tail is proportionately shorter relative to body length in *Chiappeavis* STM 29-11 (Table 2). These taxa also differ in the degree of gradation (measured as the difference in length between the longest and shortest rectrices). Subtle differences in tail shape and length can be used to understand the selective pressures responsible for producing each phenotype. Lift is determined by the maximum continuous width, therefore any elongation beyond this point is considered the product of sexual selection, being not optimized for flight (Thomas and Balmford, 1995). In one test area, 80% of all bird species were found to have tail displays of some kind (Fitzpatrick, 1997). Although two tails of equal width have the same lift, longer tails generate greater moments for turning; the trade-off is that longer tails require greater muscle force and incur more drag (Thomas and Balmford, 1995). Thus the huge diversity of avian tail morphologies represents the product of these and the numerous other selective forces that exist in the varied ecologies and lifestyles occupied by birds. The graded morphology in *Sapeornis* and even the round morphology in ornithuromorphs indicate that although capable of generating lift, these tails were not optimized for aerodynamic function, being also shaped by sexual/signal selection. The difference between the longest and shortest rectrices is highest in

chinaXiv:201711.01925v1

ChinaXiv合作期刊

Sapeornis and *Chiappeavis* suggesting this influence was strongest in these taxa. Shorter tails tend to be adapted for higher flight speeds and greater lift to drag ratios, whereas longer tails increase maneuverability and are found in woodland birds where the cluttered environment selects for increased maneuverability and high-speed flight is infrequent (Thomas, 1997; Thomas and Balmford, 1995). Thus the presence of long round-tails in most ornithuromorphs indicates these taxa well adapted for the forested Jehol paleoenvironment (Zhou, 2004). Since longer tails require greater muscle force, the proportionately shorter tail in *Chiappeavis* supports inferences based on pygostyle morphology that rectricial bulbs, if present, were poorly developed in enantiornithines. Some extant birds have a pygostyle similar to that of enantiornithines in which the dorsal surface is expanded (having a dorsal platform and thus no dorsally blade-like pygostyle lamina) to provide additional surface area for the attachment of enlarged caudal levator muscles, yet these taxa retain rectricial bulbs (Wang and O'Connor, in press). Thus the absence of a pygostyle lamina does not exclude enantiornithines from having this structure.

Fig. 8 Rectricial fan morphology in Early Cretaceous ornithothoracines
A. photograph of the tail impression preserved in *Chiappeavis magnapremaxillo* STM 29-11, scale bar equals 1 cm. Reconstructions are based on the following specimens: B. *Yanornis* STM 9-19; C. *Hongshanornis* DNHM D 2945; D. *Yixianornis* IVPP V 12631; E. *Chiappeavis* STM 29-11. Rectricial fans and pygostyles are drawn to scale; scale bar equals 2 cm

In order to more directly quantify aerodynamic differences in tail shape we reconstructed the rectricial fan for several taxa based on the specimens most clearly preserving this feature (Table 2) and estimated their lift (Thomas, 1993). We recognize that the preserved width is not necessarily the optimal or maximal spread of the tail in flight, but like living birds we assume

chinaXiv:201711.01925v1

ChinaXiv合作期刊

a range of widths were possible at least in the Ornithuromorpha. We assume equal post-mortem compression of the rectricial bulbs (or comparable tail musculature in *Chiappeavis* and *Sapeornis*) resulting in a comparable degree of tail spread between Jehol specimens. Specimens preserved in lateral view were considered unsuitable for analysis. For Jehol birds these measurements represent conservative estimates of the tail's lift capabilities. The tail fan of *Chiappeavis* is estimated to have the least efficient tail shape, whereas the tails in most Jehol ornithuromorphs have almost double the lifting power for their given body mass (Table 2). These measurements support our predictions based on the shape of the pygostyle and associated rectricial fan. The limited function of the enantiornithine tail fan, quantified here for the first time, provides support for the hypothesis that this is the cause of the restricted distribution of this feature in the Enantiornithes. Paired with limited musculature (as inferred from pygostyle morphology) and the potential absence of the ability to control the spread of the tail fan, the enantiornithine aerodynamic rectricial fan may not have provided a great enough reproductive advantage to be retained through natural selection. This is at odds with derived skeletal features present in *Chiappeavis* (enlarged premaxilla, longer synsacrum), which may alternatively suggest that a tail fan was independently evolved in the *Chiappeavis* lineage.

Table 2 Comparison of tail morphologies and their associated aerodynamic benefits between Early Cretaceous birds

	rectrices	morphology	fan width (mm)	body weight (g)	delta lift (N)	lift/mass (N/g)
Archaeopteryx		frond	90	304	0.05	0.00016
Jeholornis	4–6	two-tail	80–103	606	0.04–0.07	0.00012
Chiappeavis	8	graded	50	205	0.021	0.00010
Hongshanornis	10	round	40	44	0.013	0.00028
Yanornis	8	round	75	314	0.052	0.00017
Yixianornis	8	graded	57	148	0.028	0.00019
Columba	12	round	260	350	0.42	0.0012

Body mass was estimated using humeral length and the equations by Liu et al. (2012). Note that despite differences in their tail morphology, long-tailed birds generated similar amounts of lift (O'Connor et al., 2013). The tail in the neornithine *Columba* is estimated to generate a whole order of magnitude higher lift. Data for *Columba* was taken from Gatesy and Dial (1996); measurements for the London *Archaeopteryx* were taken from Wellnhofer (2008). Measurements from fossil specimens assume similar amounts of fanning due to comparable post-mortem compression and probably do not represent maximum spread, thus representing conservative estimates of the tail's lift capabilities.

Acknowledgements We thank SHI Ai-Juan (IVPP) for assistance with figures, T. Stidham (IVPP) for useful discussions, WANG Min (IVPP) and LI Zhi-Heng (IVPP) for useful comments on an earlier version of this manuscript, and WANG Min (IVPP) for editing the Chinese abstract. This research was supported by the National Basic Research Program of China (973 Program, 2012CB821906), the National Natural Science Foundation of China (41172020, 41172016, 41372014), and the Chinese Academy of Sciences.

chinaXiv:201711.01925v1

ChinaXiv合作期刊

巨前颌契氏鸟 (鹏鸟科：反鸟类)的形态学描述及早白垩世鸟类尾羽的空气动力学功能比较

邹晶梅[1] 郑晓廷[2,3] 胡 晗[1] 王孝理[2,3] 周忠和[1]

(1 中国科学院古脊椎动物与古人类研究所，中国科学院脊椎动物演化与人类起源重点实验室 北京 100044)

(2 临沂大学地质与古生物研究所 山东临沂 276000)

(3 山东省天宇自然博物馆 山东平邑 273300)

摘要：契氏鸟(*Chiappeavis*)是首次发现保存有扇状尾羽的反鸟类，显示出尾羽球茎这一结构在较原始的反鸟类中已经发育。详细描述了巨前颌契氏鸟(*C. magnapremaxillo*)正型标本的骨骼形态学特征。契氏鸟的腭区形态与始祖鸟(*Archaeopteryx*)相似，而区别于晚白垩世的反鸟类戈壁鸟(*Gobipteryx*)。即使具有尾羽球茎，鹏鸟类的尾综骨形态也表明该结构发育较差。估算了在契氏鸟中由扇状尾羽所产生的浮力，并与其他早白垩世鸟类进行对比。结果显示，契氏鸟的扇状尾羽所产生的空气浮力小于同时代生活的今鸟型类，这有可能解释了反鸟类中具有空气动力学功能的尾羽形态普遍缺乏的现象。

关键词：中生代，热河生物群，鸟类，尾羽

中图法分类号：Q 915.865 **文献标识码**：A **文章编号**：1000−3118(2017)01−0041−18

chinaXiv:201711.01925v1

References

Brusatte S L, O'Connor J K, Jarvis E D, 2015. The origin and diversification of birds. Curr Biol, 25: R888–R898

Chiappe L M, Walker C A, 2002. Skeletal morphology and systematics of the Cretaceous Euenantiornithes (Ornithothoraces: Enantiornithes). In: Chiappe L M, Witmer L M eds. Mesozoic Birds: Above the Heads of Dinosaurs. Berkeley: University of California Press. 240–267

Chiappe L M, Norell M, Clark J, 2001. A new skull of *Gobipteryx minuta* (Aves: Enantiornithes) from the Cretaceous of the Gobi Desert. Am Mus Novit, 3346: 1–15

Chiappe L M, Zhao B, O'Connor J K et al., 2014. A new specimen of the Early Cretaceous bird *Hongshanornis longicresta*: insights into the aerodynamics and diet of a basal ornithuromorph. PeerJ, 2(e234): 1–28

Clarke J A, Zhou Z H, Zhang F C, 2006. Insight into the evolution of avian flight from a new clade of Early Cretaceous ornithurines from China and the morphology of *Yixianornis grabaui*. J Anat, 208(3): 287–308

Fitzpatrick S, 1997. Patterns of morphometric variation in birds' tails: length, shape and variability. Biol J Linn Soc, 62: 145–162

Gatesy S M, Dial K P, 1996. From frond to fan: *Archaeopteryx* and the evolution of short-tailed birds. Evolution, 50(5): 2037–2048

Gluckman T L, 2014. Pathways to elaboration of sexual dimorphism in bird plumage patterns. Biol J Linn Soc, 111: 262–273

Goloboff P A, 1993. Estimating character weights during tree search. Cladistics, 9: 83–91

Goloboff P A, Farris J S, Nixon K C, 2008. TNT, a free program for phylogenetic analysis. Cladistics, 24: 774–786

ChinaXiv合作期刊

Hu H, Zhou Z H, O'Connor J K, 2014. A subadult specimen of *Pengornis* and character evolution in Enantiornithes. Vert PalAsiat, 52(1): 77–97

Hu H, O'Connor J K, Zhou Z H, 2015. A new species of Pengornithidae (Aves: Enantiornithes) from the Lower Cretaceous of China suggests a specialized scansorial habitat previously unknown in early birds. PLoS ONE, 10(6): e0126791

Ji S A, Atterholt J A, O'Connor J K et al., 2011. A new, three-dimensionally preserved enantiornithian (Aves: Ornithothoraces) from Gansu Province, northwestern China. Zool J Linn Soc, 162: 201–219

Liu D, Zhou Z H, Zhang Y G, 2012. Mass estimate and evolutionary trend in Chinese Mesozoic fossil birds. Vert PalAsiat, 50(1): 39–52

O'Connor J K, 2009. A systematic review of Enantiornithes (Aves: Ornithothoraces). Ph. D thesis. Los Angeles: University of Southern California. 1–600

O'Connor J K, Zhou Z H, 2013. A redescription of *Chaoyangia beishanensis* (Aves) and a comprehensive phylogeny of Mesozoic birds. J Syst Palaeont, 11(7): 889–906

O'Connor J K, Chiappe L M, Bell A, 2011. Pre-modern birds: avian divergences in the Mesozoic. In: Dyke G D, Kaiser G eds. Living Dinosaurs: the Evolutionary History of Birds. New Jersey: J. Wiley & Sons. 39–114

O'Connor J K, Wang X L, Sullivan C et al., 2013. The unique caudal plumage of *Jeholornis* and complex tail evolution in early birds. Proc Natl Acad Sci USA, 110(43): 17404–17408

O'Connor J K, Wang X L, Zheng X T et al., 2016. An enantiornithine with a fan-shaped tail, and the evolution of the rectricial complex in early birds. Curr Biol, 26: 114–119

Pan Y H, Sha J G, Zhou Z H et al., 2013. The Jehol Biota: definition and distribution of exceptionally preserved relicts of a continental Early Cretaceous ecosystem. Cretaceous Res, 44: 30–38

Thomas A L R, 1993. On the aerodynamics of birds' tails. Philos Trans R Soc Lond B Biol Sci, 340: 361–380

Thomas A L R, 1997. On the tails of birds. Bioscience, 47(4): 215–225

Thomas A L R, Balmford A, 1995. How natural selection shapes bird's tails. Am Nat, 146(6): 848–868

Wang M, O'Connor J K, Zelenkov N Z et al., 2014. A new diverse enantiornithine family (Bohaiornithidae fam. nov.) from the Lower Cretaceous of China with information from two new species. Vert PalAsiat, 52(1): 31–76

Wang W, O'Connor J K, in press. Morphological co-evolution of the pygostyle and tail feathers in Mesozoic birds. Vert PalAsiat

Wang X L, O'Connor J K, Zheng X T et al., 2014. Insights into the evolution of rachis dominated tail feathers from a new basal enantiornithine (Aves: Ornithothoraces). Biol J Linn Soc, 113(3): 805–819

Wellnhofer P, 2008. *Archaeopteryx*. Der Urvogel von Solnhofen. München: Friedrich Pfeil. 1–256

Witmer L M, Martin L D, 1987. The primtive features of the avian palate, with special reference to Mesozoic birds. In: Mourer-Chauviré C ed. L'Evolution des Oiseaux d'apres le Temoignage des Fossiles. Lyon: Département des Sciences de la Terre, Université Claude-Bernard. 21–40

Zheng X T, Zhou Z H, Wang X L et al., 2013. Hind wings in basal birds and the evolution of leg feathers. Science, 339: 1309–1312

Zhou Z H, 2004. Vertebrate radiations of the Jehol Biota and their environmental background. Chin Sci Bull, 49(8): 754–756

Zhou Z H, Zhang F C, 2006. Mesozoic birds of China - a synoptic review. Vert PalAsiat, 44(1): 74–98

Zhou Z H, Clarke J, Zhang F, 2008. Insight into diversity, body size and morphological evolution from the largest Early Cretaceous enantiornithine bird. J Anat, 212(5): 565–577

chinaXiv:201711.01925v1

ChinaXiv合作期刊

第55卷 第1期
2017年1月

古 脊 椎 动 物 学 报
VERTEBRATA PALASIATICA

pp. 59–70
figs. 1–3

Elephas cf. *E. planifrons* (Elephantidae, Mammalia) from Upper Siwalik Subgroup of Samba district, Jammu and Kashmir, India

Som Nath KUNDAL Gyan BHADUR Sandeep KUMAR

(*Department of Geology*, *University of Jammu* Jammu and Kashmir 180006, India somnath.kundal@gmail.com)

Abstract One specimen of *Elephas* cf. *E. planifrons* is reported and described here in the present paper. The specimen was recovered from the mudstone horizon underlying the volcanic ash bed exposed near the Nangal village, which is the extension of geochronological dated (2.48 Ma) volcanic ash beds exposed at Barakhetar in the Nagrota Formation of Upper Siwalik Subgroup of Samba district, Jammu and Kashmir, India. Based on the crown morphological parameters (plate numbers, molars length and width, crown length, width and height, enamel thickness, dentine thickness, length and width of plates, lamellar frequency, hypsodonty index and cement thickness), the specimen has been identified and is tentatively referred to *Elephas* cf. *E. planifrons* (LM3). The recovery of this specimen is of great significance as it extends its upper limit of range zone from 3.6–2.6 to 3.6–2.48 Ma.

Key words Jammu, India; Nagrota Formation, Upper Siwalik Subgroup; *Elephas*

Citation Kundal S N, Bhadur G, Kumar S, 2017. *Elephas* cf. *E. planifrons* (Elephantidae, Mammalia) from Upper Siwalik Subgroup of Samba district, Jammu and Kashmir, India. Vertebrata PalAsiatica, 55(1): 59–70

chinaXiv:201711.01925v1

1 History of research

From time to time various authors carried out work on elephants origin, evolution and palaeoeccology, taxonomy, distribution, classification, anatomy, ecology, behaviour, phylogenetic analysis and fossil elephantids lineages (Aguirre, 1969; Maglio, 1973; Sarwar, 1977; Tassy, 1983; Shoshani and Tassy, 1996, 2005; Wei et al., 2006; Gheerbrant and Tassy, 2009; Todd, 2010a,b) from the different parts of the world.

In Indian subcontinent, the genus *Elephas* is represented by four species (*E. planifrons*, *E. hysudricus*, *E. namadicus*, and *E. maximus*). In these four species, the first three (*E. planifrons*, *E. hysudricus*, *E. namadicus*) were extinct completely from Indian subcontinent and the last one (*E. maximus*) is surviving till date. Detailed studies on geology, palaeontology, phylogeny and age of the elephantidea fauna (*Steglophodon nathotenis*, *Steglophodon latidens*, *Steglophodon cautleyi*, *Stegodon clifti*, *Stegodon bombifrons*, *Stegodon pinjorensis*,

印度UGC-BSR (编号：20-3(6)/2012)和SERB项目(编号：SR/FTP/ES-71/2013)资助。
收稿日期：2016-08-05

ChinaXiv合作期刊

Archidiskodon planifrons, *Elephas hysudricus*, *E. maximus*, *E. hysudrindicus*, *E. planifrons*, *Palaeoloxodon namadicus*) from the Siwalik of India, Pakistan and Burma were carried out by various authors (Osborn, 1942; Sahni and Khan, 1959; Chakravarti, 1965; Opdyke et al., 1979; Azzaroli and Nepoleone, 1981; Badam and Kumar, 1982; Tripathi and Basu, 1983; Nanda et al., 1991; Samiullah et al., 2014).

In Siwalik Province of Jammu, Jammu & Kashmir State, India no detailed work on Elephantidae fauna was carried out except for a few workers (Wadia, 1925; Ganjoo, 1985; Nanda, 1994; Kundal and Kundal, 2011; Sankhyan and Sharma, 2014). Wadia (1925) first time recovered a tusk (about 3.43 m) of *Stegodon ganesa* from near the Jagti village of Nagrota Formation of Upper Siwalik Subgroup of Jammu. Ganjoo (1985) recovered dental remains of *Stegolophodon* sp., *Stegodon insignis*, *Stegodon ganesa* and *Elephas* sp. from the Pleistocene deposits of Khanpur Formation (Pinjor Formation) and Tawi Formation (Boulder Formation) of Upper Siwalik Subgroup of Jammu region. The comment on certain faunal discrepancies on Upper Siwalik mammalian faunas from Chandigarh and Jammu area was given by Nanda (1994). A lot of specimens of proboscidean were collected by the Geological Survey of India from the Siwalik of Jammu and other part of Siwalik of India and these specimens have been published in the Catalogue series no. 5 in the year 2002. An appraisal of diversity and habitats of Siwalik mammals of the Jammu Sub-Himalaya was discussed by Basu (2004). Recently, Kundal and Kundal (2011) recovered an upper right third molar (M3) of *Elephas maximus indicus* from the post Siwalik deposits of Jammu Province near Kharian village, Jammu and Kashmir, India. A few workers (Prasad et al., 2005; Bhat et al., 2008; Bhandari and Kundal, 2008; Kundal and Prasad, 2011; Kundal et al., 2011; Kundal, 2012, 2013, 2015) carried out detailed studies on fossils recovered from mudstone horizons associated with geochronologically dated volcanic ash occurring in Upper Siwalik of Jammu and its depositional environment. In the present study, the systematics and biochronology of *Elephas* cf. *E. planifrons* recovered from the Nangal village of Nagrota Formation, Upper Siwalik Subgroup of Samba district of Jammu and Kashmir has been carried out. The area in this study is given in Fig. 1A.

Geological, palaeontological and palaeomagnetic studies of type sections of Siwalik in Indian subcontinent have been carried out from time to time by various workers (Colbert, 1935; Lewis, 1937; Wadia, 1957; Keller et al., 1977; Opdyke et al., 1979, 1982; Johnson et al., 1982, 1985; Barry et al., 1982, 2002, 2013; Barry and Flynn, 1990; Flynn et al., 1995, 2013; Badgley et al., 2005, 2008; Patnaik, 2013) and revealed that the boundaries are time transgressive in between most of Formations of the Siwalik Group and that temporal mammals ranges are not usually fixed within the time limits of these Formations. A generalized stratigraphic framework of Siwalik in Indian Subcontinent is given in Fig. 1D.

The local classifications of Upper Siwalik Subgroup of Jammu–Samba district of Jammu Province based on palaeontology, magnetostratigraphy and radiometric date of ash beds were given by Ranga Rao et al. (1988), Agarwal et al. (1993) and Gupta (2000). A comparative lithostratigraphic classification of Siwalik Group of Jammu Province in Jammu and Kashmir,

chinaXiv:201711.01925v1

ChinaXiv合作期刊

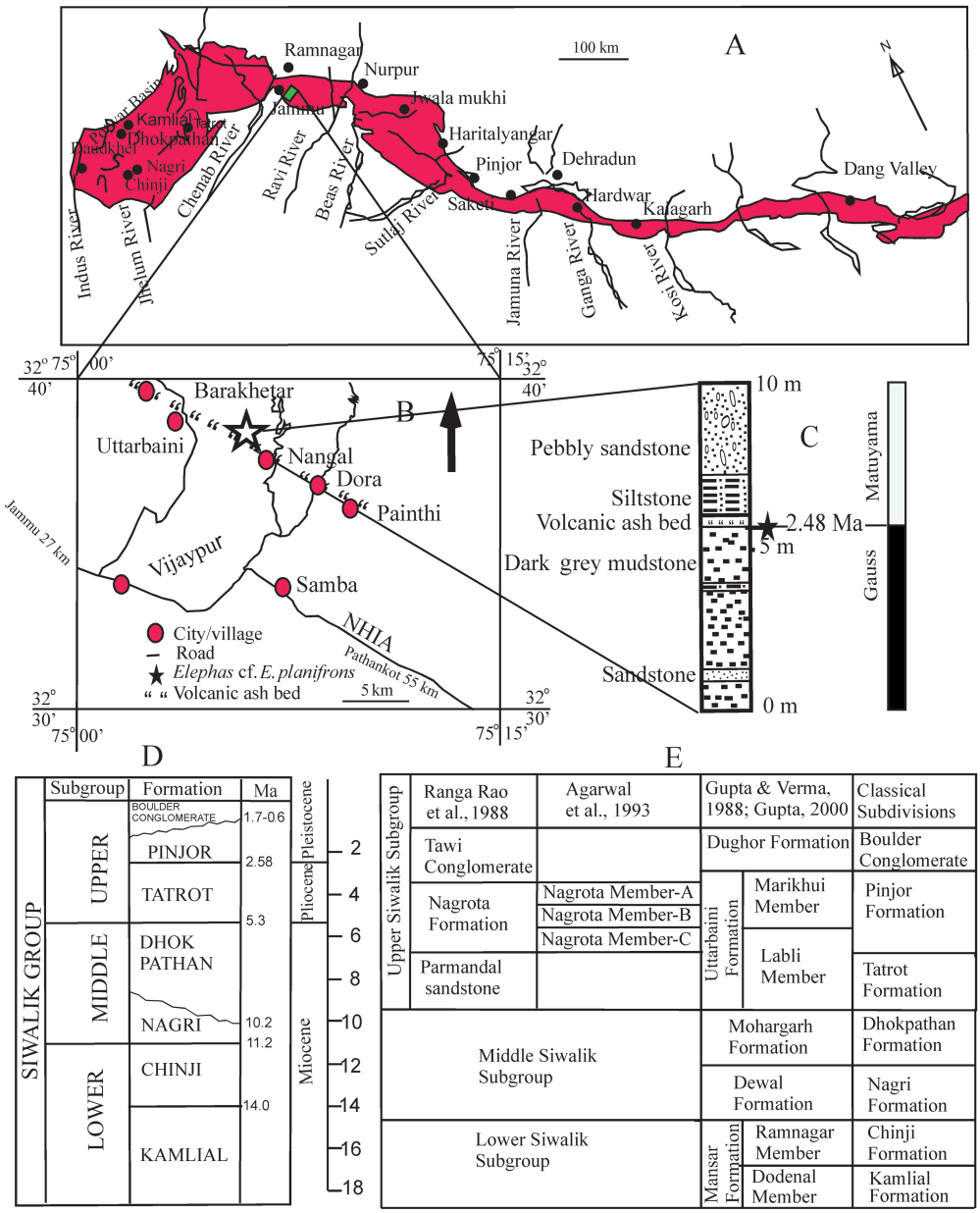

Fig. 1 Map showing range of Siwalik Hills and area under study (small box) (A), locality of *Elephas* cf. *E. planifrons* (B), position of *Elephas* cf. *E. planifrons* in the lithocolumn and the ash bed (2.48 Ma) act as transition between Gauss Normal and Matuyama Reversed Polarity Epochs (C), a generalized stratigraphic framework of the Siwalik sequence (D) (Modified from Behrensmeyer and Barry, 2005; dates from Johnson et al., 1985; Ranga Rao et al., 1988; Barry et al., 2002), and comparative local lithostratigraphic classifications of the Siwalik sequence of Jammu-Samba Region (E)

India is given in Fig. 1E. In Pinjor/Nagrota Formation, a volcanic ash bed is occurring at near Barakhetar and Nagrota villages which have been geochronologically dated 2.48 Ma. These ash beds straddle across Gauss-Matuyama boundary in the Siwalik of Jammu-Samba district

chinaXiv:201711.01925v1

ChinaXiv合作期刊

of Jammu and Kashmir, India (Ranga Rao et al., 1988). The specimen described in the present study was discovered from the mudstone horizon immediately underlying geochronologically dated 2.48 Ma volcanic ash bed at Nangal village which is the extension of Barakhetar ash bed and now is preserved in the vertebrate palaeontology laboratory, Geology Department of Jammu University, under catalog number JU/GD/VPL/9001.

2 Systematic palaeontology

Class Mammalian Illiger, 1811

Order Proboscidea Gray, 1821

Family Elephantidae Gray, 1821

Genus *Elephas* Linnaeus, 1735

***Elephas* cf. *E. planifrons* Falconer & Cautley, 1845**

(Fig. 2A–C)

Referred material JU/GD/VPL/9001, left M3 with broken roots and broken anterior two plates.

Locality River cutting section 15 km northwest of Samba city near the village Nangal, J&K, India.

Stratigraphic horizon Mudstone horizon underlying volcanic ash bed in Nagrota Formation (Ranga Rao et al., 1988)/Uttarbaini Formation (Gupta and Verma, 1988)/Pinjor Formation (Pilgrim, 1934).

Age Late Pliocene–Early Pleistocene.

Measurements (in mm) Number of plates, 9 ($2^{1/2}$ broken out + $6^{1/2}$ preserved); length of molar, 140+50 (broken anterior two plates); width of molar, 82; length/width ratio, 1.70; number of plates preserved, $6^{1/2}$ ($4^{1/2}$ worn + 2 unworn); average length of plates (occlusal), 72; average width of plates (occlusal), 17.16; lamellar frequency (lf), 6; average enamel thickness (et) of worn plates, 3.5; average cement thickness (ct) between plates, 10; average dentine thickness (dt) of worn plates, 4.64; crown length, 140; crown width, 92; maximum crown height, 80; hypsodont index (H/W×100), 87.

Description JU/GD/VPL/9001 has well preserved plates with broken roots. The anterior two and half plates of molar are broken out. The shape of the molar tapers at the posterior end (ovate); molar curvature is straight; inclination of plates to occlusal surface is weak; molar roots are strong and broken; enamel height above the cement is high; enamel figures are parallel sided with median loop, lateral sides of enamel are rounded and turn slightly anteriorly; the enamel are symmetrical in line with the long axis of the molar; medial edges of enamel of two middle plates are in contact, undulating folded; amplitudes of enamel folding in few plates are high to low; and space between enamel folds in few plates are tight to lose. The plates are well compact with cement and are widely spaced. The plates are slightly slanting towards posterior side. The specimen has four and a half worn plates and two unworn

chinaXiv:201711.01925v1

ChinaXiv合作期刊

plates. The width of the molar increased from posterior to centre and then decreased slightly towards anterior side. Except the four and half worn plates, three plates have developed strong expansion of loops at the middle which are in connection with the adjacent ones. The enamel layer is quite simple and thick.

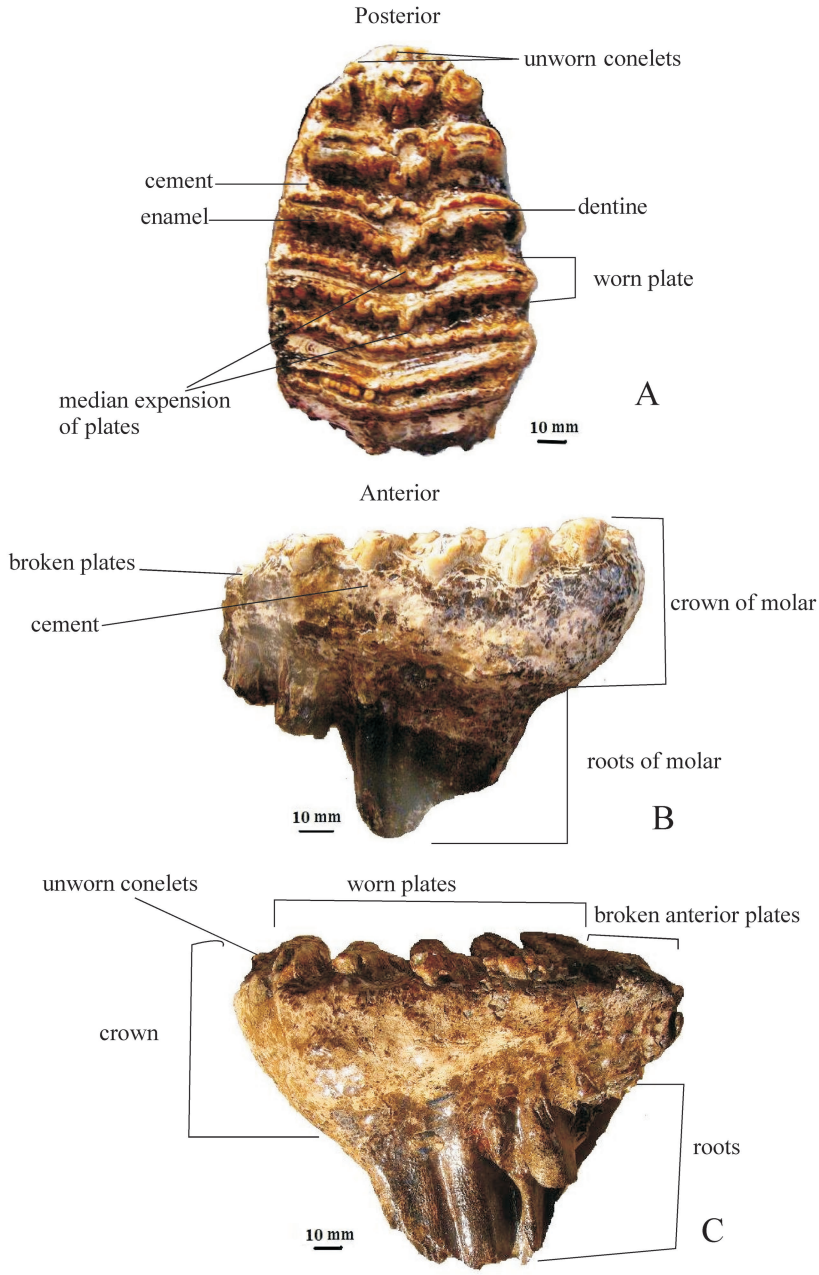

Fig. 2 Left M3 of *Elephas* cf. *E. planifrons*, JU/GD/VPL/9001
A. occlusal view; B. labial view; C. lingual view

chinaXiv:201711.01925v1

ChinaXiv合作期刊

3 Comparative study of specimen JU/GD/VPL/9001 with allied species of *Elephas*

By using the dental morphological characters (number of plates, length of molar, height and width of crown, lamellar frequency, enamel thickness and hypsodonty index), the specimen JU/GD/VPL/9001 under study is compared with allied species of *Elephas* (*E. namadicus*, *E. hysudricus*, *E. hysudrindicus*, *E. maximus*, *E. naumani*, and *E. planifrons)* described earlier (Maglio, 1973). The details of parameters described are given in Table 1.

Table 1 Comparative measurements (observed range and mean) of JU/GD/VPL/9001 with allied species of *Elephas* (M3) (mm)

	E. namadicus	*E. hysudricus*	*E. hysudrindicus*	*E. maximus*	*E. naumani*	*E. planifrons*	JU/GD/VPL/9001
Number of plates	12–16	12–15	18–21	22–27	17–19	8–12	$6^{1/2}+2^{1/2}=9$
	14.3	13.5	19.5	24.5	18	10	
Length of molar	223–317	235–302	293.2–316.6	244–282	211–278	201–292	190
	271.3	267.2	304.9	271.9	244.5	238.2	
Width of crown	61–101	93–107	72.3–82.5	80–98	81–95	86–111	92
	84	97.2	77.4	89	88	98.7	
Height of crown	137–218	108–137.2	128.4–149.3	187–214	195–251	76–129	80
	175.5	125.4	138.8	200.5	223	94.2	
Lamellar frequency	4.5–7.7	3.9–6.5	6.5	5–9	6–7	2.6–5.5	6
	5.7	5.4		7	6.5	4.2	
Enamel thickness	1.8–3.0	2.5–4.8	2.6–2.7	2.5–3.0	2.0–3.2	2.8–4.8	3.5
	2.4	3.2	2.6	2.75	2.6	3.9	
Hypsodonty index	135.6–298	112.5–147	177.5–182.3	150–250	230–320	80–110	87
	212.4	131.1	179.9	200	275	97.6	

Elephas namadicus differs from the JU/GD/VPL/9001 in number of plates (12–16), length of molar (223–317), width of crown (61–101), height of crown (137–218), enamel thickness (1.8–3.0) and hypsodonty index (135.6–298). The parallel lophs and absence of median expansion is very characteristic of *E. namadicus* which differentiate it from JU/GD/VPL/9001.

Elephas hysudricus differs from JU/GD/VPL/9001 in number of plates (12–15), length of molar (235–302), width of molar (93–107), height of crown (108–137), lamellar frequency (3.9–6.5) and hypsodonty index (112.5–147.2). Lack of median expansion and strong plication of lophs is the characteristic of *E. hysudricus* which is differentiated it from the JU/GD/VPL/9001 (Ganjoo, 1992).

Elephas hysudrindicus differs from JU/GD/VPL/9001 in number of plates (18–21), molar length (293.2–316.6), crown width (72.3–82.5), crown height (128.4–149.3), lamellar frequency (6.5), enamel thickness (2.6–2.7) and hypsodonty index (177.5–182.3). *E. hysudrindicus* is the most advanced member of *Palaeoloxodon namadicus* group.

Elephas maximus differs from JU/GD/VPL/9001 in number of plates (22–27), molar length (244–282), crown width (80–98), crown height (187–214), lamellar frequency (5–9), enamel thickness (2.5–3.0) and hypsodonty index (150–250). JU/GD/VPL/9001 has anterior and posterior columns along the median line (lenticular) which is absent in the *E. maximus*.

chinaXiv:201711.01925v1

ChinaXiv合作期刊

E. maximus has narrow folding enamel structure, whereas JU/GD/VPL/9001 has thick folded enamel structures.

The molar characters such as range of hypsodonty index, enamel thickness, lamellar frequency, height of crown, width of crown, length of molar and number of plates of *Elephas naumani* are 230–320, 2.0–3.2, 6–7, 195–251, 81–95, 211–278 and 17–19 respectively, whereas the hypsodonty index, enamel thickness, lamellar frequency, height of crown, width of crown, length of molar and number of plates of JU/GD/VPL/9001 are 87, 3.5, 6, 80, 92, 190 and 9 respectively, which are different from *E. naumani.*

JU/GD/VPL/9001 specimen understudy is broad and brachydont with expanded strong anterior and posterior columns along the median line (lenticular) which are the characteristic features of the *Elephas planifrons* (Osborn, 1942). The average enamel thickness of molar is 3.5 mm which precisely equals to the *E. planifrons* at the Indian Museum, Calcutta. The lamellar frequency of *E. planifrons* given by different authors is, Osborn (1942): up to 6; Hooijer (1955): up to 5; Maglio (1973): 2.6–5.5.

The lamellar frequency of molar under study is 6 and this specimen is also compared with the *Elephas planifrons* collected by Gupta (1981–1982) field session, from the Marikhui Member of Uttarbaini Formation which was published in GSI Catalogue No. 5 (pictorial catalogue of Siwalik vertebrate fossils from NW Himalaya in the year, 2002 (pp.130, figure 1)). JU/GD/VPL/9001 is compared with the most primitive specimen (M3) of *E. planifrons* (number 19965, American Museum) collected by Barnum Brown from Upper Pliocene Pinjor horizon of the Siwalik near the Siswan, India. The specimen resembles with JU/GD/VPL/9001 in outline as well as dental characters such as plate numbers, enamel thickness, molar length, etc. JU/GD/VPL/9001 is also compared with the specimen No. WIF/A 423 (Nanda et al., 1991) which favours *E. planifrons.*

Based on the above comparative studies of parameters such as plate number, lamellar frequency, hypsodonty index, straight molar curvature, greatest height of crown at posterior end, molar shape tapered at posterior end (ovate), thick cement on the sides and valleys, enamel highly crenulated, molar roots strong and broken, high enamel height above the cement, parallel sided with median loops expansion, rounded lateral sides of enamel and symmetrical in line with long axis of molar and discussion, JU/GD/VPL/9001 shows close affinity to *Elephas planifrons* and tentatively referable as *Elephas* cf. *E. planifrons.*

4 Biozones/faunal interval zones

Various biostratigraphic interval zones of Siwalik Group of Pakistan have been recognized based on fauna and lithology and magnetostratigraphy by number of workers (Pilgrim, 1913; Barry et al., 1982; Azzaroli, 1985; Hussain et al., 1992). In India, Verma (1988) recognised two biozones based on his work in the Markanda valley of Himachal Pradesh. These biozones are *Equussivalensis–Elephas hysudricus* (EE) Biozone and *Stegodon insignis*–

chinaXiv:201711.01925v1

ChinaXiv合作期刊

Hipparion theoboldi–Hexaprotodon sivalensis (SHH) Biozone.

The SHH biozone evidently corresponds to the *Hexaprotodon sivalensis* Interval Zone of Potwar Plateau (Pakistan) ranging from 5.3–2.9 Ma B.P. (Barry et al., 1982) and EE biozone corresponds to the *Elephas planifrons* Interval Zone ranging from 2.9–1.5 Ma B.P. and Pinjor Faunal Zone of the type area respectively. The SHH biozone is restricted to the Saketi Formation and exhibits a high frequency of aquatic forms in Himachal Pradesh and EE biozone is characterised by the presence of *Equus*, absence of *Hipparion*, presence of some aquatic forms and terminates at the end of Pinjor Formation.

The range of *Elephas planifrons* Interval Zone was modified by Hussain et al. (1992) from 2.9–1.5 to 3.4–2.7 Ma and also recognised a fifth zone known as *Elephas hysudricus* Range Zone (2.7–? Ma). Later the upper limit of the *E. hysudricus* Range Zone was proposed by Nanda (1997) up to 0.6 Ma based on the fossils available in the Indian Siwalik. The lower limit of *E. planifrons* Interval Zone was modified by Agarwal et al. (1993) and was extended up to 3.6 Ma based on dated *E. planifrons*. Nanda (1997) recognised two biostratigraphic interval zones of the Upper Siwalik Subgroup with their lower and upper limits as: 1) *E. hysudricus* Range Zone (contains most of taxa of Pinjor fauna), 2.6–0.6 Ma; 2) *E. planifrons* Interval Zone (contains most of taxa of Tatrot fauna), 3.6–2.6 Ma.

Based on the presence of fauna in the Pabbi Hills of Upper Siwalik of Pakistan, Dannell et al. (2006) divided the *Elephas hysudricus* Range Zone of Hussain et al. (1992) into *Elephas hysudricus–Crocuta–Ursus–Panthera* faunal zone, 1.7–0.9 Ma, and *Elephas hysudricus–Sivatherium* faunal zone, 2.7–1.7 Ma.

As the *Elephas* cf. *E. planifrons* in the present study has been recovered from the mudstone horizon underlying geochronologically dated (2.48 Ma) volcanic ash beds (Ranga Rao et al., 1988), the upper limit of range zone of *Elephas planifrons* may be extended from 2.6 (Nanda, 1997) to 2.48 Ma (proposed). The biostratigraphic interval and range zones of the elephant fauna by various authors and proposed range zone of *Elephas planifrons* are given in Fig. 3.

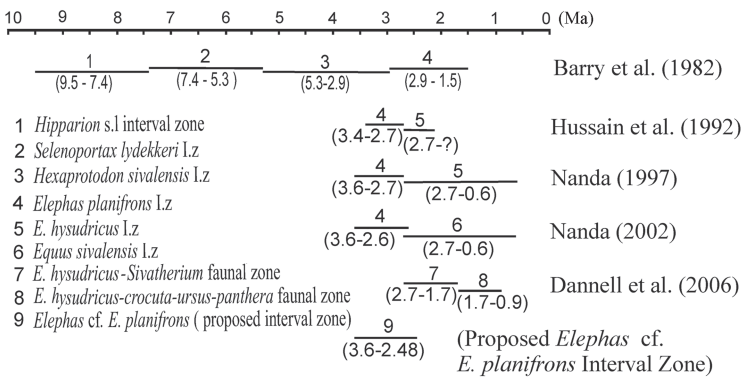

Fig. 3 Faunal interval zones suggested by various authors and proposed *Elephas planifrons* Interval Zone

chinaXiv:201711.01925v1

ChinaXiv合作期刊

5 Conclusion

The recovery of *Elephas* cf. *E. planifrons* specimen from the mudstone underlying geochronologically dated (2.48 Ma) volcanic ash bed indicates that the age of the specimen is not younger than the volcanic ash beds exposed in the Upper Siwalik Subgroup of Samba districts. The upper limit of the *Elephas* cf. *E. planifrons* Interval Zone is also extended from 2.6 (Nanda, 1997) to 2.48 Ma (proposed) in the present study as the specimen recovered from underlying geochronologically dated ash bed.

Acknowledgements The author is thankful to UGC, New Delhi, India for financial support under UGC-BSR project (No. 20-3(6)/2012 dated 30.3.2013) and SERB NO. SR/FTP/ES-71/2013 dated 24.6.2015. Thanks are also due to Liqun Shi, Executive Editor, Vertebrata PalAsiatica (IVPP), for closely review the manuscript.

chinaXiv:201711.01925v1

查谟-克什米尔桑巴地区上西瓦立克亚群中的平额象化石

Som Nath KUNDAL Gyan BHADUR Sandeep KUMAR

(印度查谟大学地质系 查谟 180006)

摘要：报道和描述了一件平额象左侧M3化石。新材料产自Nangal村附近火山灰层之下的泥岩层，该火山灰是出露于查谟-克什米尔桑巴地区Barakhetar上西瓦立克亚群Nagrota组中年龄为2.48 Ma的火山灰层的延伸。根据齿板数，臼齿长和宽，齿冠长、宽和高，釉质和齿质厚度，齿板长和宽，齿脊频率，冠高指数以及白垩质厚度等齿冠形态参数，暂时将之归为*Elephas* cf. *E. planifrons*。新材料的发现将该种的分布上限从2.6 Ma提高到2.48 Ma。

关键词：印度查谟，上西瓦立克亚群，Nagrota组，象类

中图法分类号：Q915.878 **文献标识码**：A **文章编号**：1000−3118(2017)01−0059−12

References

Agarwal R P, Nanda A C, Prasad D N et al., 1993. Geology and biostratigraphy of the Upper Siwalik of Samba area, Jammu foothills. Him Geol, 4(2): 227–236

Aguirre E, 1969. Evolutionary history of elephants. Science, 164: 1366–1376

Azzaroli A, 1985. Provinciality and turnover events in late Neogene and early Quaternary vertebrate faunas of the Indian Subcontinent. In: Gupta V J ed. Geology of Western Himalaya. Delhi, India: Hindustan Publishing Corp. 27–38

Azzaroli A, Nepoleone G, 1981. Magnetostratigraphic investigation of the Upper Siwalik near Pinjor, India. Riv Ital Paleont, 87(4): 739–762

Badam G L, Kumar A, 1982. Fossil Proboscidea from the Siwalik of Raipur Rani, Ambala, Hayrana. Bull Deccan Coll Res Inst, 41: 1–10

Badgley C J, Nelson S V, Barry J C et al., 2005. Testing models of faunal turn over with Neogene mammals from Pakistan.

ChinaXiv合作期刊

In: Lieberman D E, Smith R H, Kelley J eds. Interpreting the Past: Essays on Human, Primate and Mammals Evolution. Boston: Brill. 29–46

Badgley C J, Barry J C, Morgan M E et al., 2008. Ecological changes in Miocene mammal's record show impact of prolonged climatic forcing. Proc Nat Acad Sci, 105: 12145–12149

Barry J C, Flynn L J, 1990. Key biostratigraphic events in the Siwalik sequence. In: Lindsay E H, Fahlbusch V, Mein P eds. European Neogene Mammal Chronology. New York: Plenum Press. 557–571

Barry J C, Lindsay E H, Jacobs L L, 1982. A biostratigraphic zonation of the Middle and Upper Siwalik of Potwar Plateau of northern Pakistan. Palaeogeogr Palaeoclimat Palaeoecol, 37: 95–130

Barry J C, Morgan M E, Flynn L J et al., 2002. Faunal and environmental change in the Late Miocene Siwalik of northern Pakistan. Palaeobiol Mem, J Palaeont Soc India, 3: 1–71

Barry J C, Behrensmeyer A K, Badgley C E et al., 2013. The Neogene Siwalik of Potwar Plateau, Pakistan. In: Wang X M, Flynn L J, Fortelius M eds. Fossil Mammals of Asia: Neogene Biostratigraphy and Chronology. New York: Columbia University Press. 373–399

Basu P K, 2004. Siwalik mammals of Jammu Sub-Himalaya, India: an appraisal of their diversity and habitat. Quat Int, 1: 105–118

Behrensmeyer A K, Barry J C, 2005. Biostratigraphy surveys in the Siwaliks of Pakistan: a method for standardized surface sampling of the vertebrate fossil record. Palaeont Electron, 8(1), 15A: 24, http://palaeo-electronica.org/2005_1/behrens 15/issue 1_05.htm

Bhandari A, Kundal S N, 2008. Ostrocodes from the Nagrota Formation, Upper Siwalik Subgroup, Jammu, India. Rev Espan Micropaleont, 40(1-2): 151–166

Bhat G M, Kundal S N, Prasad G V R, 2008. Depositional origin of tuffaceous units in the Pliocene, Upper Siwalik Subgroup, Jammu (India), NW Himalaya. Geol Mag, 145(2): 279–294

Chakravarti D K, 1965. A geological, palaeontological and phylogenetical study of the Elephantoidea of India, Pakistan and Burma. In: West R D ed. D. N. Wadia Commemorative Volume, Mining-2. Kolkata: Mining and Metallurgical Institute, India. 255–272

Colbert E H, 1935. Siwalik mammals in the America Museum of Natural History. Am Philos Soc Trans NS, 26: 1–401

Dennell R, Coard R, Turner A, 2006. The biostratigraphy and magnetic polarity zonation of the Pabbi Hills, northern Pakistan: an Upper Siwalik Formation (Pinjor Stage) Upper Pliocene–Lower Pleistocene fluvial sequence. Palaeogeogr Palaeoclimat Palaeoecol, 234: 168–185

Flynn L J, Barry J C, Morgan M E et al., 1995. Neogene Siwalik mammalian lineages: species longevities, rate of change and modes of speciation. Palaeogeogr Palaeoclimat Palaeoecol, 115: 249–264

Flynn L J, Lindsay E H, Pilbeam D et al., 2013. The Siwalik and Neogene evolutionary biology in South Asia. In: Wang X M, Flynn L J, Fortelius M eds. Fossil Mammals of Asia: Neogene Biostratigraphy and Chronology. New York: Columbia University Press. 353–372

Ganjoo R K, 1985. Some new fossil Proboscidea from the Siwalik of Jammu. CAS Geol, Punjab Univ, Chandigarh, 1: 177–184

Ganjoo R K, 1992. On the evolution of the Pleistocene elephants in the Indian Subcontinent and their ecological implications. Islamabad, Pakistan: Proceedings of the First South Asia Geological Congress. 46–51

Gheerbrant E, Tassy P, 2009. L'origine et l'evolution des elephants. C R Palevol, 8: 281–294

chinaXiv:201711.01925v1

ChinaXiv合作期刊

Gupta S S, 2000. Lithostratigraphy and structure of the Siwalik succession and its relationship with the Muree succession around Ramnagar area, Udhampur district, Jammu and Kashmir. Him Geol, 21: 53–61

Gupta S S, Verma B C, 1988. Stratigraphy and vertebrate fauna of the Siwalik Jammu District Group, Mansar-Uttarbaini section, J & K. J Palaeont Soc India, 33: 117–124

Hooijer D A, 1955. Fossil Proboscidea from the Malay Archipelago and Punjab. Zool Verh Mus Leiden, 28: 1–146

Hussain S T, Vandenberg G D, Steensma K J et al., 1992. Biostratigraphy of Plio-Pleistocene continental sediments (Upper Siwalik) of the Mangla-Samwal Anticline, Azad Kashmir, Pakistan. Proc K Ned Acad Wet, 95: 65–80

Johnson N M, Opdyke N D, Lindsey E H et al., 1982. Magnetic polarity stratigraphy and ages of Siwalik Group rocks of the Potwar Plateau, Pakistan. Palaeogeogr Palaeoclimat Palaeoecol, 37: 17–42

Johnson N M, Stix J, Tauxe L et al., 1985. Palaeomagnetic chronology, fluvial processes and tectonic implications of the Siwalik deposits near Chinji village, Pakistan. Geology, 93: 27–40

Keller H M, Tahirkheli R A K, Mirza M A et al., 1977. Magnetic polarity stratigraphy of the Upper Siwalik deposits, Pabbi Hills, Pakistan. Earth Planet Sci Lett, 36: 187–201

Kundal S N, 2012. Micro-Biotic composition of Nagrota Formation Upper Siwalik Subgroup of Jammu, Jammu and Kashmir, India. Int J Curr Res, 4(12): 60–65, http://www.journalcra.com

Kundal S N, 2013. Late Pliocene (Piacenzian Stage) fossil molluscs from Upper Siwalik Subgroup of Jammu, Jammu and Kashmir, India. Int Res Earth Sci, 1(4): 10–17, www.isca.in

Kundal S N, 2015. Microfossils based palaeoecology and palaeocommunity structure of Upper Siwalik deposits of Jammu, J and K, India. Int Res J Biol Sci, 4(1): 34–40, www.isca.in

Kundal S N, Prasad G V R, 2011. ? Late Pliocene-Early Pleistocene microvertebrates from the Upper Siwalik Subgroup of Jammu, Jammu and Kashmir, India. Earth Sci India, 4(3): 143–158, http://www.earthscienceindia.info/

Kundal S N, Bhat G M, Pandita S K et al., 2011. Field observations, mineralogical composition and XRD analysis of bentonitized tuff band, Jammu Province, Jammu and Kashmir, India. Int J Dev St, 5(1): 77–86

Kundal Y P, Kundal S N, 2011. *Elephas* cf. *E. maximus indicus* (Elephantidae, Mammalia) from the Post Siwalik deposits of Jammu Province, Jammu and Kashmir, India. Vert PalAsiat, 49(3): 348–361

Lewis G E, 1937. A new Siwalik correlation. Am J Sci, 5: 191–204

Maglio V J, 1973. Origin and evolution of the Elephantidae. Trans Am Philos Soc, New Ser, 63(3): 1–145

Nanda A C, 1994. Upper Siwalik mammalians from Chandigarh and Jammu regions with comments on certain faunal discrepancies. Islamabad, Pakistan: Proceedings of First South Asia Geological Congress 1992. 39–45

Nanda A C, 1997. Comments on Neogene/Quaternary boundary and associated faunas in the Upper Siwalik of Chandigarh and Jammu. In: Quaternary Geology of South Asia. Madras, India: Anna University. 20–136

Nanda A C, 2002. Upper Siwalik mammalian faunas of India and associated events. J Asian Earth Sci, 21: 47–58

Nanda A C, Gudurun C, 1992. A report on the occurrence of Tatrot and Pinjor faunas from the Siwalik Group of Nepal. Him Geol, 3(2): 209–211

Nanda A C, Sati D C, Mehra G S, 1991. Preliminary report on the stratigraphy and mammalian faunas of the Middle and Upper Siwalik west of river Yamuna, Paonta, Himachal Pradesh. Him Geol, 2(2): 151–158

Opdyke N D, Lindsay E, Johnson G D et al., 1979. Magnetic polarity stratigraphy and vertebrate palaeontology of the Upper Siwalik Subgroup of northern Pakistan. Palaeogeogr Palaeoclimat Palaeoecol, 27: 1–34

Opdyke N D, Johnson G D, Lindsay E H et al., 1982. Palaeomagnetism of the Middle Siwalik Formation of the northern

chinaXiv:201711.01925v1

ChinaXiv合作期刊

Pakistan and rotation of the salt range decollement. Palaeogeogr Palaeoclimat Palaeoecol, 23: 1–15

Osborn H F, 1942. Proboscidea: a Monograph of the Discovery of Evolution, Migration and Extinction of Mastodonts and Elephants of the World. 2. Stegodontioidea and Elephantoidea. New York: The American Museum Press. 805–1676

Patnaik R, 2013. Indian Neogene Siwalik mammalian biostratigraphy: an overview. In: Wang X M, Flynn L J, Fortelius M eds. Fossil Mammals of Asia: Neogene Biostratigraphy and Chronology. New York: Columbia University Press. 423–444

Pilgrim G E, 1913. The correlation of the Siwalik with mammal horizons of Europe. Rec Geol Surv India, 43: 264–326

Pilgrim G E, 1934. Correlation of the fossiliferous sections in Upper Cenozoic of India. Am Mus Novit, 704: 1–5

Prasad G V R, Kundal S N, Bhat G M, 2005. Mandible of *Golunda* (Rodentia, Mammalia) from the Upper Siwalik Subgroup of Jammu, India. Ann Paleont, 91: 181–196

Ranga Rao A, Agarwal R P, Sharma U N et al., 1988. Magnetic polarity stratigraphy and vertebrate palaeontology of the Upper Siwalik Subgroup of Jammu Hills, India. J Geol Soc India, 31: 361–385

Sahni M R, Khan E, 1959. Stratigraphy, structure and correlation of the Upper Siwalik east of Chandigarh. J Palaeont Soc India, 4: 61–74

Samiullah K, Akhtar M, Yasin R et al., 2014. Proboscidean fossil fauna from the Siwalik Hills of Pakistan. VIth International Conference on Mammoths and Their Relatives, Abstract Volume. Sci Ann School Geol, Spec Vol, 102: 176–177

Sankhyan A R, Sharma S L, 2014. Insitu dental remains of *Deinotherium* from northwest Indian Siwalik. Him Geol, 35(1): 75–81

Sarwar M, 1977. Taxonomy and distribution of the Siwalik Proboscidea. Zool Dept Bull, Punjab Univ, New Ser, 10: 1–172

Shoshani J, Tassy P, 1996. The Proboscidea. Evolution and Palaeoecology of Elephants and Their Relatives. New York: Oxford University Press, 30: 1–472

Shoshani J, Tassy P, 2005. Advances in proboscidean taxonomy & classification, anatomy & physiology and ecology behaviour. Quat Int, 126–128: 5–20

Tassy P, 1983. Les Elephantoidea Miocenes du Plateau du Potwar, groupe de Siwalik, Pakistan. Ann Paléont, 69: 96–136 (I); 235–297 (II)

Todd N E, 2010a. New phylogenetic analysis of the family Elephantidae based on cranial-dental morphology. Anat Rec, 293: 74–90

Todd N E, 2010b. Qualitative composition of the cranio-dental osteology of the extant elephant, *Elephas maximus* (Asian elephant) and *Loxodont africana* (African elephant). Anat Rec, 293: 62–273

Tripathi C, Basu P K, 1983. A fossil elephant from the Middle Pleistocene alluvial deposits of Narmada Valley, M. P. J Palaeont Soc India, 28: 63–66

Verma B C, 1988. Records of tooth of *Elephae* (*Hypselephas*) *hysudricus* from Upper Siwalik, Una district, H. P: phyletic relationships of the species and its bearing on age of the beds. Geoscience, 19(2): 79–85

Wadia D N, 1925. *Stegodon ganesa* in the outer Siwalik of Jammu. Rec Geol Surv India, 56: 352–355

Wadia D N, 1957. Geology of India. London: MacMillian & Company. 1–536

Wei G B, Taruno H, Kawanura Y, 2006. Pliocene and Early Pleistocene primitive mammoths of northern China: their revised taxonomy, biostratigraphy and evolution. J Geol Sci Osaka City Univ, 49: 59–101

chinaXiv:201711.01925v1

ChinaXiv合作期刊

第55卷 第1期
2017年1月

古 脊 椎 动 物 学 报
VERTEBRATA PALASIATICA

pp. 71–88
figs. 1–7

Small mammal taphonomy of three Miocene localities from Damiao, Nei Mongol, China

Leena SUKSELAINEN[1] Hannele PELTONEN[1] Anu KAAKINEN[1] ZHANG Zhao-Qun[2]

(1 *Department of Geosciences and Geography, University of Helsinki* Helsinki FI-00014, Finland leena.sukselainen@gmail.com)
(2 *Key Laboratory of Vertebrate Evolution and Human Origins of Chinese Academy of Sciences, Institute of Vertebrate Paleontology and Palaeoanthropology, Chinese Academy of Sciences* Beijing 100044, China)

Abstract Predation is the most common cause of death in small mammals. It also causes the greatest modification on their remains. Other postmortem processes, such as weathering, trampling, and transportation all modify bones and contribute to the forming assemblage. Here we examined three Miocene localities from Damiao, Nei Mongol, China with different fluvial subenvironments. The ages span from early Miocene to early late Miocene (ca. 21–11.6 Ma). We describe the sedimentary context and taphonomic features of the small mammal assemblages, and identify the responsible agents for the fossil accumulations. Our study reveals predation as primary means of accumulation for all three localities. However, there is overprinting of other means of accumulation such as fluvial transportation and possibly signs of trampling at the two younger localities. Results indicate possibly different predators for all localities; owls for the oldest one, and diurnal birds of prey or mammalian agents for the younger two. We also show that systematic excavation for small mammals can be done, and in this way it may be possible to reduce some of the damage collecting always produces.

Keywords Nei Mongol, Neogene, micromammals, digestion, predation, fluvial deposits

Citation Sukselainen L, Peltonen H, Kaakinen A et al., 2017. Small mammal taphonomy of three Miocene localities from Damiao, Nei Mongol, China. Vertebrata PalAsiatica, 55(1): 71–88

chinaXiv:201711.01925v1

1 Introduction

Taphonomy, the study of preservational processes of organic remains, connects paleontology with biology and geology (Behrensmeyer et al., 2000; Efremov, 1940). Taphonomic processes begin at the moment of death of an organism and continue till its recovery (e.g., Arcos et al., 2010; Lyman, 1994). These processes are sources of bias in the fossil record since they may remove some of the biological information but on the other hand produce information of past environments and fossilization (Arcos et al., 2010; Behrensmeyer and Kidwell, 1985; Fernández López, 1981, 1991). Taphonomic processes affecting fossil assemblages include predation, scavenging, transport, and weathering (e.g., Andrews, 1990;

国家自然科学基金(批准号: 41472003, 41402003)和国家重点基础研究发展计划项目(编号: 2012CB821904)资助。

收稿日期：2016-05-03

ChinaXiv合作期刊

Andrews and Evans, 1983; Behrensmeyer, 1978; Lyman, 1994) and they are portrayed by different taphonomic features such as breakage, intrusive corrosion, rounding, polishing, cracks, staining, scrapes, weathering, root marks, pressure damage, and enamel pitting (Table 1).

Table 1 Taphonomic features characteristic of different taphonomic agents

	Predation	Weathering	Transport	Postdepositional	Trampling
Breakage	✓	✓	✓	✓	✓
Corrosion	✓			✓	
Cracks	✓	✓		✓	
Enamel pits	✓			✓	
Polishing	✓	✓	✓		
Pressure damage				✓	
Root marks				✓	
Rounding	✓	✓	✓		
Scrapes	✓				✓
Staining	✓			✓	
Lack of skulls					✓
Abundance of isolated teeth			✓		✓
Abundance of proximal femora					✓
Abundance of distal humeri			✓		✓
Abundance of distal tibiae			✓		
Abundance of proximal ulna			✓		
Loss of distal elements	✓				
Loss of postcranial elements	✓				

Note: Based on Wolff, 1973; Mayhew, 1977; Andrews and Evans, 1983; Andrews, 1990; Fernández-Jalvo, 1995; Reed and Denys, 2011.

Due to the limited life range of small mammals they are more sensitive to the local scale environmental changes than large mammals (Demirel et al., 2011; Redding, 1978; Soligo and Andrews, 2005) and therefore they are useful indicators of past ecologies (e.g., Van Dam, 1997, 2006; Van Dam and Weltje, 1999).

One of the major causes of death of small mammals is predation (e.g., Andrews, 1990; Andrews and Evans, 1983; Fernández-Jalvo, 1995; Reed and Denys, 2011). Predation is also the cause of the greatest modification of small mammal remains (Andrews, 1990). Of different predators, mammals modify the bones of their prey the most due to the usage of their shearing teeth in breaking up the prey before ingestion and due to this damage prey of mammalian predators is less likely to become fossilized (Andrews and Evans, 1983). The least amount of bone breakage is produced by owls, while diurnal birds of prey are intermediate bone breakers (Andrews and Evans, 1983; Andrews, 1990).

Shortly after the death of a small mammal, secondary modifications of the remains takes place. These include decay, and scavenging, which are not easily recognized in fossil samples, for decay leaves little modification, and marks left by scavenging are not readily distinguished from modification by predation. Trampling is another source of modification beginning soon after death resulting in dispersal, breakage, burial or total destruction of the animal remains. (Andrews, 1990; Arcos et al., 2010; Williams, 2001). Weathering occurs when bones are lying

chinaXiv:201711.01925v1

ChinaXiv合作期刊

in the open without protection of some kind (Andrews, 1990; Behrensmeyer, 1978). However, small mammal remains are more likely to be trampled and broken or blown away than to remain exposed to weathering (Andrews, 1990).

Transport of the remains often results in breakage of the bones. However, pellets and scat structures may protect bones for some time (Andrews, 1990; Arcos et al., 2010), but when pellets disintegrate the skeletal material will be exposed to weathering and dispersal (Andrews, 1990; Korth, 1979). Small mammal remains are easily transported by flowing water (Andrews, 1990; Dodson, 1973).

In this study we examine the small mammal taphonomy from three Miocene mammal localities from Damiao in Siziwang Banner, Nei Mongol (Fig. 1). The site was identified in 2006 and has been excavated in three field seasons since. These excavations have yielded over 30 fossil localities with three main fossil horizons that are magnetostratigraphically dated to range from early Miocene to earliest late Miocene (Kaakinen et al., 2015). Although numerous, the Neogene fossil mammal localities in Central Nei Mongol are scattered, lacking continuous vertical exposures and there are few representatives of early Miocene mammals (Kaakinen et al., 2015; Wang et al., 2009). In Damiao the strata constitute one of the most continuous sequences in Nei Mongol with early, middle, and late Miocene fossil faunas in stratigraphic superposition. Damiao also hosts the latest occurrence of the humid favouring pliopithecid primate in Central Asia, in the late middle Miocene locality of DM01 (Zhang and Harrison, 2008). Out of the circa 30 localities, three rich localities of different age and sedimentology were chosen for closer inspection. The stratigraphy (Kaakinen et al., 2015) and some mammalian groups have been studied in detail (Wang and Zhang, 2011; Zhang et al., 2011). This however is the first attempt to study the small mammal taphonomy from the area.

Here we report the results of a taphonomic study of small mammals found from three localities in Damiao. The aims of the study are to characterize the sedimentary context and taphonomic features of the small mammal burials, and to identify the agent(s) responsible for the fossil accumulations. This study also shows that systematic excavation for small mammals can be done and in this way it is possible to reduce some of the damage that always results from the collecting “no matter how careful the technique” (Andrews, 1990).

2 Sedimentological and paleontological framework

The study area is located in central Nei Mongol, ca. 100 km north from Hohhot, near Damiao village in Siziwang Banner (Fig. 1). The area is distinguished by undulating topography ranging between 1250 m and 1350 m a. s. l. The Damiao fossil localities are divided into eastern and western sides that are separated by the Wulanhua-Damiao motorway. All the localities in the area are only a few kilometers from each other. The sedimentary sequence is characterized as a fluvial environment where the bulk of the fine-grained deposits in the sequence represent well-drained floodplains (Kaakinen et al., 2015).

chinaXiv:201711.01925v1

ChinaXiv合作期刊

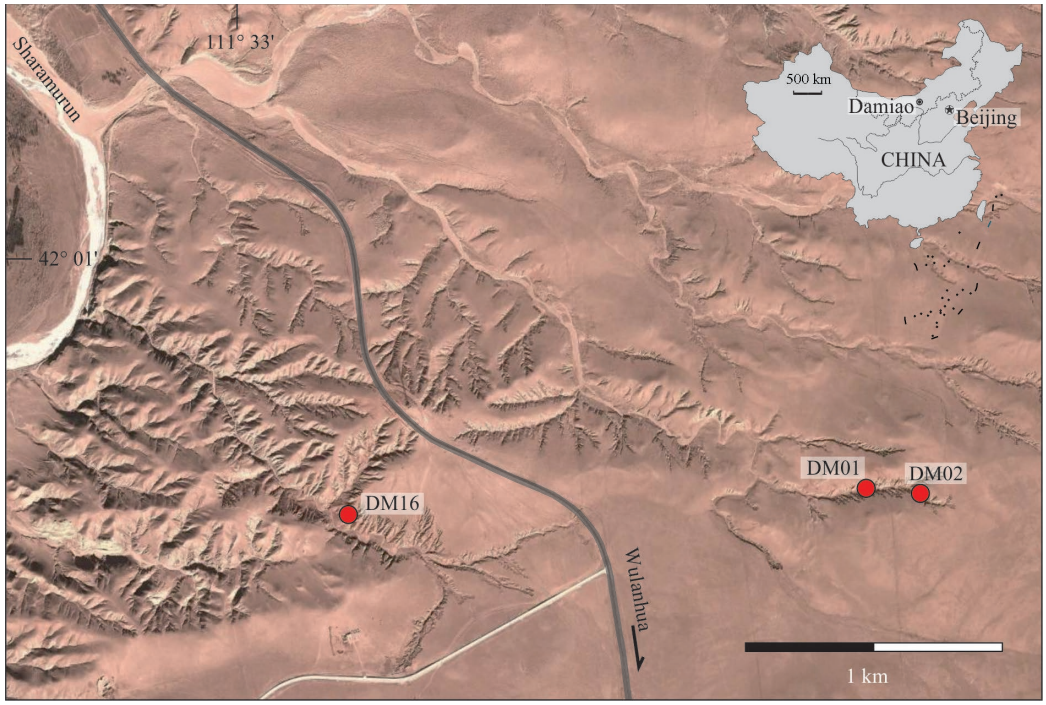

Fig. 1 Locations of the three studied localities at Damiao, Nei Mongol, China

DM16 is stratigraphically the lowest fossil site in Damiao and was paleomagnetically dated at 20–21 Ma (Kaakinen et al., 2015). It occurs within a mudstone interval comprising the basal 16 m of the sequence and extending laterally over hundreds of metres. The sediment succession at DM16 (Fig. 2) comprises rather monotonous and homogenous redbrown claystone - fine siltstones that commonly exhibit massive weathering appearance. Thin flat lamination and graded beds 1–4 cm thick are recorded in the upper portion of the section. Slickensides, spherical mm-size manganese and calcium carbonate nodules occur throughout and are locally abundant. Some fine-scale alternation of red and green coloration is discernable in the lower portion of this interval.

The productive bed is ca. 1.2 m thick, with one ca. 9 cm thick fossil-rich horizon in the middle of the bed, and is associated with root traces and few desiccation cracks. The bonebed has yielded relatively well preserved but fragmented vertebrate fossil remains, comprising mainly small mammal skeletal elements; dipodid and eomyid rodents are common as well as ochotonid lagomorphs with few insectivores. Large mammals are scarcer and represented by artiodactyls, rhinos and a mustelid. Small mammals at this level are dominated by Oligocene genera, however, by more derived species. In addition to vertebrate remains, the locality contains a dense accumulation of fossil eggshell fragments, a few gastropod shell casts and several bone-bearing pellets in the richest horizon.

Laterally extensive, massive and finely-laminated mudstones that possess a variety of features indicating paleosol development are characteristic of floodplain deposits (Miall,

chinaXiv:201711.01925v1

ChinaXiv合作期刊

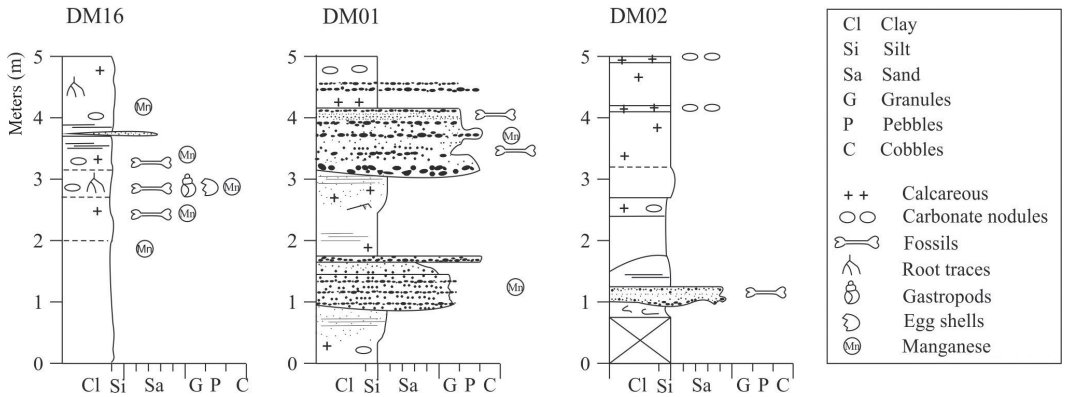

Fig. 2 Sediment lithology for three Damiao localities

1977, 1992, 1996). The sporadic desiccation cracks indicate that the mudstones were probably deposited as ephemeral ponds/lakes at the highest flood stage, and cracks were developed during desiccation (Miall, 1977, 1992).

The richest and only primate-bearing locality, DM01 is associated with latest middle Miocene Tunggur fauna with an age estimate of ca. 12.1 Ma (Kaakinen et al., 2015; Zhang et al., 2011, 2013). The DM01 section is dominated by two clast-supported conglomerate beds that stretch laterally over 60 meters. The well-sorted and densely packed clasts in these beds consist principally of spherical and well-rounded intraformational reworked calcium carbonate nodules up to 8 cm in diameter. The lower unit is up to 60 cm thick and is composed of few-cm-thick beds that often show inverse grading from coarse sand to granules. The upper conglomerate shows variable bed thickness from 1 m to 1.6 m and mainly consists of horizontally stratified pebble-granule conglomerate with subordinate layers of coarse sand and granules. In the sand-dominated parts the internal structures are trough and tabular cross bedding. The lower boundaries are erosive and exhibit discrete scours locally. These reworked pedogenic conglomerates show distinct rust and black colour in the outcrop; concretions have a black manganese staining and manganese and goethite highlights the bedding planes.

The sediments surrounding the conglomerates are mainly composed of well-sorted reddish yellow (7.5 YR 6/6) to light brown (7.5 YR 6/4) fine sands and silts. The primary sedimentary structures, when present, include thin parallel lamination and cross-lamination. These sediments are often calcareous but calcareous nodules are scarce and continuous concretion horizons are absent.

The nodule conglomerates are interpreted as resulting from the avulsive emplacement of channels reworking and concentrating the underlying calcic paleosols (Kaakinen et al., 2015). The abundant occurrence of goethite and manganese indicate an impeded drainage and more humid conditions, although the reworked pedogenic nodules indicate that climate was seasonally dry (cf. Van Itterbeeck et al., 2007).

Fossils occur in the sand-granule interbeds throughout the upper nodule conglomerate.

chinaXiv:201711.01925v1

ChinaXiv合作期刊

In addition to the pliopithecid, more than 30 species and more than one thousand skeletal elements were found. While large mammals are few and fragmentary, small mammals are abundant and characterized by well-preserved remains. Contrary to DM16 fauna, DM01 fauna is composed of taxa from extant families lacking any Paleogene members.

DM02 locality represents early late Miocene with estimated age of ca. 11.6 Ma (Kaakinen et al., 2015; Zhang et al., 2011, 2013). The DM02 section is predominately fine-grained (Fig. 2). Lithologies are mixtures of reddish brown (5 YR 4/4) to yellowish red (5 YR 4/6) silt and clay with variable amounts of calcium carbonate accumulation as distinct nodules and indurated layers. Most units exhibit no internal bedding structures. DM02 fossils are present in a 0.2–0.4 m thick lens-shaped sandstone body at the lowest portion of the local section. The fossiliferous unit erosionally overlies the underlying mudstone sequence and passes up with a sharp conformable contact to the overlying coarse siltstone. The sand lens is massive or displays a few centimeters thick horizontal interbeds of silt to poorly sorted coarse – very coarse sand. The constituent grains are mostly angular quartz, embedded in a silt matrix.

The fine-grained deposits that encompass the DM02 section are interpreted as pedogenically modified overbank deposits. Red coloration, carbonate nodules, pedogenic slikcensides and overall massive appearance in outcrop are all suggestive of pedogenesis. The fossil find unit, with its erosional base and heterogenous lithology, indicates sites of episodic injections of coarse sediment on the floodplain surface. Fossil fauna at DM02 contains abundant and diverse fossils of rodents and lagomorphs, together with few specimens of large mammals (Kaakinen et al., 2015). In general the fauna in DM02 is similar to DM01.

3 Material and methods

Materials Fossil specimens under study were collected from Damiao during three field seasons between 2007–2009. Material from DM01 consists of 185 fossil specimens, both teeth and postcrania. From DM02 158 fossil specimens in total were analyzed, mainly teeth and a few jaw fragments. There was no postcranial material available for our study from DM02. Fossil material from DM16 consists of 360 specimens from the grid of which 255 specimens were taphonomically analyzed. Half of the analyzed specimens are with full grid reference (i.e. coordinate and depth information). Majority of DM16 material is postcrania with few teeth and jaws (Table 2).

Methods At the pliopithecid bearing locality of DM01 as well as the adjacent DM02 a restricted area was opened and the sediments screened. A systematic sampling was carried out at the locality DM16, where a grid with 27 squares of 1 m × 1 m in size was set up and collected fossils were given a specific grid reference as well as for most collected specimens a precise location, both horizontal and vertical, within the grid. Dry-sieving of excavated material was done at the site using coarse screen.

The investigated specimens from Damiao showed a wide variety of taphonomic

chinaXiv:201711.01925v1

ChinaXiv合作期刊

modification. In order to detect, measure, and score the surface alterations on fossil specimens, each element was carefully examined under a stereoscopic light microscope. Taphonomic features analyzed from Damiao material for this study were: breakage, intrusive corrosion, rounding, polishing, cracks, staining, scrapes, weathering, pressure damage, root marks, and surface (enamel) pitting (Fig. 3).

Table 2 Analyzed material from Damiao localities

	DM16 (Σ255)	DM01 (Σ185)	DM02 (Σ158)
astragalus	3	0	0
calcaneum	3	0	0
femur	16	15	0
humerus	24	26	0
incisor	15	3	0
mandible	12	7	3
maxilla	1	0	3
metapodial	7	0	0
molar tooth	7	93	152
os coxae	8	5	0
phalanx	10	0	0
premolar	2	4	0
radius	5	6	0
rib	1	0	0
scapula	6	0	0
sternum	1	0	0
tibia	18	7	0
ulna	11	19	0
vertebra	1	0	0
unidentifiable	104	0	0

All the taphonomic features were scored on an ordinal scale of four stages of modification. The scale was developed for the purposes of this study based on Andrews' (1990) work on small mammal taphonomy. Scorings were made depending on the degree of the taphonomic modification on the specimen. The four stages are as follows: 0 = no modification; 1 = light modification; 2 = moderate modification; and 3 = strong modification (Fig. 4). Additionally in order to detect the microfossil accumulating agent the ratio of major distal elements to proximal elements was calculated as well as the ratio of cranial elements to postcranial elements following Andrews (1990).

Voorhies' Groups are a common way to examine skeletal elements according to their potentiality of being transported fluvially (Behrensmeyer, 1975; Lyman, 1994; Voorhies, 1969). Degree of transport reflects the different settling velocities of different types of bones (Behrenesmeyer, 1975; Korth, 1979). Voorhies' Groups have been recalibrated for micromammal studies and the Generalized Sequence of Korth's settling groups (Korth, 1979) was applied to the present data (Table 3).

Table 3 Generalized sequence of Korth's settling groups for DM16, DM01 and DM02

	I	I/II	II	II/III	III
	rib	atlas radius ulna pelvis	calcaneum astragalus humerus scapula femur (molar) maxilla	molar (small mammals)	mandible tibia
DM16	0.9	20.9	46.1	6.1	26.1
DM01		16.9	23.0	52.2	7.9
DM02		1.9	96.2	1.9	

Detailed sedimentological logging was done by applying the conventional methods for lithofacies analysis. Vertical heights were measured with Jacob's staff and Abney level (c.f.

chinaXiv:201711.01925v1

ChinaXiv合作期刊

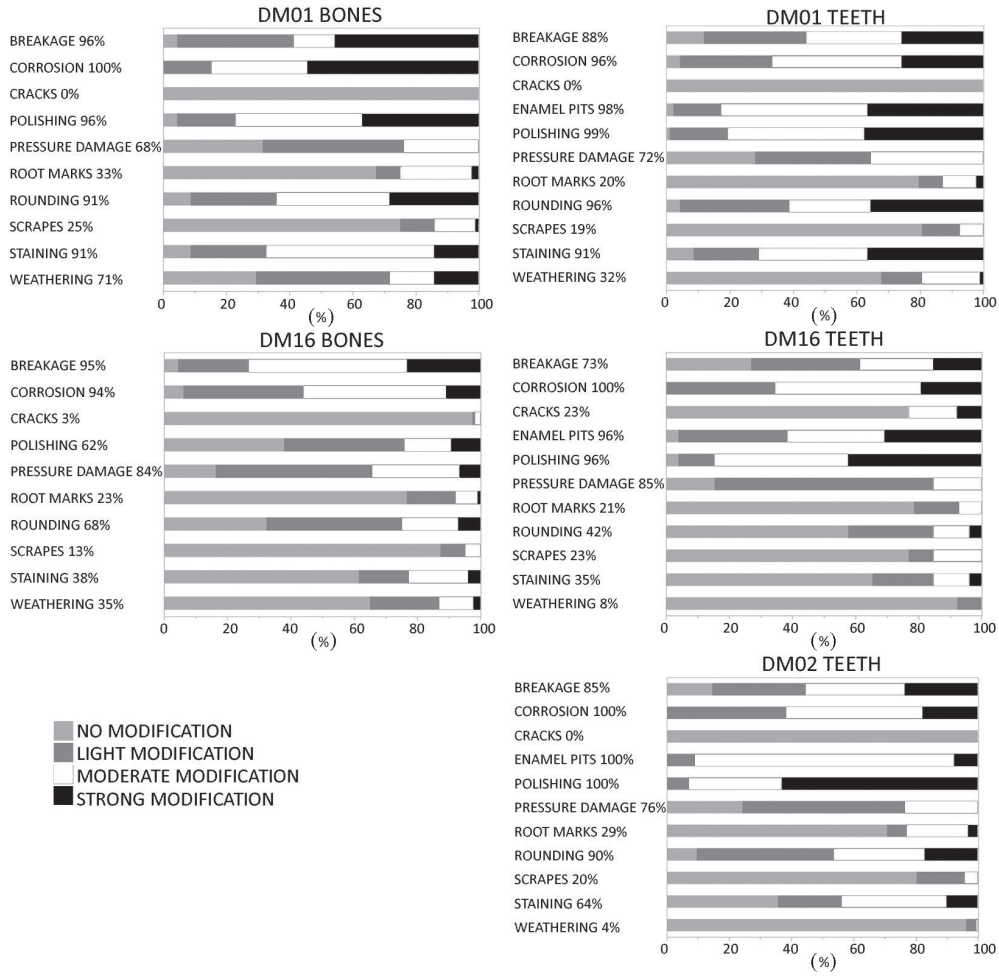

Fig. 3 Proportions of affected specimens and proportions of different stages of taphonomic features at the three Damiao localities

Fig. 4 Some examples of taphonomical features detected from Damiao fossils

A. distal end of a rodent humerus showing breakage stage 1, rounding stage 1, and intrusive corrosion stage 3; B. proximal end of a rodent ulna with shaft showing rounding stage 3, polishing stage 3, and staining stage 3; C. rodent femur with stage 2 staining, and weathering stage 3; D. distal end of rodent humerus with stage 1 staining and stage 3 intrusive corrosion; E. complete phalanx with rounding stage 1, and cracks stage 1; F. rodent incisor showing total discoloration with stage 3 breakage and stage 2 cracks. Scale bars = 1 mm

chinaXiv:201711.01925v1

ChinaXiv合作期刊

Brand, 1995), grain size was determined in the field and for selected fine-grained samples in the laboratory using a Malvern Mastersizer 2000, and sediment colours were defined as Munsell™ codes on fresh samples.

4 Results and interpretation of taphonomic features

Proportions of taphonomic features on specimens at each locality are shown in Fig. 3, bones and dental materials separately. The most prominent feature is the lack of skulls at all localities as well as lack of postcranial material at DM02 (Table 2). The ratio of major distal limb elements to proximal elements for DM16 is higher than for DM01 (Fig. 5). The ratio of cranial element to postcranial is higher in DM01 than in DM16 (Fig. 6). Both teeth and bones from DM16 showed high incidence of breakage, intrusive corrosion, rounding, polishing, cracking, enamel pitting and staining (Fig. 3), the taphonomic features that indicate predation (e.g., Andrews, 1990; Andrews and Evans, 1983; Fernández-Jalvo, 1995; Reed and Denys, 2011). The straight and spiral fracture types in broken bone specimens provide further evidence for predation (Shipman et al., 1981) as means of accumulation. Results from DM16 were also inspected with respect to the richest fossil layer. This level showed even more specimens with features associated with digestion (breakage, intrusive corrosion, and scrapes) than layers below or above it. Cracking was detected only from specimens from the richest fossil horizon and below it, and was more common in teeth than bones. Nevertheless, this feature was less common than other predation features and could result from other taphonomic agents than predation, for example from weathering during subaereal exposure of the remains. Weathering, in turn, is more common on bones than teeth but is altogether not a very common feature and can be separated from digestion by some unique features on the surface of the specimens. Weathering in small mammal remains can be identified from splitting that occurs along the collagen fiber orientation, flaking or exfoliation of the outer layer of bone (Fig. 4C) as well chipping and splitting of teeth (Andrews, 1990). Of all the localities discoloured dental specimens were found only from DM16.

The ratios of anatomical elements further suggest that predation contributed to the accumulation of the small mammals in DM16. The ratio of distal (tibia + radius) to proximal (femur + humerus) limb elements is low (Fig. 5), indicating predator assemblage, as does the ratio of postcranial to cranial elements (Fig. 6). The absence of more distal parts of limbs is a common feature in predator assemblages as is the deviation from the average skeletal proportions of postcranial to cranial elements, which indicates preferential destruction of a skeletal group - or selection against it (Andrews, 1990) -

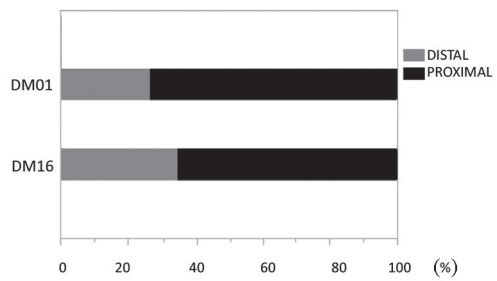

Fig. 5 Proportions of distal limb elements (tibia+ radius) to proximal limb elements (femur+ humerus) at DM16 and DM01

chinaXiv:201711.01925v1

ChinaXiv合作期刊

in this case destruction of, or selection against, cranial elements. The lack of skulls is one main feature of trampled assemblages, although in small mammals evidence of natural trampling is nearly non-existent due to the fragile nature of their bones (Andrews, 1990). Also the low number of isolated teeth at this locality suggests a source of modification of material other than trampling, such as fluvial transportation.

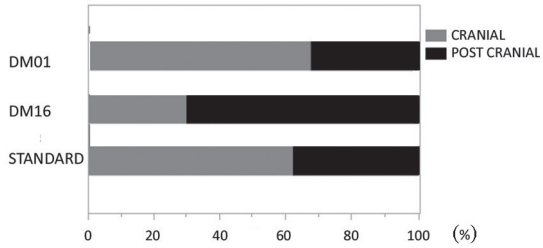

Fig. 6 Proportions of cranial to postcranial material at DM16 and DM01 compared to skeletal element ratio in an average mammal

For DM16 bones of all of Korth's settling groups are present (Table 3). However, group I (most easily affected by fluvial transport) is rather poorly represented whilst there is a high representation of least easily transported group III elements (lag deposit). The loss of group I likely results from winnowing of lighter elements during surface runoff.

Less than half of DM16 fossil bones are weathered and when they are, they mostly represent stage 1. This together with even less weathered dental material means that DM16 small mammal remains likely experienced only a short duration of exposure to weathering agents before burial. Taphonomic processes after burial in DM16 are represented by light pressure damage that is present in most specimens, and some rare light root marks. Intrusive corrosion found on specimens is likely digestive in origin as fossils are only partially affected by corrosion (Andrews, 1990).

Both teeth and bone specimens from DM01 showed high incidence of modifications related to predation (breakage, intrusive corrosion, rounding, polishing, enamel pitting and staining; e.g., Andrews, 1990; Andrews and Evans, 1983; Fernández-Jalvo, 1995; Reed and Denys, 2011). Also a high proportion of broken bones together with straight and spiral fracture types indicate predation as means of accumulation (Shipman et al., 1981). Bones from DM01 show highest incidence of stage 3 corrosion and dental material is mostly of stage 2. High incidence and high level of corrosion both on bone and dental material in DM01 suggest predation. However, the bimodal breakage distribution at DM01 could indicate two different agents forcing the accumulation. Primary means of accumulation would be predation with overprinting of other processes like transportation or trampling. It is said that much of the breakage of bone assemblages is due to transport before or after burial and transportation of small mammal bones produces high levels of breakage (Andrews, 1990). Trampling on the other hand is not well documented in small mammals since their bones are easily destroyed (Andrews, 1990). However, the lack of skulls together with a high number of isolated teeth, proximal femora and distal humeri (Fig. 7) is in accordance with the few observed trampled small mammal assemblages (Andrews, 1990). The low ratios of distal to proximal limb elements and postcranial to cranial elements in DM01 are characteristic features of many predator assemblages (Andrews, 1990) (Figs. 5, 6).

The members of group I of Korth's settling groups in DM01 are absent (Table 3). This

chinaXiv:201711.01925v1

ChinaXiv合作期刊

group is the one most easily affected by fluvial transport and might indicate DM01 is a lag assemblage (Behrenesmeyer, 1975). However, DM01 has rather low representation of group III (lag assemblage) specimens as well, and this suggests that the assemblage has been affected by fluvial transport.

In DM01 more than half of the analyzed postcranial specimens showed signs of weathering, mainly stage 1. Dental material is less often weathered but more severely, mostly stage 2, indicating short duration of exposure, but longer than in DM16. Postdepositional modification in DM01 is represented by light pressure damage that is detected on most specimens as well as rare and light root marks. Intrusive corrosion in DM01 did not affect whole surfaces and therefore is interpreted to be digestive in origin (Andrews, 1990).

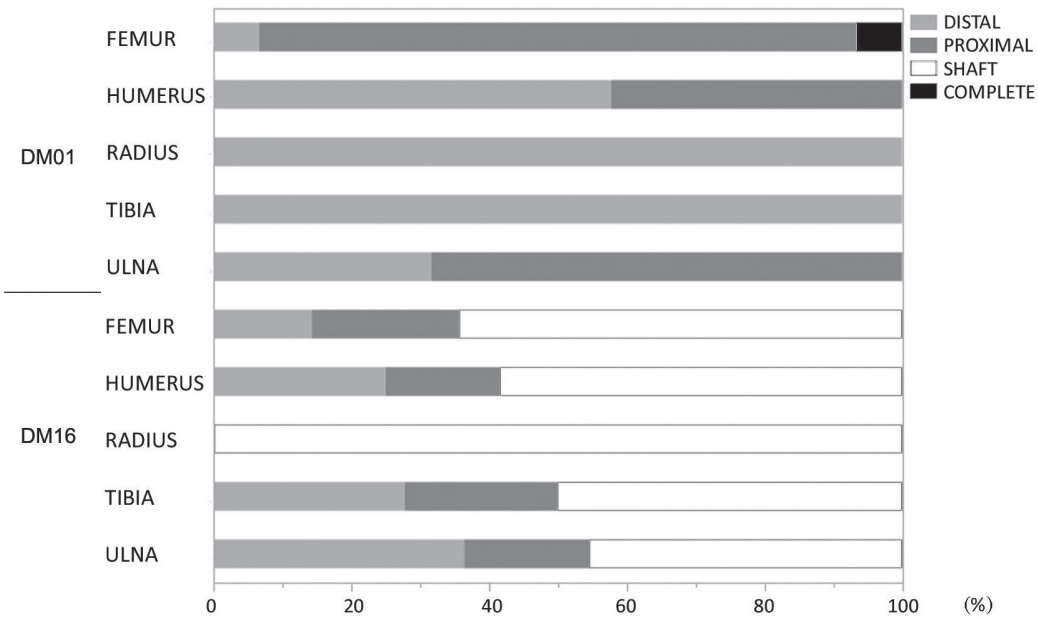

Fig. 7 Proportions of distal and proximal ends of long bones

Locality DM02 contains only small mammals and features only isolated teeth (Table 2). The dental material from DM02 presented the same taphonomic features of digestion that strongly indicate predation as for the previous unit DM01 (Fig. 3).

Trampling cannot be fully excluded as a factor affecting the DM02 small mammal fossil assemblage, since the lack of skulls may be associated with trampling (Andrews, 1990). The total absence of postcrania may also be due to trampling, since trampling causes dispersal of bones (Andrews and Cook, 1985) and in addition small mammal bones are fragile and easily broken when not protected by pellets (Andrews, 1990).

The dental material at DM02 is the least weathered of all studied localities, only 4% of teeth at DM02 showing light modification. The near lack of signs of weathering in DM02 indicates short duration of surface exposure prior to burial. After burial DM02 dental material has experienced some pressure damage and root marks, however not severe. Intrusive

chinaXiv:201711.01925v1

ChinaXiv合作期刊

corrosion is detected from all specimens but affecting only parts of the teeth suggesting digestive origins (Andrews, 1990).

5 Discussion

The large lateral continuity of the DM16 sedimentary beds, their fine-grained lithologies and associated horizontally laminated structures indicate suspension settling in the distal floodplain with periodic input of fine sands. The small mammal remains represent larger grain sizes than the range represented in the sediment matrix and therefore are not likely to have experienced much fluvial transport to the site; the low representation of lighter elements is considered as resulting from winnowing during surface runoff. Sedimentological evidence suggests that conditions were at least periodically oxidizing and conducive for soil formation as evidenced by carbonate nodules, root traces and occasional presence of mottling. The presence of bird eggshells indicates nesting sites and consequently substantiates the subaerial conditions. However, the fairly unweathered bone and teeth surfaces in DM16 do not suggest a prolonged period of subaerial exposure during dry seasons prior to burial.

The sedimentological data indicate that fossil bearing beds at DM01 resulted from reworking of the resistant pedogenic carbonate nodules into an intraformational conglomerate by fluvial avulsion. Some mechanical damage produced by transport is evident in the remains, although in light to moderate stages. It is also easily observed that DM01 shows element sorting by transport processes. The lack of skulls and high proportion of isolated teeth, distal humerus, distal tibia, and proximal ulna as well as fragmentary mandibles (cf. Wolff, 1973; Andrews, 1990) all point to fluvial transportation as a means of accumulation (Fig. 7). Weathered specimens were more common at DM01 than at DM16 although their dominantly light to moderate stages do not indicate extended subaerial exposure. Therefore it is obvious that DM01 contains materials harvested from the floodplain but, based on the relatively well-preserved nature of the remains, they have probably not been transported very long nor far.

The stratified bed of poorly sorted sand that typifies DM02 suggests relatively high-energy injection of sediment to the floodplain. Taphonomical features at DM02 locality are identical to DM01, except that the most prominent feature of DM02 is the total absence of skulls and postcranial elements. This may be due to transportation of all the lighter, more easily moved material away leaving only molars and a few mandibles behind, however, with total absence of postcrania this is uncertain. Another option could be trampling, which could have destroyed the fragile small mammal bones. However, due to the fragile nature of small mammal bones, natural trampling is rarely evidenced in small mammals (Andrews, 1990).

Natural causes of death usually leave animals well preserved, with all parts of the skeleton unbroken and typically one or only a few species present at the bone accumulations (Andrews, 1990). In the three discussed localities from Damiao this seems not to be the case. The fossils are fragmentary, with missing skeletal elements. While the identifications

chinaXiv:201711.01925v1

ChinaXiv合作期刊

of specimens are uncertain and in some cases impossible due to the fragmentary nature of material, a variety of species of small mammals were present (Tables 4–6).

Table 4 Faunal list for DM16

Artiodactyla		**Rodentia**	
Cervidae	*Lagomeryx* sp.	Muridae	*Tachyoryctoides* sp. nov.
	Stephanocemas sp. nov.	Distylomyidae	*Prodistylomys wangae*
	gen et sp. indet.		*Distylomys* cf. *D. tedfordi*
Moschidae	*Micromeryx* sp.	Dipodidae	*Sinodonomys* sp.
Insectivora			*Plesiosminthus* sp.
Erinaceidae	*Metexallerix gaolanshanensis*		*Heterosminthus* sp.
Lagomorpha		Eomyidae	*Pseudotheridomys* sp. nov.
Ochotonidae	*Sinolagomys ulunguensis*		gen. et sp. nov.

Table 5 Faunal list for DM01

Artiodactyla			*Desmatolagus morgenensis*
Cervidae	*Euprox alticus*	**Rodentia**	
	Stephanocemas sp. 1	Sciuridae	*Atlantoxerus orientalis*
	Stephanocemas sp. 2		*Eutamias* sp.
	Stephanocemas sp. 3	Dipodidae	*Heterosminthus orientalis*
Moschidae	*Micromeryx* sp.		*Protalactaga grabaui*
Carnivora		Muridae	*Gobicricetodon flynni*
Mustelidae	gen. et sp. indet.		Gobicricetodontinae gen. et sp. nov.
Insectivora			*Plesiodipus* sp.
Erinaceidae	*Mioechinus*? *gobiensis*		*Prosiphneus* sp.
Talpidae	*Desmanella storchi*		*Democricetodon* sp.
Primates		Aplodontidae	*Ansomys* sp.
Pliopithecidae	gen. et sp. indet.		gen. et sp. indet.
Lagomorpha		Castoridae	*Stenofiber hesperus*
Ochotonidae	*Bellatona fosythmajori*	Eomyidae	*Leptodontomys*
	Ochotona sp.		*Kermidomys*
	Alloptox sp.	Gliridae	*Microdyromys*

Table 6 Faunal list for DM02

Artiodactyla		**Rodentia**	
Cervidae	*Stephanocemas* sp.	Dipodidae	*Protalactaga*
Moschidae	*Micromeryx* sp.		*Lophocricetus*
Lagomorpha			*Eozapus*
Ochotonidae	*Desmatolagus*		*Gobicricetodon*
	Bellatona fosythmajori	Muridae	*Prosiphneus qiui*
	Ochotona sp.		*Nannocricetus wuae*
	Alloptox sp.		gen. et sp. indet.
Insectivora		Gliridae	gen. et sp. indet.
Erinaceidae	*Mioechinus*	Eomyidae	gen. et sp. indet.
Talpidae	gen. et sp. indet.	Aplodontidae	gen. et sp. indet.
		Castoridae	gen. et sp. indet.

Small mammal (fossil) assemblages most often result from predation (e.g., Andrews, 1990; Arcos et al., 2010; Fernández-Jalvo, 1995; Fernández-Jalvo et al., 2016). Owls are commonly cited as a source for accumulations of small vertebrate fossils (Andrews, 1990; Andrews and Evans, 1983; Dodson and Wexlar, 1979), but there is rich evidence of various other predators like diurnal raptors and mammalian carnivores involved in the accumulation of small mammal vertebrate remains as well (Andrews and Evans, 1983 and references

chinaXiv:201711.01925v1

ChinaXiv合作期刊

chinaXiv:201711.01925v1

therein). Predation seems to be a likely agent of accumulation for all localities in Damiao, however, there are differences in the intensities of digestion-associated features between localities (Fig. 3), which might point to different predator species as dominant accumulation agents. Mammalian carnivores have a complete digestion and high levels of gastric acidity and therefore digestive corrosion (Andrews, 1990). Nocturnal owls, in turn, have relatively low levels of acidity of gastric juices and corrosion whilst diurnal birds of prey feature intermediate acidity and corrosion of bone and dental remains. Signs of intrusive corrosion in Damiao specimens are very great for both bone and dental material in all three localities, being most severe in DM01 (Fig. 3) and least pronounced but abundant in DM16. DM02 molars exhibits similar distribution of corrosion stages as dental material in both DM01 and DM16. However, incisors and molars are known to have different response to digestion (Andrews, 1990; Fernández-Jalvo et al., 2016) and when excluding incisors, it is evident that DM02 and DM01 are more alike. The high incidence of intrusive corrosion could also be of pedogenic rather than digestive origin. However, the former should affect all parts of the bone rather than just small parts of it (Andrews, 1990). Considering that the fossils from Damiao are partially affected by corrosion and show other abundant predation-related taphonomic features, corrosion seems more likely to be the result of digestion for these localities.

In addition to corrosion, indications of predation in Damiao localities is evidenced by several other taphonomic features. Nearly all of the dental material from the three localities showed signs of pitting. Breaking, rounding and staining of dental material were common features in DM01 or DM02 but less abundant in DM16. These taphonomic features on both dental specimens and bones indicate predation as an accumulating agent for all localities and possibly similar, more destructive predation for DM01 and DM02 than for DM16.

Relative proportions of skeletal elements may reveal the identity of the bone accumulator since all predators produce bone loss (Andrews, 1990; Andrews and Evans, 1983; Lyman, 1994). Mammalian predators produce the largest relative loss of distal limb parts, while the opposite occurs for owls. Diurnal raptors are set in between the two groups (Andrews, 1990; Lyman, 1994). The relatively high proportion of distal limb elements and low ratio of cranial to postcranial material together with lightly digested elements suggest the involvement of owls in DM16. Several fossilized predator pellets at or right above the richest fossil layer further support this interpretation. Additionally, a few discoloured teeth indicate that diurnal raptors may have contributed to the formation of the assemblage (cf. Andrews, 1990; Mayhew, 1977). For DM01, the relatively low proportion of distal limb elements and high ratio of cranial to postcranial material point to diurnal raptor or mammalian predator as possible producers of the assemblage even without the discoloration which may be concealed by strong manganese coloration. Significant alteration by digestive processes in nearly all elements could favour a mammalian predator origin. For DM02 the teeth exhibit similar evidence of digestion as in DM01, perhaps suggesting the same predator implicated in the deposit formation.

At all localities some transportation of material is indicated, transportation of different

ChinaXiv合作期刊

duration for all localities and this results in selective loss and/or destruction of elements (e.g., Andrews, 1990; Behrensmeyer, 1975; Behrensmeyer et al., 2000; Korth, 1979). However, the fluvial transportation has not been extensive for any of the localities as the taphonomy and preservational state of specimens suggest.

All field collecting methods may play an important role in bone modification and some damage is always done (Andrews, 1990). In our study we conducted systematic excavation at DM16, and this material shows less severe stages of breakage compared to DM01 or DM02, both for bone and dental specimens. It seems likely that this method is slightly less destructive, but the differences are not statistically significant, preventing a definitive conclusion concerning the reason for breakage. The systematic sampling in DM16 did result in a clearly more representative set of specimens than DM01 (not to mention DM02) with more comprehensive representation of different skeletal elements (Table 2). However, it did not produce higher species diversity than at the two younger localities (Tables 4–6).

Large mammal fauna from Damiao has relatively stable pattern through time with cervoids as ruling group excluding the dominance of widespread open environment for the sequence (Kaakinen et al., 2015). Indication of closed and humid environment for DM01 comes from the presence of the humid favouring pliopithecoid primate (Zhang and Harrison, 2008) as well as anchitheriine horse and the cervid *Euprox alticus* (Kaakinen et al., 2015; Wang and Zhang, 2011). Sedimentological evidence also supports this with abundant goethite and manganese occurrence indicating more humid climate for DM01. However, the small mammal fauna in the entire sequence is dominated by rodents with only relatively few insectivores, which might indicate more dry and open environment (Klietmann et al., 2015; Van den Hoek Ostende, 2001) than that inferred from the large mammals. Taphonomy and preservational state of the specimens suggest that small mammals were collected within the fluvial system, however, the primary accumulators were predators. Predators, however, often prey outside their living habitats affecting the faunal composition of the fossil accumulation and further paleoecological interpretations based on the exposed fauna (e.g., Fernández-Jalvo et al., 2016) and therefore small mammals from Damiao may represent habitats of some distance away. Yet many small mammal predators, even if hunting outside their living/nesting habitats, are rarely foraging far but within few kilometers distance depending on the stage of the breeding cycle and season (e.g., Hardey et al., 2009 and references therein). It can be hypothesized that all three localities were predator accumulations that encountered fluvial transportation to the final burial sites. Based on taphonomy, sedimentology and fauna the environment was likely predominantly closed with more open surrounding areas as a gallery forest with surrounding grassland. The youngest locality, DM01, was likely the most humid.

6 Conclusions

The bone material in Damiao was mainly accumulated by predators and deposited in a fluvial setting. Some reworking by fluvial process took place in DM01 and DM02. DM16

chinaXiv:201711.01925v1

ChinaXiv合作期刊

represents distal part of the flood plain whereas DM01 portrays a channel-fill, and DM02 is a result of an episodic flood discharge to the floodplain.

Accumulating predators were likely owls for DM16, and diurnal birds of prey for DM01 and DM02. However, mammals are not fully excluded for contributing to DM01 fossil assemblage.

Systematic sampling of DM16 resulted in a wider range of skeletal material, however, it did not produce taxonomically richer sample than the more traditional excavation methods used at DM01 and DM02. Breakage was less pronounced in the systematic sample, but the difference was not statistically significant.

Environmental conditions for Damiao were rather stable throughout. It represents fluvial system, with mosaic grassland-forest environment (perhaps gallery forest with surrounding grassland). DM01, the only primate bearing locality, seems to have been the most humid, although seasonally dry.

Acknowledgements We thank the fieldwork team: Elina Hernesniemi, Aleksis Karme, Liu Liping, Liu Yan, Luo Zhiqiang, Benjamin H. Passey, Wang Lihua, and Yang Xingkai. We are grateful to Mikael Fortelius for useful comments and discussion during the process, and Liqun Shi, Lawrence Flynn, and Deng Tao for their valuable and thorough reviews on this article. Hannele Peltonen thanks Anna K. Behrensmeyer for insipiration and guidance to the secrets of taphonomy. This research was funded by Waldemar von Frenckell Foundation, the Academy of Finland, National Natural Science Foundation of China (41472003, 41402003), the Major Basic Research Projects (2012CB821904) of MST of China, the Emil Aaltonen Foundation, and the Ella and Georg Ehrnrooth Foundation.

chinaXiv:201711.01925v1

内蒙古大庙中新世小哺乳动物化石埋藏学研究

Leena SUKSELAINEN[1] Hannele PELTONEN[1] Anu KAAKINEN[1] 张兆群[2]

(1 芬兰赫尔辛基大学地球科学与地理学系 赫尔辛基 FI-00014)

(2 中国科学院古脊椎动物与古人类研究所，中国科学院脊椎动物演化与人类起源重点实验室 北京 100044)

摘要：捕食是小哺乳动物死亡最常见的原因，也导致被捕食动物遗骸发生明显改变。动物死亡后的风化、踩踏、搬运等过程也会改变动物的骨骼并影响到化石组合的形成。本文研究了内蒙古大庙三个中新世化石地点，时代从早中新世到晚中新世早期 (约 21~11.6 Ma)。通过分析各小哺乳动物化石组合的沉积背景以及埋藏学特征识别化石埋藏的主要成因。结果显示出捕食是三个地点小哺乳动物化石埋藏的基本成因，而在两个年轻的地点中也有流水搬运与可能的踩踏因素的叠加。三个地点可能存在不一样的捕食者：早中新世地点以猫头鹰捕食为主，中、晚中新世地点则以日间活动的鸟类或哺乳类为主要捕食者。研究还显

ChinaXiv合作期刊

示小哺乳动物的系统发掘是可行的，在一定程度上可以减少采样过程中产生的破坏。

关键词：内蒙古，新近纪，小哺乳动物，消化，捕食，河流沉积

中图法分类号：Q 915.873　　**文献标识码**：A　　**文章编号**：1000−3118(2017)01−0071−18

References

Andrews P, 1990. Owls, Caves and Fossils. London: Natural History Museum Publication. 1–231

Andrews P, Cook J, 1985. Natural modifications to bones in a temperate setting. Man, 20: 675–691

Andrews P, Evans E M N, 1983. Small mammal bone accumulations produced by mammalian carnivores. Paleobiology, 9: 289–307

Arcos S, Sevilla P, Fernández-Jalvo Y, 2010. Preliminary small mammal taphonomy of FLK NW level 20 (Olduvai Gorge, Tanzania). Quaternary Res. 74: 405–410

Behrensmeyer A K, 1975. The taphonomy and paleoecolgy of Plio-Pleistocene vertebrate assemblages east of Lake Rudolf, Kenya. Bull Mus Comp Zool, 146: 473–578

Behrensmeyer A K, 1978. Taphonomic and ecologic information from bone weathering. Paleobiology, 4: 150–162

Behrensmeyer A K, Kidwell S M, 1985. Taphonomy's contributions to paleobiology. Paleobiology, 11: 105–119

Behrensmeyer A K, Kidwell S M, Gastaldo R A, 2000. Taphonomy and paleobiology. Paleobiology, 26(4 Supp): 103–147

Brand L, 1995. An improved high-precision Jacob's staff design. J Sed Res, 65: 561

Demirel A, Andrews P, Yalcinkaya I et al., 2011. The taphonomy and palaeoenvironmental implications of the small mammals from Karain Cave, Turkey. J Archaeol Sci, 38: 3048–3059

Dodson P, 1973. The significance of small bones in paleoecological interpretation. Contrib Geol, Univ Wyo, 12: 15–19

Dodson P, Wexlar D, 1979. Taphonomic investigation of owl pellets. Paleobiology, 5: 275–284

Efremov I, 1940. Taphonomy: a new branch of paleontology. Panam Geol, 74: 81–93

Fernández-Jalvo Y, 1995. Small mammal taphonomy and the Middle Pleistocene environments of Dolina, northern Spain. Quat Int, 33: 21–34

Fernández-Jalvo Y, Andrews P, Denys C et al., 2016. Taphonomy for taxonomists: implications of predation in small mammal studies. Quat Sci Rev, 139: 138–157

Fernández López S, 1981. La evolución tafonómica (un planteamiento neodarwinista). Bol R Soc Esp Hist Nat (Geol), 79: 243–254

Fernández López S, 1991. Taphonomic concepts for a theoretical biochronology. Rev Esp Paleontol, 6: 37–49

Hardey J, Crick H, Wernham C et al., 2009. Raptors: a Field Guide to Surveys and Monitoring. 2nd ed. Edinburgh: Scottish Natural Heritage and the Stationary Office. 1–370

Kaakinen A, Aziz H A, Passey B H et al., 2015. Age and stratigraphic context of *Pliopithecus* and associated fauna from Miocene sedimentary strata at Damiao, Inner Mongolia, China. J Asian Earth Sci, 100: 78–90

Klietmann J, Van den Hoek Ostende L W, Nagel D et al., 2015. Insectivore palaeoecology. A case study of a Miocene fissure filling in Germany. Palaeogeogr Palaeoclimatol Palaeoecol, 418: 278–289

Korth W W, 1979. Taphonomy of microvertebrate fossil assemblages. Annls Carneg Mus, 48: 235–285

Lyman R L, 1994. Vertebrate Taphonomy. Cambrige: Cambridge University Press. 1–524

Mayhew D F, 1977. Avian predators as accumulators of fossil mammal material. Boreas, 6: 25–31

Miall A D, 1977. A review of the braided river depositional environment. Earth Sci Rev, 13: 1–62

chinaXiv:201711.01925v1

ChinaXiv合作期刊

Miall A D, 1992. Alluvial deposits. In: Walker R G, James N P ed. Facies Models – Response to Sea Level Change. Waterloo: Geological Association of Canada. 119–142

Miall A D, 1996. The Geology of Fluvial Deposits: Sedimentary Facies. Basin Analysis and Petroleum Geology. Berlin: Springer-Verlag. 1–582

Redding R W, 1978. Rodents and the archaeological palaeoenvironment: considerations, problems and the future. In: Meadow R H, Zeder M A eds. Approaches to Faunal Analysis in the Middle East. Bull Peabody Mus, 2: 64–68

Reed D N, Denys C, 2011. The taphonomy and paleoenvironmental implications of the Laetoli micromammals. In: Harrison T ed. Paleontology and Geology of Laetoli: Human Evolution in Context. Volume 1: Geology, Geochronology, Paleoecology and Paleoenvironment, Vertebrate Paleobiology and Paleoanthoropology. New York: Springer. 265–278

Shipman P, Bosler W, Davis K L, 1981. Butchering of giant geladas at an Acheulian site. Curr Anthropol, 22: 257–268

Soligo C, Andrews P J, 2005. Taphonomic bias, taxonomic bias and historical non-equivalence of faunal structure in early hominin localities. J Hum Evol, 49: 206–229

Van Dam J A. 1997. The small mammals from the upper Miocene of the Teruel-Alfambra region (Spain): paleobiology and paleoclimatic reconstructions. Geol Ultraect, 156: 1–204

Van Dam J A. 2006. Geographic and temporal patterns in the late Neogene (12-3 Ma) aridification of Europe: the use of small mammals as paleoprecipitation proxies. Palaeogeogr Palaeoclimatol Palaeoecol, 238: 190–218

Van Dam J A, Weltje G J, 1999. Reconstruction of the Late Miocene climate of Spain using rodent paleocommunity successions: an application of end-member modeling. Palaeogeogr Palaeoclimatol Palaeoecol, 151: 267–305

Van den Hoek Ostende L W, 2001. Insectivore faunas from the lower Miocene of Anatolia, Part 8: stratigraphy, palaeoecology, palaeobiogeography. Script Geol, 122: 101–122

Van Itterbeeck J, Missiaen P, Folie A et al., 2007. Woodland in a fluvio-lacustrine environment on the dry Mongolian Plateau during the Paleocene: evidence from the mammal bearing Subeng section (Inner Mongolia, PR China). Palaeogeogr Palaeoclimatol Palaeoecol, 243: 55–58

Voorhies M R, 1969. Taphonomy and population dynamics of an early Pliocene vertebrate fauna, Knox County, Nebraska. Contrib Geol, Univ Wyo, Spec Pap, 1: 1–69

Wang L H, Zhang Z Q, 2011. A new species of *Euprox* (Cervidae, Mammalia) from the Middle Miocene of Damiao, Nei Mongol, China. Vert PalAsiat, 49: 365–376

Wang X M, Qiu Z D, Li Q et al., 2009. A new Early to Late Miocene fossiliferous region in central Nei Mongol: lithostratigraphy and biostratigraphy in Aeorban strata. Vert PalAsiat, 47: 111–134

Williams J P, 2001. Small mammal deposits in archaeology: a taphonomic investigation of *Tyto alba* (barn owl) nesting and roosting sites. Ph. D thesis. Sheffield: University of Sheffield. 1–447

Wolff R G, 1973. Hydrodynamic sorting and ecology of a Pleistocene mammalian assemblage from California (USA). Palaeogeogr Palaeoclimatol Palaeoecol, 13: 91–101

Zhang Z Q, Harrison T, 2008. A new middle Miocene pliopithecid from Inner Mongolia, China. J Hum Evol, 54: 444–447

Zhang Z Q, Wang L H, Kaakinen A et al., 2011. Miocene mammalian faunal succession from Damiao, central Nei Mongol and the environmental changes. Quaternary Sci, 31: 608–613

Zhang Z Q, Kaakinen A, Liu L P et al., 2013. Mammalian biochronology of the Late Miocene Bahe Formation. In: Wang X M, Flynn L J, Fortelius M eds. Fossil Mammals of Asia: Neogene Biostratigraphy and Chronology. New York: Columbia University Press. 187–202

chinaXiv:201711.01925v1